Journal of Medicinal Chemistry

Article

Heterocyclic Diamidine DNA ligands as HOXA9 Transcription Factor Inhibitors: Design, Molecular Evaluation and Cellular Consequences in HOXA9-Dependant Leukemia Cell Model

Sabine Depauw, MELANIE LAMBERT, Samy Jambon, Ananya Paul, Paul Peixoto, Raja Nhili, Laura Marongiu, Martin Figeac, Christelle Dassi, Charles Paul-Constant, Benjamin Billoré, Arvind Kumar, Abdelbasset A. Farahat, Mohamed A Ismail, Ekaterina Mineva, Daniel P. Sweat, Chad E Stephens, David W. Boykin, W. David Wilson, and Marie-Hélène David-Cordonnier

J. Med. Chem., **Just Accepted Manuscript** • DOI: 10.1021/acs.jmedchem.8b01448 • Publication Date (Web): 15 Jan 2019

ACS Publications

is published by the American Chemical Society. 1155 Sixteenth Street N.W., Washington, DC 20036

	Wilson, W.; Georgia State University, Department of Chemistry David-Cordonnier, Marie-Hélène; Université Lille-Nord de France, Institut de Recherches sur le Cancer de Lille

Heterocyclic Diamidine DNA ligands as HOXA9 Transcription Factor Inhibitors: Design, Molecular Evaluation and Cellular Consequences in HOXA9-Dependant Leukemia Cell Model.

Sabine Depauw,[‡,1] Mélanie Lambert,[‡,1] Samy Jambon,[‡,1] Ananya Paul,[2] Paul Peixoto,[†,1] Raja Nhili,[1] Laura Marongiu,[1] Martin Figeac,[3] Christelle Dassi,[1] Charles Paul-Constant,[1] Benjamin Billoré,[1] Arvind Kumar,[2] Abdelbasset A. Farahat,[2,4] Mohamed A. Ismail,[2,5] Ekaterina Mineva,[2] Daniel P. Sweat,[6] Chad E. Stephens,[6] David W.Boykin,[2] W. David Wilson,[2] and Marie-Hélène David-Cordonnier*[,1]

[1] UMR-S1172-JPARC (Jean-Pierre Aubert Research Center), INSERM, University of Lille, Centre Hospitalier Universitaire de Lille, Institut pour la recherché sur le Cancer de Lille (IRCL), F-59045 Lille, France.

[2] Department of Chemistry, Georgia State University, Atlanta, GA 30303, United States.

[3] Functional and Structural Genomic Platform, Lille University, F-59000 Lille, France.

[4] Department of Pharmaceutical Organic Chemistry, Faculty of Pharmacy, Mansoura University, Mansoura 35516, Egypt.

[5] Department of Chemistry, Faculty of Science, Mansoura University, Mansoura 35516, Egypt.

[6] Department of Chemistry and Physics, Augusta University, Augusta, GA 30904, United States

* To whom correspondence should be addressed. Tel: +33 320 169 223; Fax: +33 320 538 562; Email: marie-helene.david@inserm.fr, ORCID ID: 0000-0001-9831-5577.

‡ The authors wish it to be known that, in their opinion, these authors should be regarded as joint First Authors

Present Address: † Peixoto Paul, EA3922, University of Bourgogne Franche-Comté, Besançon, France.

ABSTRACT:

Most transcription factors were for long time considered as undruggable targets due to the absence of binding pockets for direct targeting. HOXA9, implicated in acute myeloid leukemia, is one of them. To date, only indirect targeting of HOXA9 expression or multi-target HOX/PBX protein/protein interaction inhibitors has been developed. As an attractive alternative by inhibiting the DNA binding, we selected a series of heterocyclic diamidines as efficient competitors for HOXA9/DNA interaction through binding as minor groove DNA ligands on the HOXA9 cognate sequence. Selected DB818 and DB1055 compounds altered HOXA9-mediated

transcription in luciferase assays, cell survival and cell cycle, but increased cell death and granulocyte/monocyte differentiation, two main HOXA9 functions also highlighted using transcriptomic analysis of DB818-treated murine Hoxa9-transformed hematopoietic cells. Altogether, these data demonstrate for the first time the propensity of sequence-selective DNA ligands to inhibit HOXA9/DNA binding both in vitro and in a murine Hoxa9-dependent leukemic cell model.

INTRODUCTION

Transcription factors are often associated with different phases of the oncogenic process (initiation, development, invasion, metastasis…) and represent ~20% of the established targets in cancers. However, only a few of them are targeted in cancer therapies. The different approaches for targeting transcription factors are i) to directly target the protein via a functional pocket, ii) to target protein-protein interactions and iii) to interfere with the transcription factor's ability to interact with its cognate binding site on a targeted DNA sequence.[1–4] Only a few of them can be targeted through their ligand binding pocket. Hormone/retinoid receptors are a notable example, and more precisely the retinoid receptor RARα, which can be targeted by all-trans retinoic acid (ATRA). This compound has been used in human therapy for three decades in PML-RARα-rearranged acute promyelocytic leukemia (APL) through the induction of differentiation.[5] Other transcription factors families have been considered as undruggable targets.[6] Alternatives are protein/protein inhibitors, that can for example target the p53 and mdm2/mdmx interface[7], BCL6[8] and STAT3 homodimers[9], YAP/TAZ[10,11] or CBP/βcatenin[12] interactions, or the development of drugs from phenotypic screening as against NRF2[13] or HSF1[14]. Only a limited

number of strategies are dedicated to direct targeting of transcription factor-DNA binding domains and a recent example is the PAX2 transcription factor DNA binding domain.[15] Alternatively, another manner to target a transcription factor at the DNA binding level is to develop molecules that target the DNA promoter sequence and compete with transcription factor binding to its cognate sequence. This is the case for a variety of minor groove DNA binding structures. Many different series of DNA minor groove binders are also in preclinical development such as mithramycines, polyamides and diamidine heterocyclic derivatives.[1,4,16,17] Among this group, mithramycin A and some of its derivatives inhibits SP1/DNA,[18] which is associated with the deregulation of many SP1-driven genes such as MYC, FOXM1, p21, Ki-67, CRABP1, BAK or KLF5.[4] Mithramycin A and derivatives also block EWS-Fli-1/DNA interaction[19] and have entered clinical trials against refractory Ewing sarcoma[20]. Interestingly, two other minor groove DNA binders recently showed interesting anti-leukemic activities by targeting transcription factors associated with acute myeloid leukemia (AML): the alkylating agent–conjugated pyrrole-imidazole polyamide Chb-M against RUNX1[21] and DB2313 against PU.1[22].

HOXA9 is a well-known transcription factor implicated in oncogenic and leukemic processes. Besides its implication in some solid tumors,[23–27] HOXA9 is clearly associated with different hematologic malignancies.[28–32] Indeed, HOXA9 is over-expressed in ~70 % of AML or fused to NUP98 in the t(7;11)(p15;p15) translocation leading to the hybrid protein NUP98-HOXA9 responsible for 2-5 % of AML[33,34] and 5 % of myelodysplasic syndromes (MDS)[35]. Functionally, HOXA9 is involved in the differentiation blockade, resulting in the accumulation of leukemic blasts in patients.[28,29,32,36] Such leukemic activity is directly attributable to the HOXA9 DNA binding activity. Indeed, deletion of its homeodomain abolishes the propensity of HOXA9 to

induce leukemia in mice.[37–39] Furthermore, HOXA9 was found quite recently as one of the genes associated with leukemic stem cell signature and resulting in poor prognosis.[40] The HOXA9 transcription factor is therefore a good candidate for the development of new targeted therapies for differentiation that would be intended for a large number of patients suffering from AML.

HOXA9 binds to it regulatory DNA sequence at a 5'-tgATTTAt site (JASPAR MA0594.1), as defined by ChIP-seq in a murine model expressing a tagged-Hoxa9 protein.[41] DNA recognition occurs through the interaction between the third α-helix of its homeodomain and the DNA major groove, and between the amino-terminal unfolded module of its homeodomain which makes deep contacts in the minor groove of the AT-rich segment of the consensus binding site.[42] In the present study, we evaluated a focused library of heterocyclic diamidine DNA ligands as functional inhibitors of human HOXA9/DNA binding activity. We evaluated their mode of binding to DNA in vitro and the cellular consequences of the protein-DNA complex inhibition. We further selected DB818 and DB1055 for additional investigation and evidenced their inhibitory effect on HOXA9-induced transcription control by using HOXA9-driven luciferase gene expression. The compound effects on cell survival and clonogenic activity of Hoxa9-transformed murine bone marrow cells argues for cell differentiation process, as highlighted by transcriptomic analyses of DB818-treated leukemic cells. These results clearly show for the first time the selection of direct functional inhibitors of HOXA9/DNA binding through the targeting of the HOXA9 consensus binding site by DNA ligands.

RESULTS AND DISCUSSION

Design of the evaluated compounds

In order to develop inhibitors for the HOXA9 transcription factor at its DNA binding level, we took advantage of the HOXA9 DNA binding domain particularities. Indeed HOXA9 binds through a direct interaction of the third α-helix and the N-terminal portion of its homeodomain with the major and minor grooves, respectively. The key interaction are with the 5'-ATT(A/T) sequence of the 5'-tgATTTAt defined consensus site.[41,42] We were specifically interested in heterocyclic diamidine compounds that have been previously reported to be potent in vitro transcription factor DNA binding inhibitors: DB293 against Pit-1 and Brn-3[43] and DB1255 against the ERG transcription factor[44,45]. The AT specific minor groove binding diamidines evaluated as HOXA9 inhibitors were obtained from our large library of heterocyclic diamidines synthesized as potential anti-parasitic agents. The selections were made from a number of structurally diverse diamidine types with many selected for their binding to AT-rich, ATT(A/T) or ATGA binding to DNA [46,47] and new structures were designed on the basis of three central aromatic groups R_1, R_2 and R_3 flanked by an amidine moiety at each extremity (Table 1). A series of 39 compounds are classified based on the presence of R_2 as a 5- or 6-membered ring, on the nature or R_3 rings (general with a phenyl or a benzimidazole). Modifications of the R_1 ring and the amidine extremities (R_4 and R_5) offer a large diversity of molecules to expand structure/function relationships (Table 1).

Approximately two-thirds of those selected have been previously reported and references to their synthesis are provided in Supplementary Information. The syntheses of those previously unreported are described below.

The synthesis of three furan benzimidazole analogues (4a-c; DB915, DB928, DB995) is outlined in Scheme 1. The 2-cyanoaryl-5-formyl furans were prepared employing standard Stille cross-coupling conditions allowing 2-(tri-n-butylstannyl) - 5-(dimethoxymethyl) furan- to react

with the various cyanoaryl bromides in the presence of tetrakis (triphenylphospine) palladium. The required bis-nitriles were obtained by oxidative coupling of 3, 4-diaminobenzonitrile with the various 2-cyanoaryl-5-formyl furans using benzoquinone as the oxidant. The diamidines were prepared by first converting the bis-nitrile into the corresponding amidoximes, which were acetylated, and subsequently subjected to hydrogenolysis to yield the desired diamidines. In the case of DB928, the hydrogenolysis in addition to cleaving the N-OAc bond also cleaved the benzyl group.

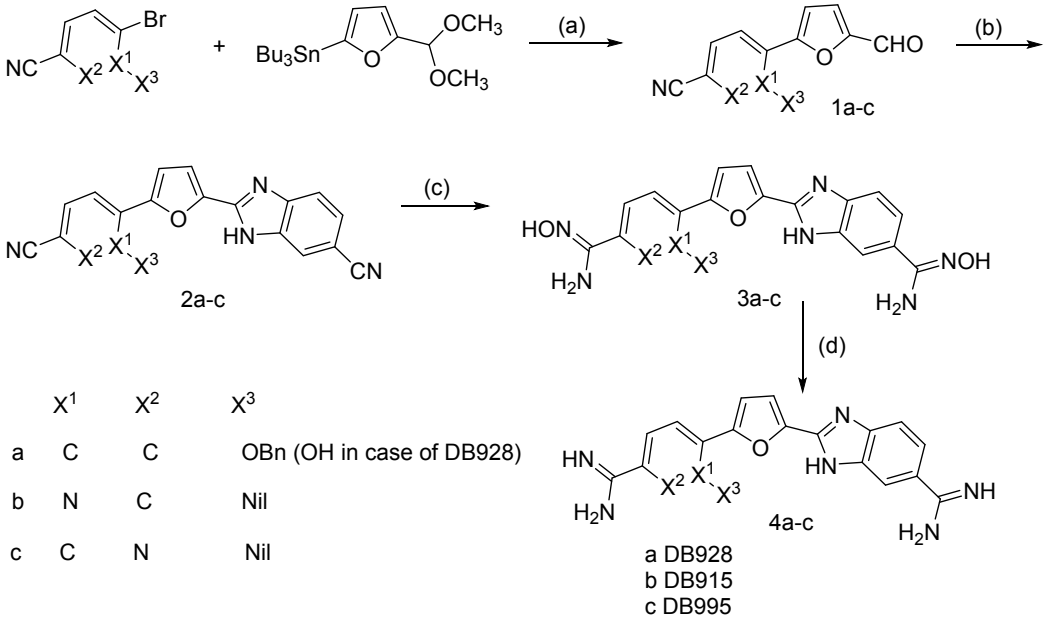

	X^1	X^2	X^3
a	C	C	OBn (OH in case of DB928)
b	N	C	Nil
c	C	N	Nil

Scheme 1. Reagents and conditions: (a) i. Pd(PPh3)4, 1,4-dioxane,ii. 2.0 M HCl; (b) 3,4-diaminobenzonitrile, 1,4-benzoquinone, EtOH; (c) NH_2OH-HCl/KO-t-Bu, DMSO; (d) i. AcOH/Ac_2O, ii. H_2/Pd-C, AcOH.

The route employed for synthesis of the thiazole benzimidazole (7; DB2651) is shown in Scheme 2. In this case Suzuki cross-coupling between 5-bromothiazole-2-carbaldhyde and 4-cyanophenylboronic acid was utilized to obtain 5-(4-cyanophenyl) thiazole-2-carbaldehyde. In this example, the bis-nitrile was achieved by oxidative coupling of 3, 4-diaminobenzonitrile and the thiazole aldehyde using sodium metabisulfite as the oxidant. The diamidine was obtained from the bis-nitrile using classical Pinner methodology.

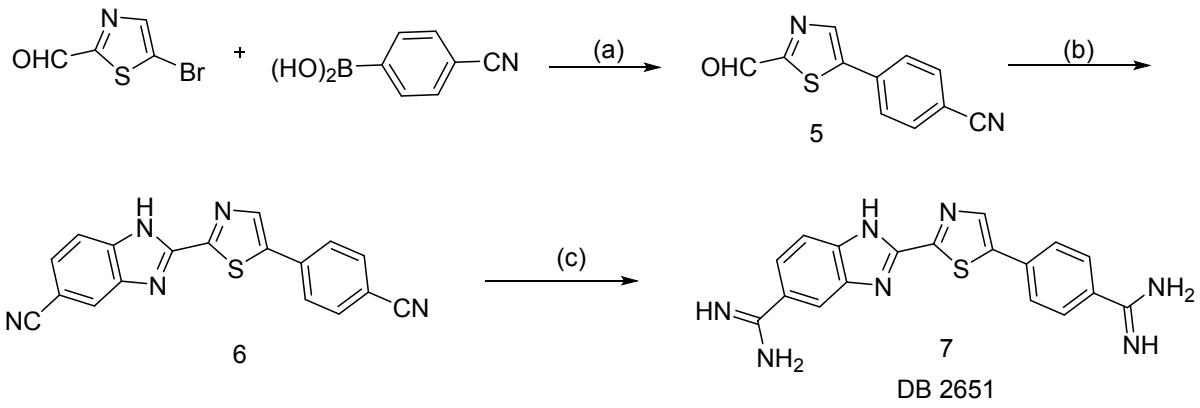

Scheme 2. Reagents and conditions: (a) $Pd(PPh_3)_4$, Na_2CO_3/H_2O, dioxane, reflux; (b) 3,4-diaminobenzonitrile, $Na_2S_2O_3$/ DMSO, 140 ^oC; (c) i HCl(g), EtOH, ii NH_3 (g), EtOH.

In Scheme 3 the synthesis approach to five (11a-e; DB1478, DB1481, DB1879, DB2005, DB2529) heteroaryl indole diamidines is presented. The 2-arylcyanofurans and thiophenes were obtained using Stille coupling between 2-(tri-n-butylstannyl) furan and 2-(tri-n-butylstannyl) thiophene with the indicated cyanoaryl bromides. NBS bromination of the 2-aryl furans and thiophenes at room temperature yielded the corresponding 5-bromo-2-aryl furans and thiophenes. Reaction of either the Boc-protected 5 or 6-cyano-2-(trimethlystannyl) indole with the 5-bromo-2-aryl furans or thiophenes yield the Boc-protected bis-nitriles. The bis-nitriles were converted into the diamidines by reaction with lithium bis(trimethylsilyl) amide.

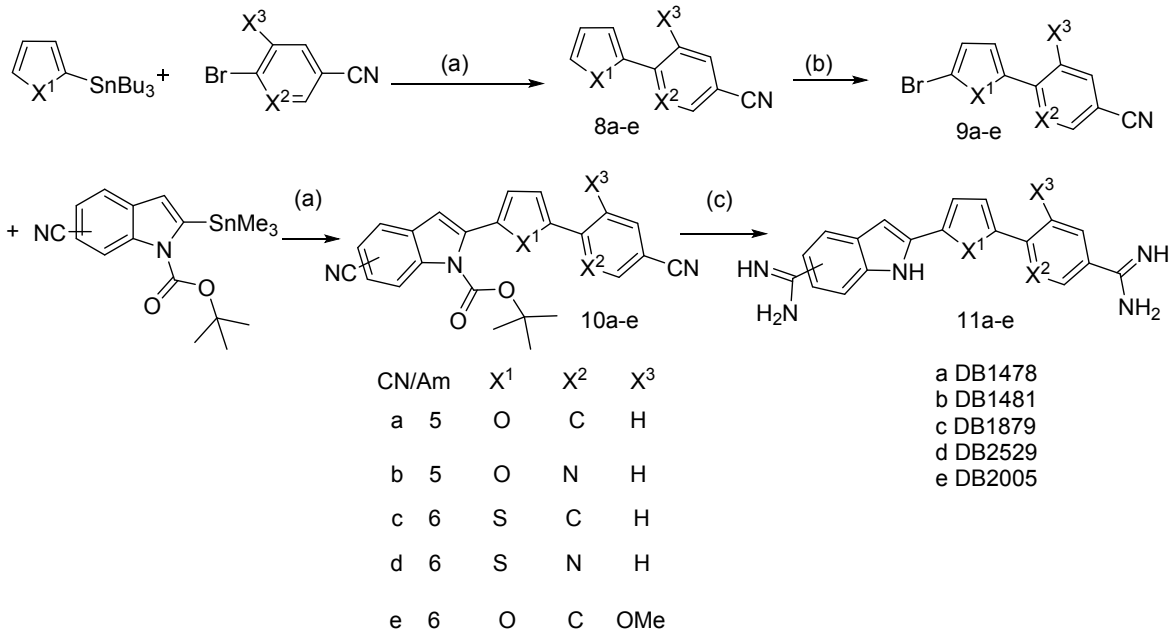

Scheme 3: Reagents and conditions; (a) $Pd(PPh_3)_4$, Dioxane; (b) NBS,DMF, rt; (c) i $LiN(TMS)_2$/THF, ii$^-$ HCl(g), EtOH.

The synthesis of the bis-N-(4-nitrophenylethyl) analogue (12a; DB421) of furamidine and the tellurophene analogue (12b; DB1751) of furamidine is presented in Scheme 4. The former was obtained from the bis-nitrile by conversion into the corresponding imidate ester, which on reaction with 4-nitrophenethyl amine yielded DB421. Reaction of 2, 5-bis-(4-cynophenyl) tellurophene with lithium bis(trimethylsilyl)amide provided DB1751.

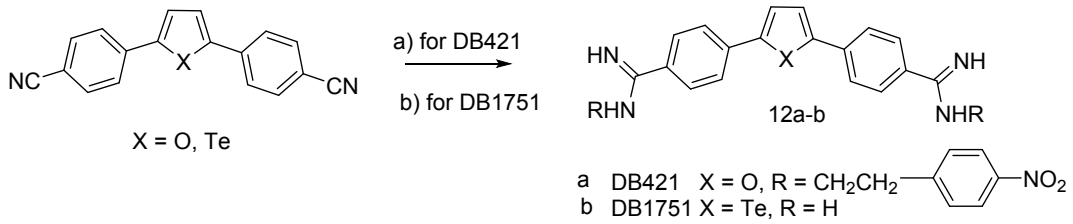

Scheme 4. Reagents and conditions; (a) i HCl(g), EtOH ii 4-nitrophenethylamine, EtOH; (b) i $LiN(TMS)_2$,THF, rt, ii HCl(g), EtOH.

The synthesis of the N-methylbenzimidazole analogue (14; DB1314) is shown in Scheme 5. The required bis-nitrile was obtained by oxidative coupling of 3-(methylamino)-4-

aminobenzonitrile with 4-cyano-3'-formyl-1, 1'-biphenyl using sodium metabisulfite as the oxidant. The mentioned lithium bis(trimethylsilyl)amide method was used to convert the bis-nitrile into the diamidine.

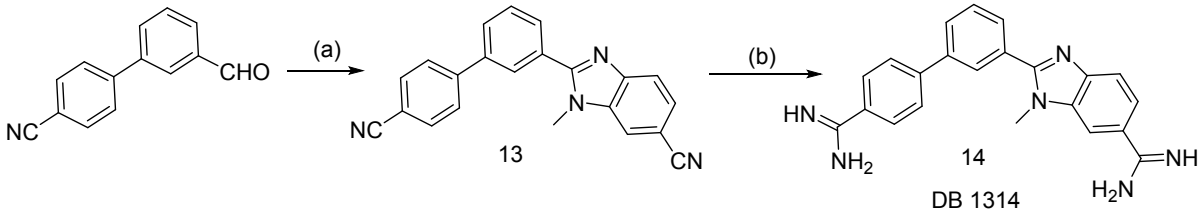

Scheme 5. Reagents and conditions: (a) 4-amino-3-(methylamino)benzonitrile, $Na_2S_2O_3$, DMF, reflux. (b) i $LiN(TMS)_2$, THF, rt ii HCl(g), EtOH.

The route utilized for synthesis of the quinoline analog (18; DB1504) is outlined in Scheme 6. The Pfitzinger reaction between 2-acetylthiophene and 6-bromoisatin provided six-bromo-2-(thiophen-2-yl)quinoline-4-carboxylic acid which on heating in the presence of copper(I)cyanide results in both decarboxylation and replacement of the bromo group with a cyano group. Once again, NBS bromination of the 2-aryl thiophene at room temperature yielded the desired 5-bromo-2-aryl thiophene analogue. Reaction of 4-cyanphenylboronic acid with the 5-bromo-2-aryl thiophene derivative under standard Suzuki coupling conditions provided the needed bis-nitrile. Again, the lithium bis(trimethylsilyl)amide methodology was employed to obtain the diamidine DB1504.

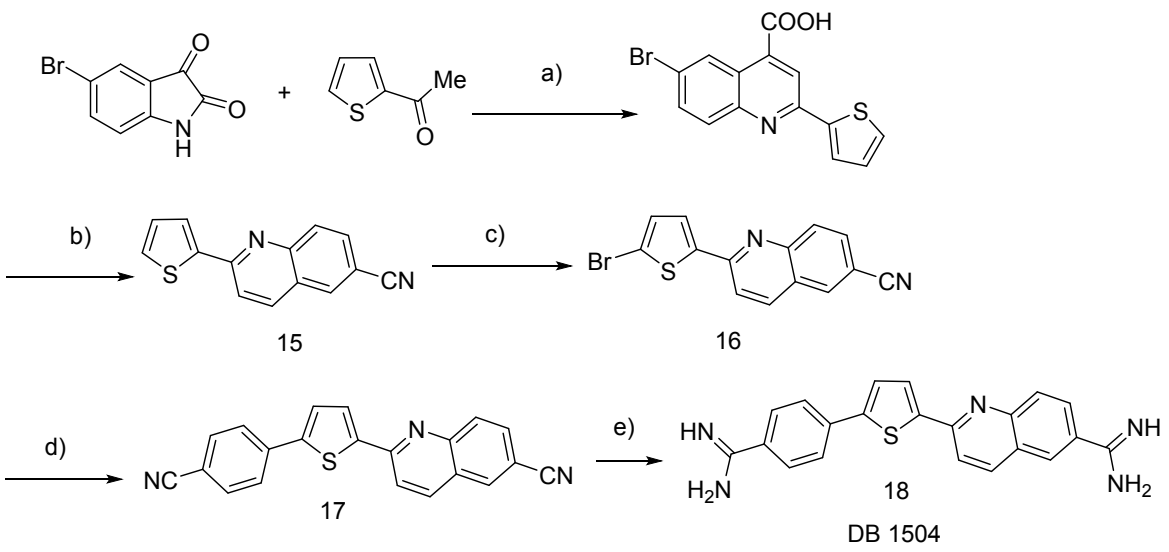

Scheme 6. Reagents and conditions: (a) NaOH, H_2O,100^oC, overnight; (b) CuCN, DMF, 140^oC (c) NBS, DMF, rt ;(d) 4-cyanophenylboronic acid, 1,4-dioxane, $Pd(PPh_3)_4$, 2M K_2CO_3, 70^oC, overnight; (e) i $LiN(TMS)_2$, THF, rt, 48 h, ii HCl(g), EtOH.

Scheme 7 shows the approach used for the synthesis of the bis-N-methylbenzimidazole analogue (19; DB2572). In this case, the bis-aldehyde was oxidatively coupled, mediated by benzoquinone, with 3-amino-4-(methylamino)benzamidine to directly yield DB2572.

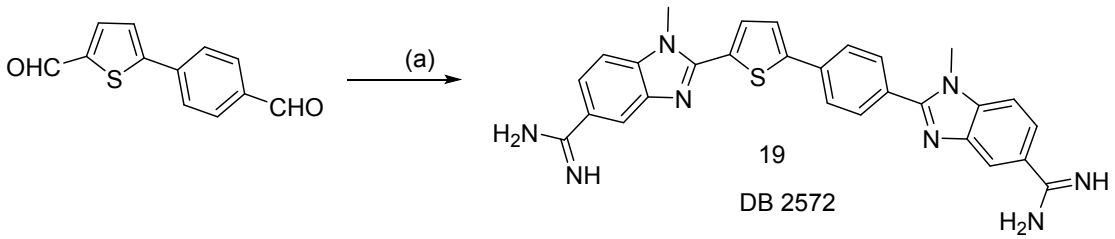

Scheme 7. Reagents and conditions: (a) 3-amino-4-(methylamino)benzamidine, benzoquinone, EtOH, reflux.

Selection of HOXA9/DNA binding inhibitors

An ELISA-derived DNA binding inhibition assay was first used to evaluate this series of compounds for the inhibition of the HOXA9 protein interaction with its cognate DNA binding

sequence 5'-aTGATTTA (HBS for HOXA9-binding site) which is 5'-biotinylated in order to be immobilized on streptavidin-coated 96-wells plates. Specific (HBS) and nonspecific (NS) oligonucleotides (sequences in Supplementary Table S1) were used as competitor DNAs to validate the experimental conditions for selective protein/DNA inhibition experiments. The previously characterized AT-rich DNA ligand DB75 and the ATGA-site DNA binding compound DB293 were used as controls. Among those evaluated, ten compounds showed significant activity on HOXA9/DNA binding (grey and white box for at least 50% and 75% inhibition, respectively) (Figure 1A) and were further evaluated using EMSA (representative gels presented in Figure 1B and Supplementary Figure S1). HOXA9 protein expressed using a reticulocyte lysate system was incubated with radiolabelled HBS-double stranded oligonucleotide (sequence in supplementary Table S1) and increasing concentrations of the tested compounds. The retarded band on the gel shows the formation of the HOXA9/HBS complex (bound, ***b***), separated from the free HBS DNA (***f***). This conclusion was further validated by addition of HOXA9-directed antibody (Ab) and by the absence of the retarded band using reticulocyte lysate prepared in the absence of HOXA9-expressing vector (first and last lanes "0" from the upper left panel in Figure 1B). Quantification of the HOXA9/DNA inhibition from EMSA is presented in Figure 1C. This result demonstrated that DB818, DB1055, DB884, DB1879 and DB2529 are highly potent inhibitors of HOXA9/DNA binding with more that 90% inhibition at 2.5 μM ("High" panel). DB1177, DB883 and DB2223, on the other hand, are less efficient ("Medium" panel) with 90% inhibition reached using 7.5 μM. By contrast, DB1620, DB1878 and DB911 are poor inhibitors ("Low" panel) while others are considered to be inactive (right panel, "Inactive").

In terms of structure activity relationship, DB818, DB1879 and DB2529 are structurally related compounds that share a common central thiophene ring but differ by the presence or absence of a nitrogen atom that converts (i) the indole ring of DB1879 to a benzimidazole ring in the DB818 for R_3 position or (ii) a phenyl ring in R_1 position of DB1879 and to a pyridine ring in DB2529. Neither modification alters their propensity to inhibit the HOXA9/DNA interaction. By contrast, changing the thiophene ring of DB818, DB1879 or DB2529 to a furan (DB293, DB1878 or DB915, respectively) or a thiazole ring (DB2651) in the benzimidazole series strongly reduces HOXA9 inhibition efficacy whereas a pyrazole ring modification still confers some weaker inhibitory activity to DB2223. Surprisingly, such modification of the thiophene ring to a thiazole ring in the di-phenyl series changes an inactive compound (DB351) to an effective (but low) inhibitor of HOXA9/DNA binding (DB1620). The addition of a methyl group on the benzimidazole ring (DB818) at the R_3 position or changing the DB818 benzimidazole ring to a quinoline ring or to a N-isopropyl-benzimidazole-phenyl moiety strongly alters its propensity to inhibit the HOXA9/DNA interaction (see DB2429, DB1504 or DB2708) relative to DB818. A methyl group on the phenyl ring in R_1 also alters the inhibitory effect of DB1878 (unmethylated) as shown using DB2005 (methylated) (Figure 1A). Moreover, the addition of a methyl group to the benzimidazole ring in the R_3 position alters the HOXA9 inhibition efficiency as observed with the highly active unmethylated compounds DB818 and DB2529, relative to their inactive methylated counterparts DB2429 and DB2430 (of note, this latter also differs by the presence of a furan 5-membered ring in R_2 position instead of a thiophene). Finally, the two pyrrole derivatives bearing an additional ring (phenyl for DB884 or pyridine for DB883) at both the R_1/R_5 positions are identified as high (DB884) and medium (DB883) inhibitors.

The results obtained from ELISA-derived DNA binding inhibition assay and EMSA are in good agreement and highlight DB818, DB1055, DB883, DB1879 and DB2529 as interesting inhibitors of HOXA9/DNA binding. By contrast, DB828, that failed to inhibit HOXA9/DNA binding, was selected as a negative control for further analyses. It is also worth noting that neither DB818 nor DB1055 inhibits the DNA binding of the HMG-box protein, a protein known to interact with DNA on AT-rich sites (Supplementary Figures 1B-C).

Direct DNA binding of the selected HOXA9/DNA inhibitors into the groove of DNA

Thermal melting experiments allow a robust screening for the relative binding affinity of the ligands with DNA sequences. In order to understand ligand-DNA complex stability, we conducted thermal melting studies of different diamidine compounds with cognate HBS sequences. Ligand and HBS duplex DNA sequences were prepared at a ratio of 1:1 and 2:1 (Figures 2A). At R=1:1, DB818, DB1055 and DB2529 showed ΔTm values of 7-10°C. The thermal stability of the complex increase at R=2:1 ligand-DNA ratio (ΔTm >10°C) for DB818, DB1055, DB2529, DB1879 and DB1878. On the other hand, DB884 and DB1177 showed moderate binding with the HBS duplex (ΔTm = 8-9 °C). However, DB883, DB884, DB2223 and DB1620 bind very weakly with the cognate HBS sequence.

To evaluate the binding mode of diamidine compounds with the same HOXA9-binding site the circular dichroism (CD) spectral experiment was performed (Figure 2B). Neither the duplex DNA nor the free diamidines compound exhibits CD signals in the compound absorption region above 300 nm. Adding increasing amount of diamidine compounds that evidenced in vitro positive results, leads to a substantial positive induced CD signals (ICD) for the complex formation with DNA at the wavelengths between 300 and 400 nm. This observation indicates

that the diamidine compounds bind within the groove of the HBS DNA sequence, more likely within the minor groove as strongly evidenced in the crystal and/or NMR structure for DB818, DB1055, DB884 or DB293 to 5'-AATT-containing DNA (PDB: 1VZK, 2I5A, 2I2I, 2GYX)[47–49]. On the other hand, DB828 induces only weak CD changes at the highest drug concentrations in agreement with the low ΔTm. All tested compounds except DB1177 and DB828 changed the positive ellipticity band of the DNA helix (positive CD band near 275 nm), suggesting that they induce modification of the stacking of the successive bases of the DNA.

HOXA9/DNA inhibitors directly bind to HOXA9-cognate sequence

To define the specific drug/DNA binding sequence, DNaseI footprinting experiments were used for selected compounds from the "High" (DB818, DB1055, DB1879, DB2529), "Medium" (DB1177, DB883), "low" (DB1878) and "inactive" (DB828) subgroups for HOXA9/DNA binding inhibition. As can be seen from Figure 3A, DNase I generated DNA fragments were separated upon electrophoretic migration from top to bottom. Some of the cleavage sites were protected from DNaseI digestion around the 50bp position with addition of increasing concentrations of selected diamidine compounds. The protected site was clearly evidenced on the corresponding densitometric analysis located on the HOXA9 binding site 5'-ATTTA for compounds from the "High" subgroup DB818, DB1055, DB1879 and DB2529 (Figure 3B). By contrast, DB828 and DB883 failed to recognize the 5'-ATTTA sequence, whereas DB1878 and DB1177 has a much weaker binding activity of the 5'-ATTTA site (Figure 3B). These results are in agreement with the DNA melting temperature studies on the HBS sequence (Figures 2A). We used the same UV/vis DNA melting approach to evaluate the binding of DB818, DB1055 and DB828 on the mutated HBS-oligonucleotide sequences. We have mutated the sequence at the 5'-ATGA (HBS-ATGAm) or the AT-rich (HBS-ATm) or containing both mutations (HBS-2mut)

(oligonucleotide sequences are presented in Supplementary Table S1). For the HBS-ATGAm sequence, the ΔTm values obtained with DB818 and DB1055 were similar to that obtained with wild-type HBS oligonucleotide, which suggests that the diamidine compounds do not bind at the 5'-ATG binding site of HBS (Figure 3C). By contrast, when the 5'-ATTTA site was mutated alone for HBS-ATm or together with the ATGA portion for HBS-2mut, ΔTm values decreased by 4°C, which is similar to the observed value for the DB828. From the previous experiment (Figure 2A) it has been observed that DB828 binds with HBS as a weak nonspecific binder. This result is in agreement with the DNase I footprinting experiments which suggest that, among other, DB818 and DB1055 interact at the 5'-ATTTA-sequence of the HOXA9 binding site (Figure 2) but did not bind to an HBS-mutated DNA as shown in Supplementary Figure S2. This sequence specific binding evidenced DB818 and DB1055 as competitors for HOXA9 binding to its cognate sequence on the DNA helix.

Surface plasmon resonance (SPR) experiments were applied to measure the dissociation constants K_D for DB818 or DB1055 on HBS or HBS-2mut sequences (Figure 4). DB818 and DB1055 have similar strong K_D values on HBS sequence (4.6 nM and 5.5 nM, respectively). The dissociation constant is much greater on the mutated sequence (0.35 μM and 1.7 μM, respectively), highlighting that DB818 is ~75-fold more selective for HBS than to HBS-mutated sequence whereas DB1055 is even more selective with >300-fold difference in K_D values (Figure 4).

To gain structural insight into the mechanism by which the DB818 and related diamidines compounds inhibit HOXA9 binding to the cognate HBS, we performed a 100 ns molecular dynamics simulation (MD) of the DB818 binding to ATGATTTA sequence (Figure 5,

Supplementary Figure S3, Supplementary Table S2). The HBS-bound complex showed that DB818 is selectively bound to the minor groove of AT-rich 5'-$A_1T_2T_3T_4A_5$/5'-T_5,A_4,A_3,A_2,T_1, binding site and makes excellent van der Waals interactions with the walls of the minor groove (Figure 5A-B). Two amidine groups, −N−Hs form H-bond either with T=O of dT_1, base or A-N3 of dA_5 base (Figure 5C-D) that are an average of 2.3 Å in length. The third strong H-bond is formed with the T=O of dT_4 base to the H-N-benzimidazole of DB818 with 2.0 Å bonding length, to account for much of the binding selectivity of DB818 (Figure 5D). Additional selectivity in binding is provided by the −CH group of the six-member ring of benzimidazole that points deeply into the minor groove and forms a dynamic close interaction with A-N3 of the dA_4, base of the A•T bp. Interaction of the phenyl ring with dT base further stabilizes DB818/DNA interaction and increases sequence selectivity. The sum of these numerous relatively stabilizing interactions, marks DB818 a strong ATTTA sequence binder within the minor groove which may explain how DB818 inhibits the binding of the HOXA9 protein at the major groove and minor groove of its cognate binding site (see conclusions section).

HOXA9/DNA binding inhibitors are effective at entering cells and localizing to the nucleus.

In order to address the cellular consequences of HOXA9 inhibitors, we used MigA9 cells, resulting from retroviral transduction of the murine Hoxa9 gene in murine bone marrow cells that were injected in sub-lethally irradiated mice and then collected from the bone marrow after leukemia burden and cultured in appropriate medium as described.[26] We first evaluated the cytotoxic effect of a series of diamidine compounds. Cell survival activity (IC_{50}) on MigA9 cells was measured at 72 hours of treatment by using a colorimetric assay based on the reduction of a MTS tetrazolium dye. The IC_{50} values of diamidine compounds are at micromolar range, except

DB828 which has very high $IC_{50,}$ and supports previous in vitro observations. Surprisingly, DB2223, as an effective in vitro inhibitor of the HOXA9/DNA binding complex, failed to alter MigA9 cell survival (Table 2). We also evaluated their susceptibilities to enter cells and localize in the nucleus by using fluorescence microscopy as previously described for DB75 and its derivatives.[50] Most of the diamidines have intrinsic fluorescence properties in blue wavelengths. Compounds were evaluated either on MigA9 murine leukemia cell line (Figure 6A and Supplementary Figure S4) and/or HT-29 adherent cell line (Supplementary Figure S5). All evaluated compounds entered the nucleus except DB911 which could not be detected due to the lack of intrinsic fluorescence properties. DB828, which also localized to the nucleus but failed to inhibit HOXA9 DNA binding, was used as a negative control in the following cellular studies.

DB818 and DB1055, but not DB828, inhibit HOXA9-dependant transcription control

In order to address the inhibitory effect of DB818 and DB1055 on the HOXA9-mediated transcriptional control, we performed luciferase assays. We used a pGL3-promoter vector in which the minimal promoter is under the control of 6-repeated HBS sequences, either the wild-type or mutated sequence at the 5'-ATTTA binding site (HBS and HBS-mut oligonucleotides, Supplementary Table S1). Cell transfection was performed in the K562 cell line as a leukemic cell model that is known for its lack of internal HOXA9 expression.[51] The absence of HOXA9 expression has been validated by using qRT-PCR and western-blotting, personal information and Supplementary Figure S6A, respectively. In this cell line, both DB818, DB1055 and DB828 compounds have no effect on cell survival and clonogenic propensities (Supplementary Figure S5B, Table 4, top lanes). Extrinsic HOXA9 protein was expressed by transfecting the pCMV-AD-HOXA9 vector in the K562 HOXA9-negative cells (Supplementary Figure S6A). HOXA9 protein has only low propensity to transactivate by itself in the absence of co-factors. Therefore,

the region encoding the transactivation domain (AD) of NF-κB was fused in frame to the HOXA9 full length open-reading frame in order to express the HOXA9-AD fused protein that presents increased transactivation properties relatively to HOXA9 alone (personal information, see also Material and Methods section). Luciferase assays were performed in the presence versus absence of evaluated compounds of DB818 and DB1055 as HOXA9/DNA binding inhibitors, or DB828 as a negative control. The results showed that both DB818 and DB1055, but not DB828, were able to inhibit HOXA9-mediated transactivation in the presence of wild-type HBS sequences by controlling luciferase expression but not in the presence of HBS-mut sequences (Figure 6B). These results also suggested that the HBS binding site is required for selective inhibition of HOXA9 transcriptional activity.

Gene expression analysis of MigA9 cells treated with DB818 highlights induced cell death processes.

In order to investigate the cellular mechanistic action of selected diamidine HOXA9/DNA inhibitors, we initially used a global gene expression analysis of MigA9 cells which were treated with DB818 (2.5μM) for 6, 12 and 24 hours. Co-deregulated genes with |mean fold changes| ≥ 1.5 are presented as heatmap in Figure 7A (|mean fold changes| ≥ 1.5). GSEA analyses on MSigDB C2-Chemical and Genetic Perturbation gene sets (Figure 7B) evidenced that the significant genes up-regulated in DB818-treated MigA9 cells at the different time correspond to genes that were down-regulated in human CD34+ cells transduced with NUP98-HOXA9 fusion (TAKEDA TARGETS OF NUP98 HOXA9 FUSION 8D DN), Figure 7B. Similarly, the list of significant commonly down-regulated genes in DB818-treated MigA9 cells are highlighted in geneset enrichments corresponding to genes up-regulated in murine HoxA9+Meis1 transformed cells (WANG IMMORTALIZED BY HOXA9 AND MEIS1 UP). Both results of CGP genesets

enrichments suggest that the gene deregulation in opposite way between the transformation of hematopoietic progenitors with HoxA9+Meis1 or NUP98-HOXA9 and the inhibition of HOXA9 activity by DB818 in MigA9. Other genesets associated with HOXA9 expression control (NUYTTEN EZH2 TARGETS UP),[52] genes controlled by HOXA9 (GABRIELY MIR21 TARGETS),[53] leukemic stem cell inhibition (GAL LEUKEMIC STEM CELL DN) and AML-induced differentiation (MARTENS TRETINOIN RESPONSE DN) were also found as significantly enriched in our dataset (Figure 7B). Ingenuity Pathway Analysis (IPA) of deregulated genes highlights the activation of macrophage differentiation, a reduced quantity of hematopoietic cells and an increase in apoptosis (Figure 7C). Analysis of the BloodSpot database (www.bloodspot.eu) found multiple commonly deregulated genes (identified as arrows in Figure 7A) which are significantly associated with the differentiation of granulocyte-monocyte progenitors (GMP) to granulocytes and monocytes (Supplementary Figure S7). Among them, the well-known monocyte/macrophage expressing the integrin Itgam (CD11b) is expressed upon differentiation of AML blasts[54,55] and the Oasl2 enzyme that is also associated with the differentiation of monocytes and dendritic cells[56]. Such over-expression of Itgam and Oasl2 were validated by qRT-PCR after a 48 hours of treatment with DB818 (5 or 10µM), as were validated the over-expression of Akap13 and Arfgef1 (Figure 7D) as examples of genes associated with granulocyte and/or monocyte differentiation (Supplementary Figure S7). Similar results of overexpression of these genes were also observed for DB1055, (Figure 7D) but DB828 failed to achieve the similar results. Recently, Sun et al. (2018) identified murine Hoxa9 DNA binding sites by ChIP-seq analysis of a murine leukemia model obtained by transformation of murine progenitor cells by co-expression of hemagglutinin (HA)-tagged HOXA9 and MEIS1 using an anti-HA antibody.[57] Among Hoxa9 ChIP-peaks, the sequence identified as “DE-651 peak”

located at position chr7:82861417-82863417 (from NCBI37/mm9 mouse reference genome) is positioned within Akap13 gene. Interestingly, we identified a cognate HOXA9 binding sequence within DE-651 peak sequence (Figure 8A). An oligonucleotide overlapping this HBS site (Akap13-HBS, Supplementary Table S1) was synthesized and radiolabeled to then be evaluated using EMSA for HOXA9 binding and DB818 or DB1055 inhibitory effect. As evidenced in Figure 8B, HOXA9 interacts with this sequence and such HOXA9/DNA binding is inhibited by the addition of increasing concentrations of DB818 or DB1055. Such interaction and its inhibition are possible option to explain HOXA9-mediated control of Akap13 expression, assuming that HOXA9 binding is associated with an inhibition of Akap13 expression. DB818 and DB1055 would abolish such negative control of Akap13 expression by HOXA9, leading to an overexpression of Akap13 as evidenced by qRT-PCR (Figure 7D) for this gene which over-expression is associated with granulocyte and monocyte differentiation (Supplementary Figure S7).

As highlighted above using the global list of deregulated genes, IPA verified two main biological processes that were altered following DB818 treatment on MigA9 cells: cell differentiation (up-regulated) and cell proliferation (down-regulated). Based on this *in silico* transcriptomic analysis, cellular analyses were then performed to address the impact of DB818 and its derivatives on the cell proliferation and differentiation in MigA9 cells.

Inhibition of MigA9 cell proliferation

MTS measurements (Table 2) showed that most of the diamidines (except DB828 and DB2223) reduced the cell survival of the HoxA9-transformed cell line MigA9. Comprehensive changes in cell survival, determined by using MTS, may be due to multiple cellular processes such as cell

death, cell cycle arrest and cell differentiation processes among others. Consequently, we then further addressed the impact of diamidine compound treatment on each of those cellular processes to have a better insight into the mechanism of action of those molecules. First, we validated the induction of cell death by DB818, as highlighted in transcriptomic analysis, using both the quantification of the proportion of propidium iodide-positive cells (PI^+) and of subG1 population, two markers of cell death addressed from cell cycle analysis. The results in Table 2 show an increase in the PI-positive population for both 24 and 48 hours treatment and for the subG1 proportion at 48 hours treatment with DB818. These results suggest that DB818 induces apoptotic cell death, in agreement with transcriptomic analyses that highlighted expression of gene sets associated with a decrease of the quantity of blood cells upon treatment with DB818 (Figure 7). Using the same experimental approaches, we showed that DB1878, DB1879 and DB2529, as close derivatives of DB818, also strongly induce cell death (Table 2). Interestingly, the five ring containing compounds DB883 and DB884 were the most active in terms of cell death, suggesting that cell death is the main cellular process that is responsible for the decrease of cell survival by DB883 and DB884. By contrast, DB1055 does not induce cell death after 24 or 48 hours treatment to explain its effect on global cell survival. The impact of drug treatment on cell cycle resulted in a strong reduction in the proportion of MigA9 cells in S-phase upon treatment with DB818 and derivatives (DB1878/1879/2529), as well as with DB1055 and DB1620 (Table 3). This reduction of cycling cells is associated with a strong increase in the G0/G1 phase (DB1055, DB1878, DB2529), in the G2/M phase (DB818) or in both phases (DB1879, DB1620) at the tested concentrations and at 48H treatment.

Anti-clonogenic activities were then performed by using DB818, DB1055 and DB828 to address cell death and cell differentiation processes. This experiment first highlights the impact of both

DB818 and DB1055 on global clonogenic propensity of the HOXA9-positive MigA9 cell line, but not on the HOXA9-negative K562 cell line (Table 4 and Supplementary Figure S6C-D). Surprisingly, the intrinsic fluorescence of DB818 and DB828 were still visible even after 10 days of culture in Methocult using fluorescence microscopy with DAPI-filters, which indicates very high stability of the diamidine compounds within the cells (Supplementary Figure S6D). Results for clonogenic assays clearly show reduction in the number of colony sub-types obtained in the presence of DB818 or DB1055, but not DB828, for the untreated wells (CTR) (Table 4).

Induction of granulocyte/monocyte differentiation.

Finally, using the same anti-clonogenic experiment, we proved that the global decrease in the colony number is associated with a reduced proportion of CFU-GM (granulocyte and monocyte) in favor of an increase of CFU-M (monocyte only) and CFU-G (granulocyte only). These results suggest that both DB818 and DB1055 induced a decrease in the number of the most immature hematopoietic progenitors cells (CFU-GM) and favored the development of colonies that are more engaged in granulocytic or monocytic differentiation (CFU-G, CFU-M). This result is in agreement with gene expression analyses with DB818 (GSEA, IPA analyses), confirmed by qRT-PCR for both DB818 and DB1055 (but not for DB828) on Itgam (CD11b) as well as on CD14 expression as two markers of monocytic to macrophagic differentiation. Altogether these molecular and cellular experiments highlight the leukemic cell differentiation process associated with treatment with the HOXA9/DNA binding inhibitors DB818 and DB1055.

CONCLUSIONS

In the present work, we selected a series of heterocyclic diamidines and derivatives as sequence-selective DNA ligands that directly inhibit HOXA9/DNA binding (Figure 1, Figure 2A) through groove binding (Figure 2B) on the HOXA9 cognate DNA sequence (Figure 3). Particularly, we identified DB818, DB1055, DB884, DB1879 and DB2529 as strong inhibitors of HOXA9/DNA binding using both an ELISA-derived DNA binding inhibition assay (Figure 1A) and EMSA with more than 90% inhibition at 2.5 μM (Figure 1B-C). Those compounds also strongly stabilize the DNA helix based on DNA melting temperature results (Figure 2A). DB818, DB1055 and DB2529 were the most efficient compounds based on results obtained at the lower drug/DNA ratio (R=1:1). The recognition occurs at the HOXA9 cognate DNA sequence as demonstrated using DNase I footprinting experiments (Figure 3), through groove binding, as shown using circular dichroism (Figure 2B), pointing deeply in the minor groove and making close contacts with AT bases of the HBS sequence as evidenced using molecular modeling studies (Figure 5). DNase I footprinting experiments also evidenced that DB818 and DB1055 appeared to be very active and selective compounds on binding to the HOXA9-binding site (Figure 3) but not to the mutated HBS sequence (Supplementary Figure S2). Moreover, DB818 and DB1055 failed to inhibit DNA binding of the HMG-box protein used as a specificity control (Supplementary Figure S1B-C). We therefore selected DB818 and DB1055 as highly potent inhibitors that compete with HOXA9 for binding to its cognate sequence. DB818 and DB1055 were previously shown to interact with AT-rich DNA sequences[45] with binding K_D values of 9 nM and 17 nM respectively. Our K_D measurements obtained with the HBS-containing DNA sequence highlight stronger interaction with values of 4.6 and 5.5 nM, respectively (Figure 4). The binding of DB818 and DB1055 to HBS requires the presence of the 5'-ATTTA portion of HBS since mutation of the HBS site on this AT-rich site abolished binding

of DB818 and DB1055 to the DNA. More precisely, the interaction of DB818 or DB1055 in the minor groove of DNA (Figures 2 and 5) is an interesting point regarding the mode of DNA binding of the HOXA9 transcription factor that implies the correct orientation of three alpha-helices of HOXA9 homeodomain. The HOXA9 helix-3 binds in the major groove of the DNA helix, whereas the amino-terminal part of its homeodomain deeply bound in the minor groove of the AT-rich portion of the HOXA9-binding site.[42] This interaction with the minor groove is associated with direct contact of Arg-5 with $A_{2'}$ on the lower strand and T_3 on upper strand of the HOXA9/DNA binding site (upper strand/lower strand: $A_1T_2T_3T_4A_5$/5'-$T_{5'}A_{4'}A_{3'}A_{2'}T_{1'}$). Water-mediated additional contacts of Arg-5 with $A_{3'}$ of the lower strand, and water-mediated contacts of Arg-2 with both $A_{4'}$ and $T_{5'}$ on lower strand reinforce the DNA binding.[42] This AT-rich portion is the exact position where DB818 and DB1055 are lying in the minor groove, which allows them to block the correct positioning of HOXA9 homeodomain to its cognate site. HOXA9 binding to the DNA is associated with a DNA bending of ~20° resulting from minor groove compression in order to allow deep contacts of helix-3 to an enlarged major groove on the opposite side. Such DNA distortion towards the minor groove results from interaction of amino acids of the amino-terminal arm (Pro-7 and Tyr-8) with helix-1 of the homeodomain of HOXA9 (Thr-13). Binding of DB818 and DB1055 to the HOXA9 binding site may also not be compatible with minor groove compression by helix-3 binding in the major groove and may enhance HOXA9/DNA binding inhibition by DB818/1055. At the cellular level, both DB818 and DB1055 control HOXA9-directed transcription based on luciferase gene expression assays (Figure 6B) and induce, among other derivatives, cell death, cell cycle arrest and cell differentiation in a model of Hoxa9-transformed murine MigA9 leukemia cell line (Tables 2-4, Figure 7 and Supplementary Figure S6). Interestingly, DB828, used here as a control as an

unselective minor groove DNA binding drug that failed to interact with HOXA9 cognate sequence (Figure 3) and to inhibit HOXA9/DNA interaction in vitro (based on ELISA and EMSA experiments, Figure 1) and in vivo (based on luciferase assays, Figure 6B). DB828 also failed to alter cell survival (MTS, Table 2), to induce cell death (PI-positive or sub-G1 populations analysis, Table 2) and MigA9 cell differentiation (anti-clonogenic activities and CD11b/CD14 differentiation markers expression, Table 4 and Figure 7).

Up to now, no direct HOXA9/DNA binding inhibitors have been discovered. Only indirect inhibition strategies have been developed. The first approach is by targeting proteins of the MLL complex that controls HOXA9 gene expression. This is the case with inhibitors of DOT1L such as EPZ-5676 (pinometostat, currently in a phase I clinical trial) that reduce HOXA9 gene expression and induce cell differentiation[58,59] or of inhibitors of the menin/MLL interaction[60,61]. The second approach is the targeting of the HOX/PBX interface of multiple HOX proteins with their co-factors of the PBX family by the HXR9 peptidomimetic developed against a variety of solid tumors and hematopoietic malignancies.[62]

Some other heterocyclic diamidines were previously identified as transcription factors inhibitors, DB293 against Pit-1 and Brn-3,[43] DB1255 against ERG[44,45] and DB2113 against PU.1[22,63] but none were previously evaluated against the HOXA9 transcription factor.

Identification of DB818 and DB1055 as HOXA9/DNA binding competitors and inducers of granulocyte/monocyte differentiation offers an exciting new opportunity to target the HOXA9 transcription factor. HOXA9 is one of the master regulators of the differentiation blockade in acute myeloid leukemia[28,29,32,36], being at the crossroads of many cell signaling perturbations resulting from well-characterized mutations or translocations defining AML subgroups such as

for instance MLL translocations, MYST3-CREBBP or NUP98-NSD1 fusion proteins and NPM1 or EZH2 mutations.[30,31] Therefore, treatment of such AML subtypes with DB818/DB1055 needs to be further evaluated in the future to offer new potential differentiation therapies. HOXA9 is also associated with different solid tumor models such as glioblastoma, gastric and prostate cancers[23–26] against which DB818, DB1055 and/or derivatives might also be evaluated to propose future therapeutic strategies. This DNA targeting approach to inhibit HOXA9/DNA binding and function is a very promising strategy with the potential to develop new anti-cancer treatments and particularly new differentiation therapies in leukemia.

Experimental Section

1. Chemistry

References for previously reported diamidines are provided in the Supplementary Information. The synthesis of the previously unreported diamidines follows below and in the Result and Discussion section. Representatives ^{1}HNMR spectra for the diamidines are provided in the Supplementary Information. The purity (≥95%) of all compounds evaluated in this study was established by elemental analysis and ^{1}H high resolution NMR spectroscopy. Elemental Analysis was performed by Atlantic Microlab Inc., Norcross, GA.

General procedure for the synthesis of compounds 1a-c

To a stirred solution of the bromo compounds[64] (10 mmol), 5-(dimethoxymethyl)furan-2-yl-tri-n-butylstannane[65] (10 mmol) in 30 mL anhydrous 1,4-dioxane was added tetrakis-triphenylphosphine palladium (300 mg). The stirred mixture was warmed to 90–100 ^{o}C for 16 h.

The solvent was removed under reduced pressure; the residue was extracted using 200 mL of dichloromethane from aqueous solution containing 3 mL of concentrated ammonia, then washed with water, and passed through celite. The organic layer was evaporated and the oily residue was mixed with 15 mL 2.0M HCl, and stirred for 2 h, the separated precipitate was filtered off and washed with ethanol. The product was crystallized from ethanol.

3-Benzyloxy-4-(5-formylfuran-2-yl)-benzonitrile (1a).73% yield, mp 164-165 ^{o}C. ^{1}H NMR (DMSO-d_6); δ 5.38 (s, 2H), 7.16 (d, J = 3.6 Hz, 1H), 7.40-7.46 (m, 3H), 7.51-7.56 (m, 3H), 7.61 (d, J = 3.6 Hz, 1H), 7.80 (s, 1H), 8.00 (d, J = 8.1 Hz, 1H), 9.63 (s, 1H). MS (m/z, rel.int.); 303 (M^+, 40), 275 (25), 198 (10), 91 (100).

6-(5-Formylfuran-2-yl)nicotinonitrile (1b). Yield 60%, mp 204-205^{o}C (EtOH). ^{1}H NMR (DMSO-d_6); δ 7.56 (d, J = 3.6 Hz, 1H), 7.71 (d, J = 3.6 Hz, 1H), 8.07 (d, J = 8.4 Hz, 1H), 8.44 (dd, J = 8.4, 2.1 Hz, 1H), 9.09 (d, J = 2.1 Hz, 1H), 9.72 (s, 1H). MS (m/z, rel.int.); 199 (M^+ +1, 100).

5-(5-Formylfuran-2-yl)picolinonitrile (1c). Yield 62%, mp 191-192 ^{o}C (EtOH). ^{1}H NMR (DMSO-d_6); δ 7.66 (d, J = 3.6 Hz, 1H), 7.74 (d, J = 3.6 Hz, 1H), 8.17 (d, J = 8.1 Hz, 1H), 8.46 (dd, J = 8.1, 2.1 Hz, 1H), 9.25 (d, J = 2.1 Hz, 1H), 9.71 (s, 1H). MS (m/z, rel.int.); 198 (M^+, 100), 197 (70), 141 (30).

2-{5-[(2-Benzyloxy)-4-cyanophenyl]-furan-2-yl}-1*H*-benzimidazole-6-carbonitrile(2a).

Prepared adopting reported methodology.[66] Yield 81%, mp 247-248.5 ^{o}C (DMF). ^{1}H NMR (DMSO-d_6); δ 5.39 (s, 2H), 7.18 (d, J = 3.6 Hz, 1H), 7.40-7.49 (m, 4H), 7.55-7.67 (m, 4H), 7.74-

7.79 (m, 2H), 8.14 (s, 1H), 8.30 (d, J = 8.0 Hz, 1H), 13.0 (s, 1H). MS (m/z, rel.int.); 417 (M^++1, 100), 397 (10), 323 (60).

2-[5-(5-Cyanopyridin-2-yl)furan-2-yl]-1*H*-benzimidazole-6-carbonitrile(2b).Prepared adopting reported methodology.[66] Yield 74%, mp > 300 °C (DMF). ^{1}H NMR (DMSO-d_6); δ 7.51 (d, J = 3.6 Hz, 1H), 7.56 (d, J = 3.6 Hz, 1H), 7.64 (d, J = 8.1 Hz, 1H), 7.78 (d, J = 8.1 Hz, 1H), 8.16 (d, J = 8.1 Hz, 2H), 8.49 (dd, J = 8.1, 2.1 Hz, 1H), 9.06 (d, J = 2.1 Hz, 1H), 13.70 (s, 1H). MS (m/z, rel.int.); 312 (M^+ +1, 100).

2-[5-(6-Cyanopyridin-3-yl)furan-2-yl]-1*H*-benzimidazole-6-carbonitrile(2c).Prepared adopting reported methodology.[66] Yield 75%, mp 279-281 °C (DMF). ^{1}H NMR(DMSO-d_6); δ 7.50 (d, J = 3.6 Hz, 1H), 7.64 (d, J = 3.6 Hz, 1H), 7.65-7.80 (m, 2H), 8.10-8.21 (m, 2H), 8.50 (dd, J = 8.1, 1.8 Hz, 1H), 9.32 (d, J = 1.8 Hz, 1H), 13.72 (s, 1H). MS (m/z, rel.int.); 312 (M^+ +1, 100).

***N*-Hydroxy-2-{5-[(2-benzyloxy)-4-(*N*-hydroxyamidino)phenyl]-furan-2-yl}-1*H*-benzimidazole-6-amidine (3a)**. Prepared adopting reported methodology.[67] Yield 94%, mp 253-255 °C. ^{1}H NMR (DMSO-d_6); δ 5.35 (s, 2H), 5.86 (s, 2H), 5.97 (s, 2H), 7.05 (d, J = 3.6 Hz, 1H), 7.29 (d, J = 3.6 Hz, 1H), 7.40-7.81 (m, 10H), 8.16 (d, J = 8.1 Hz, 1H), 9.61 (s, 1H), 9.80 (s, 1H), 13.11 (s, 1H). MS (m/z, rel.int.); 483 (M^++1, 10), 465 (5), 432 (5), 392 (55), 375 (100).

***N*-Hydroxy-2-{5-[5-(*N*-hydroxyamidino)pyridin-2-yl]furan-2-yl}-1*H*-benzimidazole-6-amidine (3b)**. Prepared adopting reported methodology.[66] Yield 91%, mp > 300 °C. ^{1}H NMR (DMSO-d_6); δ 5.89 (s, 2H), 6.08 (s, 2H), 7.38 (d, J = 3.6 Hz, 1H), 7.40 (d, J = 3.6 Hz, 1H), 7.53-7.66 (m, 2H), 7.99-8.06 (m, 2H), 8.22 (dd, J = 8.4, 2.4 Hz, 1H), 8.95 (d, J = 2.4 Hz, 1H), 9.64 (s,

1H), 9.97 (s, 1H), 13.22 (s, 1H). MS (m/z, rel.int.); 378 (M^++1, 80), 286 (10), 256 (18), 240 (100).

***N*-Hydroxy-2-{5-[6-(*N*-hydroxyamidino)pyridin-3-yl]furan-2-yl]-1*H*-benzimidazole-6-amidine (3c)**. Prepared adopting reported methodology.[66] Yield 90%, mp 285-287 ^oC. ^1H NMR (DMSO-d_6); δ 5.88 (s, 2H), 5.92 (s, 2H), 7.38 (d, J = 3.6 Hz, 1H), 7.41 (d, J = 3.6 Hz, 1H), 7.55-7.63 (m, 2H), 7.83-7.99 (m, 2H), 8.29 (dd, J = 8.4, 2.1 Hz, 1H), 9.16 (d, J = 2.1 Hz, 1H), 9.63 (s, 1H), 10.05 (s, 1H), 13.17 (s, 1H). MS (m/z, rel.int.); 378 (M^++1, 40), 362 (8), 101 (100).

2-[5-(4-Amidino-2-hydroxyphenyl)furan-2-yl]-1*H*-benzimidazole-6-amidine acetate (4a, DB928). Prepared adopting reported methodology.[66] Yield 78%, mp 277-279 ^oC. ^1H NMR (D_2O/DMSO-d_6); δ 1.78 (s, 3 x CH_3), 7.18-7.43 (m, 4H), 7.52-7.75 (m, 2H), 8.04 (s, 2H). ESI-HRMS: m/z calculated for $C_{19}H_{17}N_6O_2$: 361.1413, found: 361.1410 (M^+ + 1). Anal. Calcd. For $C_{19}H_{16}N_6O_2$-3.0AcOH-1.9H_2O: C, 52.24, H, 5.57, N, 14.63. Found: C, 52.04, H, 5.29, N, 14.77.

2-[5-(5-Amidinopyridin-2-yl)furan-2-yl]-1*H*-benzimidazole-6-amidine acetate (4b, DB915). Prepared adopting reported methodology.[66] Yield 84%, mp 221-223 ^oC. ^1H NMR (D_2O/DMSO-d_6); δ 1.79 (s, 2.3 x CH_3), 7.33 (s, 1H), 7.43 (s, 1H), 7.50-7.70 (m, 2H), 8.00-8.10 (m, 2H), 8.29 (s, 1H), 8.97 (s, 1H). ESI-HRMS: m/z calculated for $C_{18}H_{16}N_7O$: 346.1416, found: 346.1425 (M^+ + 1). Anal. Calcd. For $C_{18}H_{15}N_7O$-2.3AcOH-3.1H_2O: C, 50.32, H, 5.68, N, 18.17. Found: C, 50.02, H, 5.74, N, 18.36.

2-[5-(6-Amidinopyridin-3-yl)furan-2-yl]-1*H*-benzimidazole-6-amidine acetate (4c, DB995). Prepared adopting reported methodology.[66] Yield 70%, mp 222-224 ^oC. ^1H NMR (D_2O/DMSO-d_6); δ 1.87 (s, 3 x CH_3), 7.38 (s, 1H), 7.50-7.69 (m, 3H), 8.08 (s, 1H), 8.30-8.45 (m, 2H), 9.23 (s,

1H). ESI-HRMS: m/z calculated for $C_{18}H_{16}N_7O$: 346.1416, found: 346.1426 (M^+ + 1). Anal. Calcd. For $C_{18}H_{15}N_7O$-3.0AcOH-2.0H_2O-0.25EtOH: C, 51.34, H, 5.70, N, 17.10. Found: C, 51.53, H, 5.54, N, 16.70.

4-(2-Formylthiazol-5-yl)benzonitrile (5) Na_2CO_3 (20 mmol) in water (5 ml) and 4-cyanophenylboronic acid (11 mmol) methanol (10 ml) were added to a stirred solution of 5-bromothiazole-2-carbaldehyde (10 mmol) in dioxane (30 mL) and the mixture was deaerated under nitrogen for 20 min. Tetrakistriphenylphosphine palladium (0.46 g, 0.4 mmol) was added and the reaction mixture was vigorously stirred at 100 °C for 24 h. The solvent was evaporated under reduced pressure, the solid was partitioned between ethyl acetate (200 mL) and 2 M aqueous Na_2CO_3 (25 mL) containing 5 mL of concentrated ammonia, to remove palladium residues, then washed with water, passed through Celite to remove the catalyst, dried (sodium sulfate) and evaporated. The product was purified using column chromatography on silica gel with hexanes/ethyl acetate as an eluent. Brown solid (1.09 g, 51 %), mp 155-156 ^oC. ^{1}HNMR (DMSO-d_6): δ 10.02 (s, 1 H), 8.93 (s, 1H), 8.23 (d, *J* = 7.8 Hz, 2H), 7.98 (d, *J* = 7.8 Hz, 2H); ESI-HRMS: m/z calculated for $C_{11}H_7N_2OS$: 215.0274, found: 215.0272 (M^+ + 1).

2-(5-(4-Cyanophenyl)thiazol-2-yl)-1*H*-benzo[d]imidazole-5-carbonitrile(6). Sodium metabisulphite (6 mmol) was added to a solution of 3,4-diaminobenzonitrile (3 mmol) and 4-(2-formylthiazol-5-yl)benzonitrile (3 mmol) in DMSO (10 mL) and the mixture was heated at 140 ^oC for 30 min. The reaction mixture was poured into water, filtered and dried. Purification was by crystallization from acetone. Yellow solid (0.52 g, 54 %), mp > 300 ^oC. ^{1}HNMR (DMSO-d_6): δ 8.66 (br s, 1 H), 8.29 (m, 3H), 8.00 (d, *J* = 6.4 Hz, 2H), 7.69 (m, 2H); ESI-HRMS: m/z calculated for $C_{18}H_{10}N_5S$: 328.0651, found: 328.0641 (M^+ + 1).

2-(5-(4-Carbamimidoylphenyl)thiazol-2-yl)-1H-benzo[d]imidazole-6-carboximidamide trihydrochloride (7, DB 2651). The bis-nitrile (1 mmol) was suspended in dry ethanol (20 ml) and cooled in ice bath, HCl gas was bubbled through the reaction mixture for 30 min and the reaction flask was tightly sealed and stirred at room temperature for 14 days. The yellow precipitate of imidate ester hydrochloride was filtered and washed with dry ethanol and anhydrous ether and dried under vacuum at room temperature for 3 h. The imidate ester was suspended in dry ethanol and cooled in ice bath, ammonia gas was bubbled through the solution for 30 min and the reaction flask was tightly sealed and stirred at room temperature for 2 days. The formed yellow precipitate was filtered and washed with dry ethanol , acetone and dried under vacuum at 100 ^{o}C for 12 h. Yellow solid (0.18 g, 37 %), mp > 300 ^{o}C. ^{1}HNMR (DMSO-d_6): δ 9.58 (s, 2 H), 9.48 (s, 2 H), 9.33 (s, 2 H), 9.24 (s, 2 H), 8.73 (br s, 1H), 8.37 (d, *J* = 8 Hz, 2H), 8.24 (br s, 1H), 8.06 (d, *J* = 7.6 Hz, 2H), 7.85 (d, *J* = 8.4 Hz, 1H), 7.76 (d, *J* = 8.4 Hz, 1H); ESI-HRMS: m/z calculated for $C_{18}H_{16}N_7S$: 362.1182, found: 362.1177 (Amidine base M^+ + 1). Anal. Calcd. For $C_{18}H_{15}N_7S$. 3HCl. $2H_2O$. $0.1C_3H_6O$: C, 42.87; H, 4.44; N, 19.12. Found: C, 43.07; H, 4.26; N, 18.82.

Synthesis of 2-(4-Cyanoaryl)furans and thiophenes (8 a-e).

Tetrakistriphenylphosphine palladium (0.576 g, 0.5mmol) was added to a stirred mixture of the 2(tributylstannyl) furan or thiophene, (10 mmol) and the bromoarylbenzonitriles (10 mmol) in deaerated dioxane (25 mL) under nitrogen. The reaction flask was heated at 100 °C for 12 h. The solvent was concentrated under reduced pressure, the resulting paste was stirred with ether and filtered. The solid obtained was purified by column chromatography on silica gel, using hexanes/ethyl acetate as eluent.

The following compounds were previously reported 4-(furan-2-yl)benzonitrile **8a**[68], 6-(furan-2-yl)nicotinonitrile **8b**[69], 4-(thiophen-2-yl)benzonitrile **8c**[68], 6-(thiophen-2-yl)nicotinonitrile **8d**[69].

2-(2-Methoxy-4-cyanophenyl) furan (8e). White solid, yield (1.61 g, 81 %). mp 54-54.5 ^{o}C ; 1HNMR ($CDCl_3$) δ 7.95(dd, 1H, J=8Hz, 2Hz), 7.54(brs, 1H), 7.46(d, 1H, J=8Hz), 7.19(brs, 1H), 7.13(brs, 1H), 6.56 (dd, 1H, J=3.2Hz, 2Hz), 4(s, 3H); ^{13}CNMR ($CDCl_3$) δ 149.2, 143.1, 137, 134.6, 130.8, 130.1, 129.6, 127.7, 118.6, 113.6, 111.2, 53.2; ESI-MS: m/z calculated for $C_{12}H_9NO_2$: 199.2, found: 201.1 (M^++2); Anal. Calcd. For $C_{12}H_9NO_2$: C, 72.35; H, 4.55; N, 7.03. Found: C, 72.41; H, 4.71; N, 6.97.

Synthesis of 2-Bromo-5-(4-cyanoaryl)furans and thiophenes (9a-e). *N*-Bromosuccinimide (2.13 g, 12 mmol) was added portionwise to a stirred solution of the nitriles **8a-e** (10 mmol) in dimethylformamide (20 ml) in an ice bath. The reaction mixture was stirred overnight at room temperature then poured onto ice water, the obtained precipitate was collected and dried. Purification by column chromatography on silica gel, using hexanes/ethyl acetate as eluent.

The following compounds were previously reported 4-(5-bromofuran-2-yl)benzonitrile **9a**[68], 6-(5-bromofuran-2-yl)nicotinonitrile **9b**[69], 4-(5-bromothiophen-2-yl)benzonitrile **9c**[68], 6-(5-bromothiophen-2-yl)nicotinonitrile **9d**[69].

2-Bromo-5-(2-methoxy-4-cyanophenyl) furan (9e). Yellow solid, yield (2.41 g, 87 %). mp 71-71.5 ^{o}C ; 1HNMR ($CDCl_3$) δ 7.89(brs, 1H), 7.33-7.19(m, 3H), 6.47(brs, 1H), 3.99(s, 3H); ^{13}CNMR ($CDCl_3$) δ 155.1, 150.9, 126, 125.3, 122.7, 119.1, 116, 115.8, 115.7, 114.9, 111, 56.8; ESI-MS: m/z calculated for $C_{12}H_8BrNO_2$: 278.1, found: 279.2 (M^++1); Anal. Calcd. For $C_{12}H_8BrNO_2$: C, 51.83; H, 2.90; N, 5.04. Found: C, 51.59; H, 2.76; N, 5.14.

General procedure for the synthesis of the dinitriles (10a-e).

A mixture of the heteroaryl bromides **9a-e** (0.01 mole) and tert-butyl 5 or 6-cyano-2-(trimethylstannyl)-1H-indole-1-carboxylate[20,28] 4.06 g (0.01 mole) in 75 ml anhydrous dioxane with $Pd(PPh_3)_4$ 0.23 g (0.0002 mole) and the solution (under nitrogen) was heated under reflux for 12-24 h (tlc monitored). The solvent was removed under reduced pressure and the resultant solid filtered, washed with hexane and dried in air. The solid was often a mixture of *N*-Boc and non-Boced indoles. The solid was suspended in DCM (100 ml), di-*t*-butyl dicarbonate 2.18 g (0.01 mole) and 10 mg DMAP were stirred for 12 h at rt, diluted with 50 ml water, organic layer separated, dried over $MgSO_4$, filtered, concentrated and triturated with hexane and the yellow solid filtered, yields 61-82%.

***t*-Butyl 5-cyano-2-(5-(4-cyanophenyl) furan-2-yl)-1H-indole-1-carboxylate (10a).** Yield of 3.27 g (80%), mp >300°C dec; ^{1}H NMR ($CDCl_3$): 8.33 (d, 1H, J= 8.4 Hz), 7.94 (d, 1H, J= 1.6 hz), 7.80 (d, 2H, J= 8.0 Hz), 7.70 (d, 2H, J= 8.0 Hz), 7.63 (dd, 1H, J= 1.6 Hz, J= 8.4 Hz), 6.96 (d, 1H, J= 3.6 Hz), 6.90 (s, 1H), 6.78 (d, 1H, J= 3.6 Hz), 1.47 (s, 9H); ^{13}C NMR ($CDCl_3$): 152.4, 149.2, 147.3, 139.3, 134.2, 132.9, 131.4, 128.7, 128.3, 125.9, 124.0, 119.7, 118.9, 116.4, 113.0, 111.2, 110.9, 109.7, 106.8, 85.3, 27.9; HRMS-ESI-POS.: calc. for $C_{25}H_{19}N_3O_3Na$ *m/z* 432.1324 (M^++ 1), found *m/z* 432.1340.

***t*-Butyl-5-cyano-2-(5-(5-cyanopyridin-2-yl)furan-2-yl)-1H-indole-1-carboxylate (10b).** Yield of yellow solid 2.9 g (72%), mp >300°C dec; ^{1}H NMR ($CDCl_3$): 8.60 (d, 1H, J= 1.2 Hz), 8.32 (d, 1H, J= 8.4 Hz), 7.99 (dd, 1H, J= 2.4 Hz, J= 8.4 Hz), 7.94 (brs, 1H), 7.79 (d, 1H, J= 8.4 Hz), 7.63 (dd, 1H, J=1.2 Hz, J= 8.4 Hz), 7.37 (d, 1H, 3.6 Hz), 6.94 (bs, 1H), 6.84 (d, 1H, J= 3.6 Hz), 1.47 (s, 9H); ^{13}C NMR ($CDCl_3$): 152.9, 152.5, 151.4, 149.1, 148.7, 140.1, 139.3, 131.1, 128.6, 128.5,

126.0, 119.6, 117.9, 117.0, 116.5, 113.9, 113.5, 111.8, 107.5, 106.9, 85.5, 27.9; MS: HRMS-ESI-POS.: calc. for $C_{24}H_{18}N_4O_3Na$ *m/z* 433.1277 (M^++Na), found *m/z* 433.1311.

***t*-Butyl 6-cyano-2-(5-(4-cyanophenyl) thiophen-2-yl)-1H-indole-1-carboxylate (10c).** Yield of yellow solid 3.37 g (74%), mp >300°C dec; ^{1}H NMR ($CDCl_3$): 8.55 (d, 1H, J = 1.2 Hz), 7.74-7.68 (m, 5H), 7.64 (d, 1H, J = 8.0 Hz), 7.53 (d, 1H, J = 1.2 Hz, J = 8.0 Hz), 7.44 (d, 1H, J = 3.6 Hz), 7.21 (d, 1H, J = 3.6 Hz), 1.51 (s, 9H); ^{13}C NMR ($CDCl_3$): 149.2, 142.3, 138.1, 136.5, 135.7, 135.6, 132.9, 132.0, 129.8, 126.4, 126.0, 124.9, 121.5, 120.2, 120.0, 118.8, 112.0, 111.1, 107.7, 85.6, 27.8; MS: HRMS-ESI-POS.: calc. for $C_{25}H_{19}N_3O_2SNa$ *m/z* 448.1096 (M^++1), found *m/z* 448.1081.

***t*-Butyl-6-cyano-2-(5-(5-cyanopyridin-2-yl)thiophen-2-yl)-1H-indole-1-carboxylate(10d).** Yield 3.35 g (81%), mp >280°C dec; ^{1}H NMR ($CDCl_3$): 8.82 (d, 1H, J =1.6 Hz), 8.54 (s, 1H), 7.97 (dd, 1H, J = 2.4 Hz, J = 8.4 Hz), 7.77 (dd, 1H, J = 0.8 Hz, J= 8.4 Hz), 7.69 (d, J =4.0 Hz), 7.65 (d, 1H, J = 8.0 Hz), 7.52 (dd, 1H, J =1.6 Hz, J = 8.4 Hz), 7.26 (d, 1H, J = 4.0 Hz), 6.83 (s, 1H), 1.51 (s, 9H); ^{13}C NMR ($CDCl_3$): 155.1, 152.7, 149.2, 143.9, 139.9, 138.9, 136.7, 135.8, 132.0, 129.8, 126.8, 126.4, 121.7, 120.3, 120.1, 118.2, 117.0, 112.1, 107.9, 107.5, 85.7, 27.9; MS: HRMS-ESI-POS.: calc. for $C_{24}H_{18}N_4O_2SNa$ *m/z* 449.1045 (M^++Na), found *m/z* 449.1057.

***t*-Butyl6-cyano-2-(5-(4-cyano-2-methoxyphenyl)furan-2-yl)-1H-indole-1-carboxylate(10e).** Yield of yellow solid, yield 1.33 g (61 %). mp >300 ^{o}C; ^{1}HNMR (DMSO-d_6) δ 8.44 (s, 1H), 7.97(d, 1H, J=8Hz), 7.89(d, 1H, J=8Hz), 7.71(d, 1H, J=8Hz), 7.65(brs, 1H), 7.53(d, 1H, J=8Hz), 7.31-7.30(m, 1H), 7.24(s, 1H), 7.06-7.05(m, 1H), 4.04(s, 3H), 1.36 (s, 9H); ESI-MS: m/z calculated for $C_{26}H_{21}N_3O_4$: 439.46, found: 440.4 (M^++1); Anal. Calcd. For $C_{26}H_{21}N_3O_4$: C, 71.06; H, 4.82; N, 9.56. Found: C, 71.22; H, 4.83; N, 9.49.

General procedure for the synthesis of the Heteroaryl Diamidines hydrochloride (11a-e).

To a cold and stirred suspension of the dinitriles (0.001 mol) in 15 ml dry THF was added 6.0 ml, (0.006 mol) $LiN(TMS)_2$ (1M in THF), stirred for 24 h, cooled, acidified carefully with sat. ethanolic-HCl, the precipitated white solid was stirred for 2 h, solvent was removed under reduced pressure ether was added and the solid was filtered. The dark solid was collected and 10 ml ice water was added, basified with 2M NaOH to pH of ca. 10, the precipitate was filtered, washed with water and air dried. The solid was suspended in dry ethanol (15 ml) and 5 ml satd. ethanolic HCl and stirred for 6 h, the ethanol was distilled off and the resultant solid was triturated with dry ether and filtered. The solid was dried under reduced pressure at 80^0C for 12 h to yield (33-75%) diamidine hydrochlorides.

2-(5-(4-Carbamimidoylphenyl) furan-2-yl)-1H-indole-5-carboximidamide dihydrochloride (11a, DB1478). A yellow brown solid, mp >300°C; yield 2.5 g (80%), mp >300°C dec; ^{1}H NMR (DMSO-d_6): 12.59 (s, 1H), 9.50 (brs, 2H), 9.29 (brs, 2H), 9.26 (brs, 2H), 9.04 (brs, 2H), 8.12 (s, 1H), 8.13 (d, 2H, J= 8.4 Hz), 8.0 (d, 2H, J= 8.4 Hz), 7.63 (brs, 2H), 7.46 (d, 1H, J= 3.6 Hz), 7.28 (d, 1H, J= 3.6 Hz), 7.13 (d, 1H, J= 1.6 Hz); ^{13}C NMR (DMSO-d_6): 166.4, 164.8, 151.3, 147.7, 139.7, 134.4, 131.0, 129.0, 127.8, 125.0, 123.9, 123.6, 121.5, 118.9, 111.7, 111.4, 110.1, 99.6; MS: HRMS-ESI-POS: calc. for $C_{20}H_{18}N_5O$ *m/z* 344.1511 (M^++ 1), found *m/z* 344.1513; Anal. calc. for $C_{20}H_{17}N_5O.2HCl.1.25H_20$: C, 54.74; H, 4.93; N, 15.96; Found: C, 54.67; H, 5.03; N, 15.79.

2-(5-(5-Carbamimidoylpyridin-2-yl)furan-2-yl)-1H-indole-5-carboximidamide trihydrochloride (11b, DB1481). A red brown solid, 0.35 g (72%); mp >300°C dec; ^{1}H NMR(DMSO-d_6): 12.70 (s, 1H), 9.70 (br, 2H), 9.39 (brs, 2H), 9.31 (brs, 2H), 9.06 s, 2H), 9.05

(d, 1H, J=2.4 Hz), 8.41 (dd, 1H, J= 2.4 Hz, J= 8.4 Hz), 8.22 (d, 1H, J= 8.4 Hz), 8.20 (s, 1H), 7.54-7.52 (brs, 2H), 7.53 (d, 1H, J=3.6 Hz), 7.33 (d, 1H, J= 3.6 Hz), 7.18 (d, 1H, J= 2.0 Hz); ^{13}C NMR (DMSO-d_6): 166.4, 163.6, 151.6 (signal is big accounts 2 carbons), 149.3, 149.1, 139.9, 137.5, 130.8, 127.8, 122.1, 121.83, 121.77, 119.2, 118.0, 114.5, 112.0, 110.4, 100.5; Anal. calc. for $C_{19}H_{16}N_6O.3HCl.1.75H_20$: C, 47.02; H, 4.67; N, 13.31; Found: C, 47.83; H, 4.73; N, 13.49.

2-(5-(4-Carbamimidoylphenyl)thiophen-2-yl)-1H-indole-6-carboximidamide diydrochloride (11c, DB1879). A brown solid, yield 0.32 g (70%), mp >300°C dec; ^{1}H NMR (DMSO-d_6): 12.72 (d, 1H, J= 1.2 Hz), 9.57 (brs, 2H), 9.39 (brs, 2H), 9.33 (brs 2H), 9.13 (brs, 2H), 7.98-7.95 (m, 3H), 7.93(d, 2H, J= 7.6 Hz), 7.87 (d, 1H, J=3.6 Hz), 7.84 (d, 1H, J= 3.6 Hz),7.72 (d, 1H, J= 8.4 Hz), 7.48 (dd, 1H, J= 1.6 Hz, J= 8.4 Hz), 6.88 (brs, 1H); ^{13}C NMR (DMSO-d_6): 166.5, 164.9, 141.2, 138.2, 136.1, 135.9, 135.6, 132.5, 129.2, 127.3, 127.0, 126.5, 125.3, 120.6, 120.3, 119.1, 112.0, 100.0; MS: HRMS-ESI-POS: calc. for $C_{20}H_{18}N_5S$ *m/z* 360.1283 (M^++1), found *m/z* 360.1271; Anal. calc. for $C_{20}H_{17}N_5S.2HCl.1.25H_2O$: C, 45.51; H, 4.48; N, 13.26; Found: C, 45.63; H, 4.62; N, 13.56.

2-(5-(5-Carbamimidoylpyridin-2-yl)thiophen-2-yl)-1H-indole-6-carboximidamide trihydrochloride (11d, DB2529). A reddish brown solid, yield 0.35 g (74%), mp >280°C dec; ^{1}H NMR (DMSO-d_6): 12.73 (d, 1H, J=1.2 Hz), 9.74 (s, 2H), 9.44 (s, 2H), 9.39 (s, 2H), 9.14 (s, 2H), 9.02 (s, 1H), 8.34 (dd, 1H, J = 1.6 Hz, J = 8.4 Hz), 8.22 (d, 1H, J = 8.4 Hz), 8.10 (d, 1H, J = 3.6 Hz), 7.98 (brs, 1H), 7.73 (d, 1H, J = 3.6 Hz), 7.47 (dd, 1H, J= 1.6 Hz, J = 8.4 Hz), 6.99 (d, 1H, J=1.6 Hz); ^{13}C NMR (DMSO-d_6): 166.48, 163.5, 155.3, 149.2, 142.6, 138.3, 137.2, 136.2, 136.0, 132.5, 129.0, 126.9, 122.1, 120.8, 120.4, 119.1, 118.1, 112.1, 100.4; MS: HRMS-ESI-POS: calc. for $C_{19}H_{17}N_6S$ *m/z* 361.1235 (M^++1), found *m/z* 361.0285; Anal. calc. for $C_{19}H_{16}N_6S.3HCl$: C, 48.71; H, 4.09; N, 17.95; Found: C, 48.86; H, 4.12; N, 17.84

2-(5-(4-Carbamimidoyl-2-methoxyphenyl)furan-2-yl)-1H-indole-6-carboximidamide(11e, DB2005). Yellow solid, yield (0.184 g, 33%), mp >300 ^{o}C; ^{1}HNMR (DMSO-d_6) δ 12.7 (s, 1H), 9.61 (s, 2H), 9.51 (s, 2H), 9.47(s, 2H), 9.36(s, 2H), 8.42(d, 1H, J=8Hz), 8.02(s, 1H), 7.76(d, 1H, J=8Hz), 7.69-7.65(m, 2H), 7.49(d, 1H, J=8Hz), 7.34-7.32(m, 2H), 7.1(s, 1H), 4.09(s, 3H); ^{13}CNMR (DMSO-d_6) δ 166.9, 165.1, 155.2, 148.8, 147.1, 136.3, 133.1, 132.8, 127.4, 126.3, 125.9, 123.3, 121.0, 120.9, 119.5, 115.8, 112.5, 112.0, 111.2, 99.7, 56.7; ESI-MS: m/z calculated for $C_{21}H_{19}N_5O_2$: 373.41, found: 374.40 (amidine base M^{+}+1); Anal. Calcd. For $C_{21}H_{19}N_5O_2$. 2HCl. 1.75H_2O. 0.15EtOH: C, 52.77; H, 5.28; N, 14.44. Found: C, 52.42; H, 5.34; N, 14.39.

4, 4'-(Furan-2,5-diyl) bis (N-(4-nitrophenethyl) benzimidamide) dihydrochloride (12a, DB421). 4-(Nitrophenyl) ethylamine free base [prepared from HCl salt 0.405 g (0.002) mole and freshly prepared NaOMe)] in 10 ml dry ethanol was added to a suspension of imidate ester dihydrochloride prepared from 2,5 bis(4-cyanophenyl) furan[70] 0.435 g (0.001 mole in 35 ml dry ethanol, the reaction mixture was stirred at rt 12 h (TLC monitored). The solvent was removed in vac. Diluted with 20 ml ice water, basified to pH 10 with 2M NaOH (aq), the yellow solid was filtered, washed with water, dried under reduced pressure at rt. The free base was converted to it's dihydrochloride by treating with sat. ethanolic HCl, yellow solid, yield 0.52 g (77%), mp >310°C dec; ^{1}H NMR (DMSO-d_6): 10.15 (brs, 2H), 9.69 (brs, 2H), 9.44 (brs, 2H), 8.22 (d, 4H, J = 7.6 Hz), 8.09 (d, 4H, J =7.6 Hz), 7.85 (d, 4H, J =7.6 Hz), 7.69 (d, 4H, J = 7.6 Hz), 7.41 (s, 2H), 3.81 (t, 4H, J = 6.8 Hz), 3.18 (t, 4H, J =6.8 Hz); ^{13}C NMR (DMSO-d_6): 162.2, 152.4, 146.7, 146.4, 133.9, 130.4, 129.0, 127.4, 123.7, 123.5, 11.5, 43.2, 33.1; MS: HRMS-ESI-POS.: calc. for $C_{34}H_{31}N_6O5$ *m/z* 603.2356 (M^{+}+1), found *m/z* 603.2291; Anal. calc. for $C_{34}H_{30}N_6O_5$.2HCl: C, 60.45; H, 4.77; N, 12.44; Found: C, 60.33; H, 4.82; N, 12.56

2,5-Bis(4-amidinophenyl)tellurophene dihydrochloride (12b, DB1751). In a 50 mL flame-dried round bottom flask, 2,5-bis(4-cyanophenyl)tellurophene[71] (0.191 g, 0.5 mmol) was dissolved in dry tetrahydrofuran (10 mL, freshly distilled from Na). Lithium hexamethyldisilazane (LiHMDS, 1.0 M in THF, 2.5 mL) was added slowly by syringe, and the darkened mixture was stirred overnight under nitrogen. The solution was then treated with HCl-saturated EtOH (3 mL) to yield a yellow precipitate. After stirring the suspension for another 6 hrs, it was diluted with ether (~25 mL) and vacuum filtered to yield an orange solid. The solid was then triturated in water (~10 mL) to dissolve any ammonium chloride, then refiltered and dried overnight in vacuo under low heat to yield the title compound as a reddish solid (0.164 g, 63%). ^{1}H-NMR (DMSO-d_6): 7.85 (s, 8H), 8.34 (s, 2H), 9.10 (br s, 1H). ^{13}C-NMR (DMSO-d_6): 126.7, 126.7, 129.0, 137.2, 144.1, 148.1, 164.8. HRMS (ESI): calcd for $C_{18}H_{16}N_4{}^{130}Te$: 419.0516; found: 419.0531 $[M + H]^+$. Anal. Calcd for $C_{18}H_{16}N_4Te$-2HCl-2H_2O (524.89): C, 41.19; H, 4.22; N, 10.67. Found: C, 41.36; H, 4.13; N, 11.05.

2-(4'-Carbamimidoyl-[1,1'-biphenyl]-3-yl)-1-methyl-1H-benzo[d]imidazole-6-carboximidamide trihydrochloride (14, DB1314). To a stired solution of 3-(4-cyanophenyl) benzaldehyde[66] 2.07 g (0.01 mole), 4-amino-3-(methylamino) benzonitrile 1.47 g (0.01 mole) in 20 ml dry DMF under N_2 was added sodium bisulfite 2.08 (0.02 mole) and the mixture was heated under reflux for 12 hr. (tlc monitored). The solvent was removed, the residue was triturated with cold water, separated solid was filtered, washed with water and air dried. Light brown solid was stirred with 1:1 mixture of DCM-ether, filtered and dried under reduced pressure at 60°C for 4 h gave 2-(4'-cyano-[1, 1'-biphenyl]-3-yl)-1-methyl-1H-benzo[d]imidazole-6-carbonitrile (13), yield 2.3 g (69%); mp >300°C dec; ^{1}H NMR (DMSO-d_6): 8.36 (d, 1H, J= 1.2 Hz), 8.24 (t, 1H, J= 1.6 Hz), 8.03-7.97 (m, 6H), 7.88 (d, 1H, J= 8.4 Hz), 7.76 (dd, 1H, J= 8.0

Hz), 7.67 (dd, 1H, J= 1.2 Hz, J= 8.4 Hz), 4.01 (s, 3H); ^{13}C NMR (DMSO-d_6): 155.7, 145.1, 143.5, 138.6, 136.1, 132.5, 129.9, 129.3, 129.2, 128.5, 127.6, 127.5, 125.0, 119.8, 119.4, 118.2, 115.6, 110.3, 104.0, 31.7; MS: HRMS-ESI-POS: calc. for $C_{22}H_{15}N_4$ *m/z* 335.1297 (M^++1), found *m/z* 335.1307. Using 0.334 g (0.001 mole) of the previous bisnitrile **13** yielded the final diamidine **DB1314** following the LiN(TMS)$_2$ method described above; yield 0.32 g (70%), mp >300°C dec; ^{1}H NMR (DMSO-d_6): 9.51 (s, 2H), 9.50 (s, 2H), 9.26 (s, 2H), 9.20 (s, 2H), 8.35 (brs, 1H), 9.31 (brs, 1H), 8.09 (d, 2H, J= 8.4 Hz), 8.06-8.0 (m, 4H), 7.89 (brd, 1H, J= 8.8 Hz), 7.82 (t, 1H, J= 8.0 Hz), 4.06 (s, 3H); ^{13}C NMR (DMSO-d_6): 165.5, 165.2, 153.7, 144.0, 139.2, 138.2, 135.6, 130.48, 130.12, 130.07,129.07, 128.9, 127.5, 127.4, 126.4, 124.2, 123.8, 117.3, 112.9, 33.0; MS: HRMS-ESI-POS: calc. for $C_{22}H_{21}N_6$ *m/z* 369.1827 (M^++1), found *m/z* 369.1827; Anal. calc. for $C_{22}H_{20}N_6$.3.0HCl.1.5H_2O: C, 52.34; H, 5.19; N, 16.69; Found: C, 52.43; H, 5.32; N, 16.50.

2-(Thiophen-2-yl)quinoline-6-carbonitrile(15). It was synthesized from 6-bromo-2-thiophene-quinoline-4-carboxylic acid[72], product from of Pfitzinger reaction of 6-bromoisatin and 2-acetylthiophene according to the published procedure.[73] 6-Bromo-2-thiophene-quinoline-4-carboxylic acid (0.15 g, 0.45 mmol) was heated with CuCN (80 mg, 0.9 mmol) in dry DMF at 140-150 ^{o}C for 3 days. The mixture is quenched with aq. KCN and extracted with EtOAc to give 33 mg of 6-cyano-2-thiophene-quinoline in 31% yield after chromatographic purification (30% Et_2O/hexanes); mp 141.5-142.5 ^{o}C; ^{1}H NMR (DMSO-d_6) δ 8.50 (d, J = 1.8 Hz, 1H), 8.47 (d, J = 9.0 Hz, 1H), 8.20 (d, J = 8.7 Hz, 1H), 8.07 (d, J = 4.2 Hz, 1H), 8.05 (s, 1H), 7.97 (dd, J_1 = 2.1 Hz, J_2 = 6.0 Hz, 1H), 7.80 (d, J = 5.1 Hz, 1H), 7.25 (q, J_1 = 3.6 Hz, J_2 = 1.2 Hz, 1H). ^{13}C NMR (DMSO-d_6) δ 152.9, 146.9, 142.4, 135.6, 132.4, 128.8, 128.7, 128.2, 126.8, 126.2, 124.7, 117.4, 116.8, 106.9. MS (ESI) 237.08 (M^++1, 100).). IR hν (cm^{-1}): 2219 (CN).

2-(5-Bromothiophen-2-yl)quinoline-6-carbonitrile(16). It was synthesized from **15** (0.33 g, 1.6 mmol), NBS (0.3 g, 1.8 mmol) in dry DMF according to a general procedure[68,69] to give 0.47 g of **3** in 93% yield, mp 216-218 ^{o}C. ^{1}H NMR (DMSO-d_6) δ 8.57 (s, 1H), 8.50 (d, *J* = 9 Hz, 1H), 8.20 (d, *J* = 9 Hz, 1H), 8.03 (m, 2H), 7.90 (d, *J* = 3.9 Hz, 1H), 7.36 (d, *J* = 3.9 Hz, 1H). HRMS (ESI) Calcd. for $C_{14}H_8N_2BrS$ *m/z* : 314.9513, Found : 314.9592.

2-(5-(4-Cyanophenyl)thiophen-2-yl)quinoline-6-carbonitrile(17). It was synthesized under general Suzuki coupling conditions from **16** (0.37 g, 1.04 mmol), $Pd(Ph_3P)_4$ (60 mg, 0.05 mmol), 4-cyanophenylboronicacid (183.7mg, 1.25 mmol), 2M K_2CO_3 (1mL) in 1,4-dioxane (5 mL), to give **4** (280 mg), 80% yield; mp> 300 ^{o}C. ^{1}H NMR (DMSO-d_6) δ 8.59 (s, 1H), 8.53 (d, *J* = 8.4 Hz, 1H), 8.28 (d, *J* = 8.8 Hz, 1H), 8.13 (d, *J* = 6.4 Hz, 1H), 8.10 (s, 1H), 8.00 (m, 3H), 7.89 (d, *J* = 8.0 Hz, 2H), 7.83 (s, 1H). Anal. Calcd. for $C_{21}H_{11}N_3S$: C, 74.76; H, 3.29. Found: C, 74.48; H, 3.09.

2-(5-(4-Carbamimidoylphenyl)thiophen-2-yl)quinoline-6-carboximidamide trihydrochloride (18, DB1504) It was synthesized from **4** (95 mg, 0.27 mmol), $LiN(TMS)_2$ (1M, 1.6 mL, 1.6 mmol) in dry THF according to the procedure described above to give after work up 79 mg (79%) of **DB1504**, mp > 300 ^{o}C. ^{1}H NMR (DMSO-d_6) δ 9.46 (s, 2 H, exchangeable with D_2O) 9.50 (s, 2 H, exchangeable with D_2O), 9.42 (s, 2 H, exchangeable with D_2O), 9.29 (s, 2 H, exchangeable with D_2O), 8.58 (m, 2H), 8.34 (d, *J* = 8.4 Hz, 1H), 8.20 (d, *J* = 3.6 Hz, 1H), 8.10 (m, 4H), 7.94 (m, 3H). ^{13}C NMR (DMSO-d_6) δ 165.2, 164.9, 154.1, 149.3, 145.5, 145.1, 138.6, 138.4, 130.1, 129.9, 129.3, 129.2, 128.4, 127.6, 127.0, 126.2, 125.9, 125.4,

119.2. MS (ESI) *m/z*: 372.1 (M^++1). Anal. Calcd. for $C_{21}H_{17}N_5S$-3 HCl- 0.5 H_2O- 0.2 EtOH: C, 51.50; H, 4.48; N, 14.03. Found: C, 51.78; H, 4.27; N, 13.70.

2-(5-(4-(5-Carbamimidoyl-1-methyl-1H-benzo[d]imidazol-2-yl)phenyl)thiophen-2-yl)-1-methyl-1H-benzo[d]imidazole-5-carboximidamide tetrahydrochloride (19, DB2572). Reaction of 5-(4-formylphenyl) thiophene-2-carboxaldehyde[74] (0.108 g, 0.0005 mol), 3-amino-4-(methylamino) benzamidine hydrochloride[75] (0.228 g, 0.001 mole) and 1, 4-benzoquinone (0.108 g, 0.001 mol) in dry ethanol (50 ml) (under nitrogen) was heated at reflux for 12 h. The reaction mixture following standard work-up and drying at 50^0 C (12 h in vac.) yielded di hydrochloride salt, which was converted to tetra hydrochloride salt by dissolving in 15 ml ethanol and treating with 2 ml sat. ethanolic HCl; greenish solid, yield 0.25 g (72%), mp >280°C dec; ^{1}H NMR (DMSO-d_6): 9.60 (brs, 2H), 9.47 (brs, 2H), 9.34 (brs, 2H), 9.23 (brs, 2H), 8.37 (d, 1H, J= 1.2 Hz), 8.27 (d, 1H, J= 1.2 Hz), 8.12-8.55 (m, 5H), 8.03 (d, 1H, J =3.6 Hz), 7.97-7.92 (m, 3H), 7.82 (dd, 1H, J=1.2 Hz, J =8.8 Hz), 4.17 (s, 3H), 4.08 (s, 3H); ^{13}C NMR (DMSO-d_6): 165.8, 165.5, 153.3, 148.8, 145.5, 140.4, 139.7, 138.4, 136.5, 138.4, 130.93, 130.91,130.6, 126.4, 125.8, 125.5, 123.5, 123.1, 122.4, 121.7, 118.7, 117.4, 112.2, 111.1,32.6, 32.2; MS: HRMS-ESI-POS: calc. for $C_{28}H_{25}NS$ *m/z* 505.1923 (M^++1), found *m/z* 505.1876; Anal. calc. for $C_{28}H_{24}N_8S.4HCl.3.0H_20$: C, 47.73; H, 4.86; N, 15.91; Found: C, 47.93; H, 4.73; N, 15.79

2. Biological Assays.

2.1. DNA and Proteins.

All oligonucleotides (Supplementary Table S1) were purchased from Eurogentec (Belgium). The pGL3-prom-HBS-1R, pGL3-prom-HBS-6R and pGL3-prom-HBSmut-6R reporter vectors were obtained by double digestion of the pGL3-promoter plasmid (Promega, France) at MluI and NheI

(NEB, France) restriction sites localized 5' upstream to the SV40 minimal promoter, followed by ligation with phosphorylated double stranded oligonucleotides obtained from hybridization of FP-HBS-1Ra and FP-HBS-1Rb, Luc-HBS-6Ra and Luc-HBS-6Rb or Luc-HBSmut-6Ra and Luc-HBSmut-6Rb oligonucleotides. The $pcDNA_3$-HOXA9 expression vector was a kind gift from Dr Nabeel B. Yaseen (Northwestern University, Chicago, USA).[51] A TY-tag was added in 5' to HOXA9 cDNA to be expressed in reticulocyte lysate system for ELISA-derived Protein/DNA Binding inhibition assay. The pCMV-AD-HOXA9 expression vector used for luciferase assays was constructed by subcloning HOXA9 cDNA from pRc/CMV-HOXA9 (a gift from Prof. Corey Largman†, University of California, San Francisco, USA) into the pCMV-AD vector (Stratagene, France) to fuse the NF-κB activation domain to HOXA9 protein in order to improve the transactivation capacity of HOXA9 in the absence of co-activators for luciferase assays.

2.2. ELISA-derived Protein/DNA Binding inhibition assay (EPDBi)

The 96-wells screening procedure was performed essentially as described[44] with the following modifications. Streptavidin coated 96-wells plates (ThermoFicher, France) were blocked for 1h at room temperature in 200µL of blocking solution of TBS-T (Tris-HCl 10mM pH 8.0, NaCl 150mM, Tween 0.5%) supplemented with 10% skimmed milk powder. After three 5min washes at room temperature with TBS-T, 20nM of double stranded biotinylated HOXA9-binding site containing oligonucleotides (Supplementary Table S1) were immobilized per well for 20min at room temperature in 100µL of binding buffer (Tris-HCl 10mM pH7.5, EDTA 1mM pH7.5, NaCl 50mM, DTT 1mM, BSA 10µg/µL, Glycerol 6%) with or without 5 or 10µM of the tested diamidine compounds. After two 5 min washes at room temperature with 200µL of binding buffer, 40µL of binding buffer containing HOXA9 proteins expressed from reticulocyte lysate

system (Promega, Madison, Wisconsin, USA) (2µL of lysate) were incubated for 1H at room temperature with or without 50- or 100-fold excess of non-biotinylated oligonucleotides of the same HBS-containing sequence or a non-specific sequence. The unbound proteins were removed by three successive washes with the binding buffer. The HOXA9/DNA complex was revealed by addition of 85ng of a mouse anti-TY1-tag antibody (C1520054, Diagenode, Belgium) in TBS-T for 1H at room temperature followed by three washing steps and addition of a 1/2000 dilution of a secondary sheep HRP-conjugated anti-mouse antibody (NXA931, GE Healthcare, France). After three 5min washes with 200µL of TBS-T, 50µL of TMB (Promega, Madison, Wisconsin, USA) were added for 7min at room temperature. The reaction was stopped by addition of 50µL of 0.5M H_2SO_4 and the absorbance was measured at 450nm on a microplate spectrometer (Spectramax-I3, Molecular Devices). All collected data were analyzed using SoftMax Pro software.

2.3. Electrophoretic Mobility Shift Assay (EMSA)

The HBS or the Akap13-HBS double-strand oligonucleotides (Supplementary Table S1) were radiolabeled at 5'-end as described previously.[43] The binding experiments were performed as previously reported[43,44] with some modifications. Briefly, 2µL of HOXA9 protein-expressing reticulocyte lysates (TNT® coupled reticulocyte lysate system, Promega, Madison, Wisconsin, USA) were incubated 20min at 4°C in binding buffer with the radio-labeled HBS-containing DNA and diamidine compounds at the indicated concentrations. Free DNA was separated from protein-DNA complexes on a 6% native polyacrylamide gel under electrophoresis for 3H at 300V in 0.5X TBE buffer. Gels revelations were performed using a Pharos-PMI equipment (BioRad) and analyzed with the ImageQuant-3.3 software.

2.4. Circular dichroism (CD) and DNA thermal melting assay

CD spectra and DNA melting temperature studies were performed using double stranded oligonucleotides of various DNA sequences in the absence or presence of diamidine compounds essentially as previously reported,[76] with the following modifications. Double stranded oligonucleotides were obtained by equimolar hybridization of the corresponding -a and -b strands (Supplementary Table S1). For CD analysis, 5μM of double stranded HBS oligonucleotide was incubated in TNE buffer (50mM Tris-HCl pH7.8 + 100mM NaCl + 1mM EDTA) and CD spectra were collected in a quartz cell of 10mm path length as an average of three accumulations from 480 to 230nm using a J-810 Jasco spectropolarimeter at a controlled temperature of 25°C fixed by a PTC-424S/L peltier type cell changer (Jasco) as described previously[77]. DB818, DB1055 and DB828 (1, 2, 3, 4, 5, 6, 8 and 10 μM) were gradually added to the DNA sample separately and CD was measured at each drug/DNA ratio. For Tm measurements, indicated compounds and oligonucleotides were mixed in TNE buffer at drug/DNA ratio R of 1:1 or 2:1 as indicated. The DNA absorbance at 260nm was measured in quartz cells using an Uvikon XL spectrophotometer thermostated with a peltier cryostat every min over a range of 15 to 100°C with an increment of 1°C/min. The Tm values were deduced from the midpoint of the hyperchromic transition obtained from first-derivative plots. The variation of melting temperature (△Tm) were obtained by subtracting the melting temperature measurement of CT-DNA alone (control Tm) to that obtained with DNA incubated with the compounds (△Tm values = $Tm_{[compound + DNA]}$ - $Tm_{[DNA\ alone]}$).

2.5. DNase I Footprint Assay

The pGL3-prom-HBS-1R or pGL3-prom-HBSmut-1R plasmid were digested by ClaI and BglII restriction enzymes and radiolabelled at 3' termini with [α-^{32}P]-dATP (PerkinElmer, France). DNase I digestion and electrophoretic separation were performed as reported.[78] The DNA sequence was deduced from guanine positions cleaved upon DMS and piperidine treatment (G-track). The gels were exposed to storage screen for the appropriated delay at room temperature. The results were collected using Pharos-PMI equipment (BioRad).

2.6. Surface Plasmon Resonance (SPR)

SPR measurements were performed with four-channel Biacore T200 optical biosensor systems (GE Healthcare, Inc., Piscataway, NJ). A streptavidin-immobilized (SA) sensor chip was prepared for use by conditioning with a series of 60s injections of 1M NaCl in 50mM NaOH (activation buffer) followed by extensive washing with HBS buffer [10mM HEPES, 150mM NaCl, 3mM EDTA, and 0.05% P20 (pH7.4)]. Biotinylated HP-HBS and HP-HBS-ATm (Supplementary Table S1) DNA hairpins (25-50nM) were prepared in HBS buffer and immobilized on the flow cell surface by noncovalent capture as previously described.[79,80] Flow cell 1 was left blank as a reference, while flow cells 2-4 were immobilized with DNA by manual injection of DNA stock solutions (flow rate of 1 μL/min) until the desired amount of DNA response units (RU) was obtained (320−330 RU). Ligand solutions were prepared with degassed and filtered 50 mM Tris-HCl buffer pH 7.42 by serial dilutions from a concentrated stock solution. Typically, a series of different ligand concentrations (from 1 nM to 1 μM) were injected over the DNA sensor chip at a flow rate of 100μL/min until a constant steady-state response was obtained (3min), and this was followed by buffer flow for ligand dissociation (10-20 min). After each cycle, the sensor chip surface was regenerated with a 10 mM glycine solution at pH 2.5 for 30s followed by multiple buffer injections to yield a stable baseline for the following cycles.

RUobs was plotted as a function of free ligand concentration (Cfree), and the equilibrium binding constants (K_A) were determined either with a one-site binding model (K_2=0) for DB818 or with a two-site model for DB1055 (due to some non-specific interactions), where r represents the moles of bound compound per mol of DNA hairpin duplex and K_1 and K_2 are macroscopic binding constants.

$$r = (K_1 \bullet Cfree + 2K_1 \bullet K_2 \bullet Cfree_2)/(1 + K_1 \bullet Cfree + K_1 \bullet K_2 \bullet Cfree_2) \quad (1)$$

RUmax in the equation was used as a fitting parameter, and the obtained value was compared to the predicted maximal response per bound ligand to independently evaluate the stoichiometry.[80] One-site binding models have been applied for DB818 with HP-HBS and HP-HBS-ATm DNA and also for DB1055 with HP-HBS-ATm DNA. Due to some non-specific interactions, two-site interaction model has been applied for DB1055 with HP-HBS DNA. Kinetic analyses were performed by globally fitting the binding results for the entire concentration series using a standard 1:1 kinetic model with integrated mass transport-limited binding parameters as described previously.[80]

2.7. Ab-Initio Calculations and Molecular Dynamic (MD)

Simulation Optimization and electrostatic potential calculations were performed for the DB818 molecule using DFT/B3LYP theory with the 6-31+G* basis set in Gaussian 09 (Gaussian, Inc., 2009, Wallingford, CT) with Gauss-view 5.09. Partial charges were derived using the RESP fitting method (Restrained Electrostatic potential).[81] AMBER 14 (Assisted Model Building with Energy Refinement)[82] software suite was used to perform molecular dynamic (MD) simulations. Canonical B-form ds[(5'-CCATGATTTACG-3')(5'-CGTAAATCATGG-3')] DNA was built in Nucleic Acid Builder (NAB) tool in AMBER. AMBER preparation and force field parameter

files required to run molecular dynamic simulations for DB818 molecule were produced using ANTECHAMBER[83]. Specific atom types assigned for DB818 molecule (Supplementary Figure S3) were adapted from the ff99 force field. Most of the force field parameters for DB818 molecule were derived from the existing set of bonds, angles and dihedrals for the similar atom types in parm99 and GAFF force fields.[84] Some dihedral angle parameters were obtained from previously reported parametrized data.[85] Parameters of DB818 in frcmod file are listed in Supplementary Table S2.

AutoDock Vina program[86] was used to dock the DB818 in the minor groove of DNA to obtain the initial structure for DB818-DNA complex. MD simulations were performed in explicit solvation conditions where the DNA-DB818 complex was placed in a truncated octahedron box filled with TIP3P water using xleap program in AMBER. Sodium ions were used to neutralize the system. A 10 Å cutoff was applied on all van der Waals interactions. The MD simulation was carried out using the Sander module with SHAKE algorithm applied to constrain all bonds. Initially, the system was relaxed with 500 steps of steepest-descent energy minimization. The temperature of the system was then increased from 0 K to 310 K for over 10 ps under constant-volume conditions. In the final step, the production run on the system was subsequently performed for 100 ns under NPT (constant-pressure) conditions.

2.8. Cellular distribution of the compounds using fluorescence microscopy

GFP-expressing MigA9 suspension cells ($2x10^5$) were treated with the indicated compounds at 20 µM during 2h and allowed to attach onto poly-L-lysine-coated coverslips overnight prior to fixation with formaldehyde 4%. Nuclear compartment was stained through DNA binding of TO-PRO-3 iodide (1 mM, Invitrogen™, Thermo Fisher Scientific, USA) or propidium iodide

(10µg/mL, Sigma-Aldrich, USA) supplemented with RNase A (300µg/mL, Sigma-Aldrich, USA) for 30min in the dark at room temperature. Coverslips were mounted with a drop of anti-fade medium. Adherent human colon carcinoma HT-29 cells were treated with 5µM of the indicated compounds for 16H and fixed with 2% paraformaldehyde prior to addition of 75nM of $DiOC_6$ and 1µg/mL of PI supplemented with RNaseA. Based on the intrinsic fluorescence of evaluated compounds, images were acquired either on a confocal inverted LSM880 microscope (Carl Zeiss microscopy, Zeiss GmbH, Germany) or on a wide field fluorescence inverted DMi8 (Leica Microsystems, Germany) microscope, both with a x63 objective. Excitation and emission wavelengths are indicated in the legends.

2.9. Transient transfections

The K562 cell line was used as an HOXA9-negative leukemia cell model that has strong potency for transfection (AMAXA V-kit system, Lonza). K562 cells ($2x10^6$) were pre-cultured overnight in RPMI-1640 supplemented with GlutaMAX™-I (Gibco) and mixed with 2µg of the expression vector (pCMVAD-HOXA9 or pCMVAD as control), reporter vector (pGL3-Prom-HBS-6R, pGL3-Prom-HBSmut-6R or pGL3-Prom as control) and vectors for validation/normalizing of transfection efficiency pmaxGFP™ (0.5µg) and pCDNA4-βgal (0.5µg) in 100µL of BufferV to then be electroporated using a Amaxa™ Nucleofactor™ as recommended by the provider (Nucleofector® kit V, LONZA, France). Each transfected cell sample was recovered in 4mL of complete RPMI-media to be split in two equal amounts ($1x10^6$ cells) in 12-wells plates. After 6H, compounds were added at 20µM in one of them whereas the other one received vehicle (deionized H_2O). After 48H, cells were rinsed with PBS and lysed under non-denaturing conditions 20min at 4°C with 0.5mL of Lysis passive Buffer 5X (Promega, Madison, Wisconsin, USA) and supernatant was recovered after a 15min centrifugation at 13000g. For β-galactosidase

activity, 200µL of luminescent β-galactosidase detection kit-II (Clontech, France) were added to 25µL of supernatant. The fluorescence of GFP protein was detected using a 96-well fluorimeter at $\lambda_{excitation}$ = 485nm and $\lambda_{emission}$ = 535nm. The luciferase activity was finally measured using the Luciferase assay system (Promega, Madison, Wisconsin, USA) according to manual recommendations. All data were collected using a Mithras LB940 (Berthold).

2.10. DNA microarray analysis

MigA9 cells ($2x10^6$) were treated in presence and absence of 5µM of DB818 in duplicates for 6, 12 or 24H treatments. Total RNA was then purified with RNAeasy kit from Qiagen including DNAseI treatment and the duplicates were pooled. Mouse Whole Genome Agilent 44K 60-mer oligonucleotide Microarrays were performed according to the Two-Color Microarray-Based Gene Expression protocol (Agilent Technologies). Microarrays were scanned using the Agilent scanner G2505B. The expression data were extracted by Feature Extraction and processed with Limma R package,[87] combining the three data points (6, 12 and 24H) for normalization, filtering, and statistical analysis. The genes commonly up-regulated or down-regulated with adjusted p-values<0.05 and with |FoldChange|≥1.5 at 6, 12 and 24H were further analyzed with GSEA and Ingenuity Pathway Analysis softwares.

2.11. qRT-PCR

MigA9 cells were treated in presence and absence of 5 and 10 µM of DB818, DB1055 and DB828 at n=6 per condition for 48H treatments prior to the purification of total RNA. RNAs were reverse-transcribed with High-Capacity cDNA Reverse Transcription Kit (Applied Biosystems™, ThermoFisher, USA) to generate the corresponding cDNAs and amplified using qPCR primer sequences as presented in Supplementary Table S1. Specificity and efficacy of the

primers were addressed. PCR amplification was performed in duplicate using 200nM of oligonucleotide primers and SYBR Green PCR Master Mix reagent (ThermoFisher Scientific, USA) following the manufacturer's instructions on a StepOnePlus apparatus using StepOneTM Real-Time PCR software (Applied Biosystems™, ThermoFisher, USA). The mRNA levels of each target gene were normalized relatively to the mouse housekeeping gene Gapdh quantified for each sample. The relative expression ratio was calculated using the delta-delta-Ct method.

2.12. Cell survival

For the MTS assay, MigA9 cells were seeded into 96-well plates at a density of 1.5×10^4/well in 100µL of complete medium and treated with DB818, DB1055 or DB828 compounds at 0.1 to 50µM or the corresponding control vehicle for 72H before analysis using CellTiter 96® AQueous One Solution Cell Proliferation Assay kit following the manufacturer's instruction. The absorbance was detected at 490nm with a Microplate Reader (Spectramax, Molecular Devices). Measurements were performed in duplicates or triplicates and repeated at least three times.

2.13. Cell death and cell cycle analysis using flow cytometry

MigA9 cells (10^5 cells/mL) were treated for 24 and/or 48H with various diamidine compounds at the mentioned concentrations, in triplicate. For propidium iodide-positive cell labeling, $2.5x10^4$ treated cells were stained by propidium iodide (P4170, Sigma Aldrich, USA, 5µg/mL). Cells were analyzed by flow cytometry using LSR-Fortessa X20 (BD Biosciences) and data were analyzed using FlowJo software (BD Biosciences). For cell cycle analysis, 10^6 cells were first treated with 10 µM EdU for 1 hour using Click-iT® EdU Flow Cytometry Assay Kit (Molecular probes) prior to fixation using cold 70% ethanol followed by addition of propidium iodide at 50 µg/mL in the presence of RNaseA 100µg/mL for 30 min. Cell cycle was acquired by flow

cytometry using CyAn-ADP (Beckman Coulter, USA) and data were analyzed using Summit software (Beckman Coulter, USA).

2.14. Colony-forming assays

Murine MigA9 or human K562 cell line (1000 cells/well of 6-wells plates) were mixed with 1mL of complete M3434 (murine) or H4535 (human) Colony-Forming Cell Assays MethoCult® (Stemcell Technologies, France) in the presence or absence of 2.5µM of the mentioned compounds in duplicates and plated in 6-wells plates for 10 days. Full wells were then photographed under visible light and clones were quantified as individual clones for K562 and murine cell lines. For MigA9 cell line, representative clones were photographed under visible light or for intrinsic compound fluorescence using an inverted fluorescence microscope with an excitation wavelength/bandpath of 350/50nm and an emission wavelength/bandpath of 460/50nm with a dry X5 objective and the individual clones were further identified as CFU-GM, CFU-M CFU-G or BFU-E based on morphological criteria as presented by the supplier.

2.15. Statistics

Student unpaired t-tests were performed using Prism Software 7.0 (GraphPad, La Jolla, CA, USA).

AUTHOR INFORMATION

Corresponding Author

* To whom correspondence should be addressed: Dr Marie-Hélène David-Cordonnier, INSERM UMR-S1172 / JPARC, IRCL, Place de Verdun, F59045 Lille, France ; Tel: +33 320 169 223;

Fax: +33 320 538 562; Email: marie-helene.david@inserm.fr; ORCID ID: 0000-0001-9831-5577.

Present Addresses

†Present Address: Peixoto Paul, EA3922, University of Bourgogne Franche-Comté, Besançon, France.

Author Contributions

The manuscript was written through contributions of all authors. All authors have given approval to the final version of the manuscript. ‡These authors contributed equally.

Funding Sources

This work is supported by the Ligue contre le Cancer-Septentrion (Comité du Nord, Comité du Pas-de-Calais), the Association Laurette Fugain [ALF-2009/06, ALF-2016/05], the Association pour la Recherche sur le Cancer [ARC-SFI20111203669], the FEDER-Région Nord-Pas-de-Calais and the Institut pour la Recherche sur le Cancer de Lille (IRCL) to M.-H.D.-C, and by the National Institutes of Health [GM111749 to W.D.W and D.W.B].

Notes

This work is dedicated to Dr Jean-Pierre Kerckaert who generated transcriptomic data (Agilent platform of the University of Lille) and to Prof. Corey Largman who kindly provided MigA9 cells.

ACKNOWLEDGMENT

M.L. thanks the University of Lille, the French Research Ministry and the French Hematological Society (SFH), S.J. thanks the ARC Foundation, P.P. and R.N. thanks the IRCL, for their respective PhD fellowships.

M.H.-D.C. thanks the Institut pour la Recherche sur le Cancer de Lille (IRCL) for technical expertise, Dr Nabeel Yaseen (Northwestern University, Chicago, USA) for the kind gift of pcDNA3-HOXA9 expressing vector, Dr Dominique Payet-Bornet and Dr Andrew Travers (Cambridge University, UK) for the gift of purified HMG-D100 protein, Dr Samuel Meignan (Centre Oscar Lambret, Lille) for access to the confocal inverted LSM880 microscope, the University of Lille, for access to the Pharos-PMI phosphorimaging equipment and the flow cytometry platform of the BioImaging Center of Lille Nord de France (BiCeL) at IRCL for access to equipment and technical formation.

ABBREVIATIONS

Akap13, A-kinase anchoring protein 13; AML, acute myeloid leukemia; Arfgef1, ADP ribosylation factor guanine nucleotide exchange factor 1; dATP , deoxyadenosine triphosphate; ATRA, all-trans retinoic acid; APL, acute promyelocytic leukemia; BCL6, B-cell lymphoma 6 protein; CBP, CREB-binding protein; CD, circular dichroism; CFU, colony forming unit; CGP, chemical and genetic perturbations; CRABP1, cellular retinoic acid binding protein 1; CTR , control; DAPI, 4',6-diamidino-2-phenylindole; $DiOC_6$, 3,3′-dihexyloxacarbocyanine iodide; DMS , dimethyl sulfide; ELISA, enzyme-linked immunosorbent assay; EMSA, electrophoretic mobility shift assay; ERG, ETS-related gene; EWS, Ewing's sarcoma; EZH2, enhancer of zeste homolog 2; FOXM1, forkhead box M1 transcription factor; GFP, green fluorescent protein;

GMP, granulocyte-monocyte progenitors; GSEA, Gene Set Enrichment Analysis; HBS, HOXA9-binding site; HMG, high mobility group; HSF1, heat shock factor 1; HP , hairpin; HRP, horseradish peroxidase; IPA, Ingenuity Pathway Analysis; Itgam, integrin alpha M; KLF5, Kruppel like factor 5; mdm, murine double minute; MLL , mixed-lineage leukemia; NPM1, Nucleophosmin1; NRF2, nuclear factor erythroid-2-related factor 2; NS, nonspecific; NUP98, nuclear pore complex protein 98; Oasl2, 2'-5'-oligoadenylate synthetase like 2, PAX, paired box; PBS , phosphate buffer saline; PBX, Pre-B-cell leukemia homeobox; PDB, Protein Data Bank; PI, propidium iodide; RUNX1, Runt Related Transcription *Factor* 1; SPR, surface plasmon resonance; STAT3, signal transducer and activator of transcription 3; TBS, Tris buffer saline; YAP, yes-associated protein.

CONFLICT OF INTEREST

No conflict of interest.

Supporting Information Availability:

Supplementary Tables S1-2

Supplementary Figures S1-7

Supplementary Chemistry Section

Supplementary references

Representatives [1]HNMR Spectra

Molecular Formula Strings.

References

(1) Bouhlel, M. A.; Lambert, M.; David-Cordonnier, M.-H. Targeting Transcription Factor Binding to DNA by Competing with DNA Binders as an Approach for Controlling Gene Expression. *Curr. Top. Med. Chem.* **2015**, *15* (14), 1323–1358.

(2) Hagenbuchner, J.; Ausserlechner, M. J. Targeting Transcription Factors by Small Compounds—Current Strategies and Future Implications. *Biochem. Pharmacol.* **2016**, *107*, 1–13.

(3) Portugal, J.; Barceló, F. Noncovalent Binding to DNA: Still a Target in Developing Anticancer Agents. *Curr. Med. Chem.* **2016**, *23* (36), 4108–4134.

(4) Lambert, M.; Jambon, S.; Depauw, S.; David-Cordonnier, M.-H. Targeting Transcription Factors for Cancer Treatment. *Molecules* **2018**, *23*, 1479.

(5) Lo-Coco, F.; Cicconi, L. History of Acute Promyelocytic Leukemia: A Tale of Endless Revolution. *Mediterr. J. Hematol. Infect. Dis.* **2011**, *3* (1), e2011067.

(6) Dang, C. V.; Reddy, E. P.; Shokat, K. M.; Soucek, L. Drugging the "undruggable" Cancer Targets. *Nat. Rev. Cancer* **2017**, *17* (8), 502–508.

(7) Tisato, V.; Voltan, R.; Gonelli, A.; Secchiero, P.; Zauli, G. MDM2/X Inhibitors under Clinical Evaluation: Perspectives for the Management of Hematological Malignancies and Pediatric Cancer. *J. Hematol. Oncol.* **2017**, *10* (1), 133.

(8) Leeman-Neill, R. J.; Bhagat, G. BCL6 as a Therapeutic Target for Lymphoma. *Expert Opin. Ther. Targets* **2018**, *22* (2), 143–152.

(9) Furtek, S. L.; Backos, D. S.; Matheson, C. J.; Reigan, P. Strategies and Approaches of Targeting STAT3 for Cancer Treatment. *ACS Chem. Biol.* **2016**, *11* (2), 308–318.

(10) Liu-Chittenden, Y.; Huang, B.; Shim, J. S.; Chen, Q.; Lee, S. J.; Anders, R. A.; Liu, J. O.; Pan, D. Genetic and Pharmacological Disruption of the TEAD-YAP Complex Suppresses the Oncogenic Activity of YAP. *Genes Dev.* **2012**, *26* (12), 1300–1305.

(11) Gibault, F.; Bailly, F.; Corvaisier, M.; Coevoet, M.; Huet, G.; Melnyk, P.; Cotelle, P. Molecular Features of the YAP Inhibitor Verteporfin: Synthesis of Hexasubstituted Dipyrrins as Potential Inhibitors of YAP/TAZ, the Downstream Effectors of the Hippo Pathway. *ChemMedChem* **2017**, *12* (12), 954–961.

(12) Kim, Y.-M.; Gang, E.-J.; Kahn, M. CBP/Catenin Antagonists: Targeting LSCs' Achilles Heel. *Exp. Hematol.* **2017**, *52*, 1–11.

(13) Xie, W.; Pariollaud, M.; Wixted, W. E.; Chitnis, N.; Fornwald, J.; Truong, M.; Pao, C.; Liu, Y.; Ames, R. S.; Callahan, J.; Solari, R.; Sanchez, Y.; Diehl, A.; Li, H. Identification and Characterization of PERK Activators by Phenotypic Screening and theirEffects on NRF2 Activation. *PLoS One* **2015**, *10* (3), e0119738.

(14) Cheeseman, M. D.; Chessum, N. E.; Rye, C. S.; Pasqua, A. E.; Tucker, M. J.; Wilding, B.; Evans, L. E.; Lepri, S.; Richards, M.; Sharp, S. Y.; Ali, S.; Rowlands, M.; O'Fee, L.; Miah, A.; Hayes, A.; Henley, A. T.; Powers, M.; Te Poele, R.; De Billy, E.; Pellegrino, L.; Raynaud, F.; Burke, R.; van Montfort, R. L.; Eccles, S. A.; Workman, P.; Jones, K. Discovery of a Chemical Probe Bisamide (CCT251236): An Orally Bioavailable Efficacious Pirin Ligand from a Heat Shock Transcription Factor 1 (HSF1) Phenotypic Screen. J Med Chem. 2017 Jan 12;60(1):180-201.

(15) Grimley, E.; Liao, C.; Ranghini, E. J.; Nikolovska-Coleska, Z.; Dressler, G. R. Inhibition of Pax2 Transcription Activation with a Small Molecule That Targets the DNA Binding Domain. *ACS Chem. Biol.* **2017**, *12* (3), 724–734.

(16) Leung, C. H.; Chan, D. S. H.; Ma, V. P. Y.; Ma, D. L. DNA-Binding Small Molecules as Inhibitors of Transcription Factors. *Med. Res. Rev.* **2013**, *33* (4), 823–846.

(17) Fontaine, F.; Overman, J.; François, M. Pharmacological Manipulation of Transcription Factor Protein-Protein Interactions: Opportunities and Obstacles. *Cell Regen. (London, England)* **2015**, *4* (1), 2.

(18) Blume, S. W.; Snyder, R. C.; Ray, R.; Thomas, S.; Koller, C. A.; Miller, D. M. Mithramycin Inhibits SP1 Binding and Selectively Inhibits Transcriptional Activity of the Dihydrofolate Reductase Gene in Vitro and in Vivo. *J. Clin. Invest.* **1991**, *88* (5), 1613–1621.

(19) Grohar, P. J.; Woldemichael, G. M.; Griffin, L. B.; Mendoza, A.; Chen, Q. R.; Yeung, C.; Currier, D. G.; Davis, S.; Khanna, C.; Khan, J.; McMahon, J.B.; Helman, L.J. Identification of an Inhibitor of the EWS-FLI1 Oncogenic Transcription Factor by High-Throughput Screening. *J. Natl. Cancer Inst.* **2011**, *103* (12), 962–978.

(20) Grohar, P. J.; Glod, J.; Peer, C. J.; Sissung, T. M.; Arnaldez, F. I.; Long, L.; Figg, W. D.; Whitcomb, P.; Helman, L. J.; Widemann, B. C. A Phase I/II Trial and Pharmacokinetic Study of Mithramycin in Children and Adults with Refractory Ewing Sarcoma and EWS–FLI1 Fusion Transcript. *Cancer Chemother. Pharmacol.* **2017**, *80* (3), 645–652.

(21) Morita, K.; Suzuki, K.; Maeda, S.; Matsuo, A.; Mitsuda, Y.; Tokushige, C.; Kashiwazaki, G.; Taniguchi, J.; Maeda, R.; Noura, M.; Hirata, M.; Kataoka, T.; Yano, A.; Yamada, Y.; Kiyose, H.; Tokumasu, M.; Matsuo, H.; Tanaka, S.; Okuno, Y.; Muto, M.; Naka, K.; Ito K.; Kitamura, T.; Kaneda, Y.; Liu, P. P.; Bando, T.; Adachi, S.; Sugiyama, H.; Kamikubo, Y. Genetic Regulation of the RUNX Transcription Factor Family Has Antitumor Effects. *J. Clin. Invest.* **2017**, *127* (7), 2815–2828.

(22) Antony-Debré, I.; Paul, A.; Leite, J.; Mitchell, K.; Kim, H. M.; Carvajal, L. A.; Todorova, T. I.; Huang, K.; Kumar, A.; Farahat, A. A.; Bartholdy, B.; Narayanagari, S. R.; Chen, J.; Ambesi-Impiombato, A.; Ferrando, A. A.; Mantzaris, I.; Gavathiotis, E.; Verma, A.; Will,

B.; Boykin, D. W.; Wilson, W. D.; Poon, G. M.; Steidl, U. Pharmacological Inhibition of the Transcription Factor PU.1 in Leukemia. *J. Clin. Invest.* **2017**, *127* (12), 4297–4313.

(23) Shah, N.; Sukumar, S. The Hox Genes and Their Roles in Oncogenesis. *Nat. Rev. Cancer* **2010**, *10* (5), 361–371.

(24) Gonçalves, C. S.; Xavier-Magalhães, A.; Pojo, M.; Oliveira, A. I.; Correia, S.; Reis, R. M.; Sousa, N.; Rocha, M.; Costa, B. M. Transcriptional Profiling of HOXA9-Regulated Genes in Human Glioblastoma Cell Models. *Genomics Data* **2015**, *5*, 54–58.

(25) Pires-Luís, A. S.; Costa-Pinheiro, P.; Ferreira, M. J.; Antunes, L.; Lobo, F.; Oliveira, J.; Henrique, R.; Jerónimo, C. Identification of Clear Cell Renal Cell Carcinoma and Oncocytoma Using a Three-Gene Promoter Methylation Panel. *J. Transl. Med.* **2017**, *15* (1), 149–157.

(26) Malek, R.; Gajula, R. P.; Williams, R. D.; Nghiem, B.; Simons, B. W.; Nugent, K.; Wang, H.; Taparra, K.; Lemtiri-Chlieh, G.; Yoon, A. R.; True, L.; An, S. S.; DeWeese, T.; Ross, A. E.; Schaeffer, E. M.; Pienta, K. J.; Hurley, P. J.; Morrissey, C.; Tran, P. T. TWIST1-WDR5-Hottip Regulates Hoxa9 Chromatin to Facilitate Prostate Cancer Metastasis. *Cancer Res.* **2017**, *77* (12), 3181–3193.

(27) Ma, Y.; Zhang, Y.; Mou, X.; Liu, Z.; Ru, G.; Li, E. High Level of Homeobox A9 and PBX Homeobox 3 Expression in Gastric Cancer Correlates with Poor Prognosis. *Oncol. Lett.* **2017**, *14* (5), 5883–5889.

(28) Vijapurkar, U.; Fischbach, N.; Shen, W.; Brandts, C.; Stokoe, D.; Lawrence, H. J.; Largman, C. Protein Kinase C-Mediated Phosphorylation of the Leukemia-Associated HOXA9 Protein Impairs Its DNA Binding Ability and Induces Myeloid Differentiation. *Mol. Cell. Biol.* **2004**, *24* (9), 3827–3837.

(29) Faber, J.; Krivtsov, A. V.; Stubbs, M. C.; Wright, R.; Davis, T. N.; Van Heuvel-Eibrink, M. Den; Zwaan, C. M.; Kung, A. L.; Armstrong, S. A. HOXA9 Is Required for Survival in Human MLL-Rearranged Acute Leukemias. *Blood* **2009**, *113* (11), 2375–2385.

(30) Collins, C. T.; Hess, J. L. Role of HOXA9 in Leukemia: Dysregulation, Cofactors and Essential Targets. *Oncogene* **2016**, *35* (9), 1090–1098.

(31) Collins, C. T.; Hess, J. L. Deregulation of the HOXA9/MEIS1 Axis in Acute Leukemia. *Curr. Opin. Hematol.* **2016**, *23* (4), 354–361.

(32) Chen, S.; Yu, J.; Lv, X.; Zhang, L. HOXA9 Is Critical in the Proliferation, Differentiation, and Malignancy of Leukaemia Cells Both in Vitro and in Vivo. *Cell Biochem. Funct.* **2017**, *35* (7), 433–440.

(33) Xu, H.; Valerio, D. G.; Eisold, M. E.; Sinha, A.; Koche, R. P.; Hu, W.; Chen, C. W.; Chu, S. H.; Brien, G. L.; Park, C. Y.; Hsieh, J. J.; Ernst, P.; Armstrong, S. A. NUP98 Fusion Proteins Interact with the NSL and MLL1 Complexes to Drive Leukemogenesis. *Cancer Cell* **2016**, *30* (6), 863–878.

(34) Rio-Machin, A.; Gómez-López, G.; Muñoz, J.; Garcia-Martinez, F.; Maiques-Diaz, A.;

Alvarez, S.; Salgado, R. N.; Shrestha, M.; Torres-Ruiz, R.; Haferlach, C.; Larráyoz, M. J.; Calasanz, M. J.; Fitzgibbon, J.; Cigudosa, J. C. The Molecular Pathogenesis of the NUP98-HOXA9 Fusion Protein in Acute Myeloid Leukemia. *Leukemia* **2017**, *31* (9), 2000–2005.

(35) Borrow, J.; Shearman, A. M.; Stanton, V. P.; Becher, R.; Collins, T.; Williams, A. J.; Dubé, I.; Katz, F.; Kwong, Y. L.; Morris, C.; Ohyashiki, K.; Toyama, K.; Rowley, J.; Housman, D.E. The t(7;11)(P15;P15) Translocation in Acute Myeloid Leukaemia Fuses the Genes for Nucleoporin NUP98 and Class I Homeoprotein HOXA9. *Nat. Genet.* **1996**, *12* (2), 159–167.

(36) Tan, L.; Xu, H.; Chen, G.; Wei, X.; Yu, B.; Ye, J.; Xu, L.; Tan, H. Silencing of HMGA2 Reverses Retardance of Cell Differentiation in Human Myeloid Leukaemia. *Br. J. Cancer* **2018**, *118* (3), 405–415.

(37) Calvo, K. R.; Sykes, D. B.; Pasillas, M.; Kamps, M. P. Hoxa9 Immortalizes a Granulocyte-Macrophage Colony-Stimulating Factor-Dependent Promyelocyte Capable of Biphenotypic Differentiation to Neutrophils or Macrophages, Independent of Enforced Meis Expression. *Mol. Cell. Biol.* **2000**, *20* (9), 3274–3285.

(38) Hu, Y. L.; Passegué, E.; Fong, S.; Largman, C.; Lawrence, H. J. Evidence That the Pim1 Kinase Gene Is a Direct Target of HOXA9. *Blood* **2007**, *109* (11), 4732–4738.

(39) Breitinger, C.; Maethner, E.; Garcia-Cuellar, M. P.; Slany, R. K. The Homeodomain Region Controls the Phenotype of HOX-Induced Murine Leukemia. *Blood* **2012**, *120* (19), 4018–4027.

(40) Ng, S. W. K.; Mitchell, A.; Kennedy, J. A.; Chen, W. C.; McLeod, J.; Ibrahimova, N.; Arruda, A.; Popescu, A.; Gupta, V.; Schimmer, A. D.; Schuh, A. C.; Yee, K. W.; Bullinger, L.; Herold, T.; Görlich, D.; Büchner, T.; Hiddemann, W.; Berdel, W. E.; Wörmann, B.; Cheok, M.; Preudhomme, C.; Dombret, H.; Metzeler, K.; Buske, C.; Löwenberg, B.; Valk, P. J.; Zandstra, P. W.; Minden, M. D.; Dick, J. E.; Wang, J. C. A 17-Gene Stemness Score for Rapid Determination of Risk in Acute Leukaemia. *Nature* **2016**, *540* (7633), 433–437.

(41) Huang, Y.; Sitwala, K.; Bronstein, J.; Sanders, D.; Dandekar, M.; Collins, C.; Robertson, G.; MacDonald, J.; Cezard, T.; Bilenky, M.; Thiessen, N.; Zhao, Y.; Zeng, T.; Hirst, M.; Hero, A.; Jones, S.; Hess, J. L. Identification and Characterization of Hoxa9 Binding Sites in Hematopoietic Cells. *Blood* **2012**, *119* (2), 388–398.

(42) LaRonde-LeBlanc, N. A.; Wolberger, C. Structure of HoxA9 and Pbx1 Bound to DNA: Hox Hexapeptide and DNA Recognition Anterior to Posterior. *Genes Dev.* **2003**, *17* (16), 2060–2072.

(43) Peixoto, P.; Liu, Y.; Depauw, S.; Hildebrand, M. P.; Boykin, D. W.; Bailly, C.; Wilson, W. D.; David-Cordonnier, M. H. Direct Inhibition of the DNA-Binding Activity of POU Transcription Factors Pit-1 and Brn-3 by Selective Binding of a Phenyl-Furan-Benzimidazole Dication. *Nucleic Acids Res.* **2008**, *36* (10), 3341–3353.

(44) Nhili, R.; Peixoto, P.; Depauw, S.; Flajollet, S.; Dezitter, X.; Munde, M. M.; Ismail, M. A.; Kumar, A.; Farahat, A. A.; Stephens, C. E.; Duterque-Coquillaud, M.; Wilson D. W.; Boykin, D. W.; David-Cordonnier, M. H. Targeting the DNA-Binding Activity of the Human ERG Transcription Factor Using New Heterocyclic Dithiophene Diamidines. *Nucleic Acids Res.* **2013**, *41* (1), 125–138.

(45) Munde, M.; Kumar, A.; Peixoto, P.; Depauw, S.; Ismail, M. A.; Farahat, A. A.; Paul, A.; Say, M. V.; David-Cordonnier, M. H.; Boykin, D. W.; Wilson D. W. The Unusual Monomer Recognition of Guanine-Containing Mixed Sequence DNA by a Dithiophene Heterocyclic Diamidine. *Biochemistry* **2014**, *53* (7), 1218–1227.

(46) Munde, M.; Kumar, A.; Nhili, R.; Depauw, S.; David-Cordonnier, M. H.; Ismail, M. A.; Stephens, C. E.; Farahat, A. A.; Batista-Parra, A.; Boykin, D. W.; Wilson D. W. DNA Minor Groove Induced Dimerization of Heterocyclic Cations: Compound Structure, Binding Affinity, and Specificity for a TTAA Site. *J. Mol. Biol.* **2010**, *402* (5), 847–864.

(47) Liu, Y.; Kumar, A.; Depauw, S.; Nhili, R.; David-Cordonnier, M. H.; Lee, M. P.; Ismail, M. A.; Farahat, A. A.; Say, M.; Chackal-Catoen, S.; Batista-Parra, A.; Neidle, S.; Boykin, D. W.; Wilson D. W. Water-Mediated Binding of Agents That Target the DNA Minor Groove. *J. Am. Chem. Soc.* **2011**, *133* (26), 10171–10183.

(48) Mallena, S.; Lee, M. P. H.; Bailly, C.; Neidle, S.; Kumar, A.; Boykin, D. W.; Wilson, W. D. Thiophene-Based Diamidine Forms a "Super" AT Binding Minor Groove Agent. *J. Am. Chem. Soc.* **2004**, *126* (42), 13659–13669.

(49) Sheng, J.; Gan, J.; Huang, Z. Structure-Based DNA-Targeting Strategies with Small Molecule Ligands for Drug Discovery. *Med. Res. Rev.* **2013**, *33* (5), 1119–1173.

(50) Lansiaux, A.; Tanious, F.; Mishal, Z.; Dassonneville, L.; Kumar, A.; Stephens, C. E.; Hu, Q.; Wilson, W. D.; Boykin, D. W.; Bailly, C. Distribution of Furamidine Analogues in Tumor Cells: Targeting of the Nucleus or Mitochondria Depending on the Amidine Substitution. *Cancer Res.* **2002**, *62* (24), 7219–7229.

(51) Ghannam, G.; Takeda, A.; Camarata, T.; Moore, M. A.; Viale, A.; Yaseen, N. R. The Oncogene Nup98-HOXA9 Induces Gene Transcription in Myeloid Cells. *J. Biol. Chem.* **2004**, *279* (2), 866–875.

(52) Nagel, S.; Venturini, L.; Marquez, V. E.; Meyer, C.; Kaufmann, M.; Scherr, M.; MacLeod, R. A. F.; Drexler, H. G. Polycomb Repressor Complex 2 Regulates HOXA9 and HOXA10, Activating ID2 in NK/T-Cell Lines. *Mol. Cancer* **2010**, *9*, 151.

(53) Velu, C. S.; Chaubey, A.; Phelan, J. D.; Horman, S. R.; Wunderlich, M.; Guzman, M. L.; Jegga, A. G.; Zeleznik-Le, N. J.; Chen, J.; Mulloy, J. C.; Cancelas, J. A.; Jordan, C. T.; Aronow, B. J.; Marcucci, G.; Bhat, B.; Gebelein, B.; Grimes, H. L. Therapeutic Antagonists of MicroRNAs Deplete Leukemia-Initiating Cell Activity. *J. Clin. Invest.* **2014**, *124* (1), 222–236.

(54) Wu, J. J.; Cantor, A.; Moscinski, L. C. B2 Integrins Are Characteristically Absent in Acute Promyelocytic Leukemia and Rapidly Upregulated in Vivo upon Differentiation

with All-Trans Retinoic Acid. *Leuk. Res.* **2007**, *31* (1), 49–57.

(55) Fang, J.; Ying, H.; Mao, T.; Fang, Y.; Lu, Y.; Wang, H.; Zang, I.; Wang, Z.; Lin, Y.; Zhao, M.; Luo, X.; Wang, Z.; Zhang, Y.; Zhang, C.; Xiao, W.; Wang, Y.; Tan, W.; Chen, Z.; Lu, C.; Atadja, P.; Li, E.; Zhao, K.; Liu, J., Gu, J. Upregulation of CD11b and CD86 through LSD1 Inhibition Promotes Myeloid Differentiation and Suppresses Cell Proliferation in Human Monocytic Leukemia Cells. *Oncotarget* **2017**, *8* (49), 85085–85101.

(56) Jin, P.; Han, T. H.; Ren, J.; Saunders, S.; Wang, E.; Marincola, F. M.; Stroncek, D. F. Molecular Signatures of Maturing Dendritic Cells: Implications for Testing the Quality of Dendritic Cell Therapies. *J. Transl. Med.* **2010**, *8*, 4.

(57) Sun, Y.; Zhou, B.; Mao, F.; Xu, J.; Miao, H.; Zou, Z.; Phuc Khoa, L.T.; Jang, Y.; Cai, S.; Witkin, M.; Koche, R.; Ge, K.; Dressler, G.R.; Levine, R.L.; Armstrong, S.A., Dou, Y., Hess, J.L. HOXA9 Reprograms the Enhancer Landscape to Promote Leukemogenesis. Cancer Cell. **2018,** *34* (4), 643-658.

(58) Daigle, S. R.; Olhava, E. J.; Therkelsen, C. A.; Majer, C. R.; Sneeringer, C. J.; Song, J.; Johnston, L. D.; Scott, M. P.; Smith, J. J.; Xiao, Y.; Jin, L.; Kuntz, K. W.; Chesworth, R.; Moyer, M. P.; Bernt, K. M.; Tseng, J. C.; Kung, A. L.; Armstrong, S. A.; Copeland, R. A.; Richon, V. M.; Pollock, R. M. Selective Killing of Mixed Lineage Leukemia Cells by a Potent Small-Molecule DOT1L Inhibitor. *Cancer Cell* **2011**, *20* (1), 53–65.

(59) Waters, N. J. Preclinical Pharmacokinetics and Pharmacodynamics of Pinometostat (EPZ-5676), a First-in-Class, Small Molecule S-Adenosyl Methionine Competitive Inhibitor of DOT1L. *Eur. J. Drug Metab. Pharmacokinet.* **2017**, *42* (6), 891–901.

(60) Shi, A.; Murai, M. J.; He, S.; Lund, G.; Hartley, T.; Purohit, T.; Reddy, G.; Chruszcz, M.; Grembecka, J.; Cierpicki, T. Structural Insights into Inhibition of the Bivalent Menin-MLL Interaction by Small Molecules in Leukemia. *Blood* **2012**, *120* (23), 4461–4469.

(61) Xu, S.; Aguilar, A.; Xu, T.; Zheng, K.; Huang, L.; Stuckey, J.; Chinnaswamy, K.; Bernard, D.; Fernández-Salas, E.; Liu, L.; Wang, M.; McEachern, D.; Przybranowski, S.; Foster, C.; Wang, S. Design of the First-in-Class, Highly Potent Irreversible Inhibitor Targeting the Menin-MLL Protein–Protein Interaction. *Angew. Chemie - Int. Ed.* **2018**, *57* (6), 1601–1605.

(62) Morgan, R.; El-Tanani, M.; Hunter, K. D.; Harrington, K. J.; Pandha, H. S. Targeting HOX/PBX Dimers in Cancer. *Oncotarget* **2015**, *8* (19), 32322–32331.

(63) Munde, M.; Wang, S.; Kumar, A.; Stephens, C. E.; Farahat, A. A.; Boykin, D. W.; Wilson, W. D.; Poon, G. M. K. Structure-Dependent Inhibition of the ETS-Family Transcription Factor PU.1 by Novel Heterocyclic Diamidines. *Nucleic Acids Res.* **2014**, *42* (2), 1379–1390.

(64) Ismail, M. A.; Anbazhagan, M.; Stephens, C. E; Boykin, D. W. Synthesis of benzyloxybromobenzonitriles. *Synthetic Commun.* **2004**, *34* (5), 751–758.

(65) Farahat, A. A.; Kumar, A.; Barghash, A. M.; Goda, F. E.; Eisa, H. M.; Boykin, D. W. Bichalcophenes: A Concise Synthesis of Formyl Ester- and Cyano Ester-Substituted Bithiophenes, Bifurans, and Furanothiophenes. *J. Heterocyclic Chem.* **2010**, *47* (1), 167–170.

(66) Ismail, M. I.; Brun, R.; Wenzler, T.; Tanious, F. A.; Wilson, W. D.; Boykin, D. W. Dicationic biphenyl benzimidazole derivatives as antiprotozoal agents. *Bioorg. & Med. Chem.* **2004**, *12* (20), 5405–5413.

(67) Ismail, M. I.; Brun, R.; Wenzler, T.; Tanious, F. A.; Wilson, W. D.; Boykin, D. W. Novel Dicationic Imidazo[1,2-a]pyridines and 5,6,7,8-Tetrahydro-imidazo[1,2-a]pyridines as Antiprotozoal Agents. *J. Med. Chem.* **2004**, *47*, 3658–3664.

(68) Chaires, J. B.; Jinsong Ren, J.; Hamelberg, D.; Kumar, A.; Pandya, V.; Boykin, D. W.; Wilson, W. D. Structural Selectivity of Aromatic Diamidines. *J. Med. Chem.* **2004**, *47* (14), 5729–5742.

(69) Ismail, M. A.; Brun, R.; Easterbrook, J. D.; Tanious, F. A.; Wilson, W. D.; Boykin, D. W. Synthesis and Antiprotozoal Activity of Aza-Analogues of Furamidine. *J. Med. Chem.* **2003**, *46* (22), 4761–4769.

(70) Kumar, A.; Stephens, C. E.; Boykin, D. W. Palladium catalyzed reactions for the synthesis of 2,5-disubstituted furans. *Heterocyclic Communications* **1999**, *5*, 301–304.

(71) Sweat, D. P.; Stephens, C. E. Synthesis and Stille cross-coupling reactions of 2-(tributylstannyl)- and 2,5-bis(tributylstannyl)tellurophene. *Synthesis*, **2009**, *5* (19), 3214–3218.

(72) Buu-Hoi, N. G.; Royer, R.; Xuong, N. G.; Jacqignon, P. The Pfitzinger reaction in the synthesis of quinoline derivatives. *J. Org. Chem.* **1953**, *18* (9), 1209–1224.

(73) Kalluraya, B.; Sreenivasa, S. Synthesis and Pharmacological properties of some quinoline derivatives. *Il Farmaco* **1998**, *53* (6), 399–404.

(74) Ajdačić, V.; Senerovic, L.; Vranić, M.; Pekmezovic, M.; Arsic-Arsnijevic, V.; Veselinovic, A.; Veselinovic, J.; Šolaja, B. A.; Nikodinovic-Runic, J.; Opsenica, I. M. Synthesis and evaluation of thiophene-based quanylhydrazones(iminoguanidines) efficient against panel of voriconazole-resistant fungal isolates. *Bioorg. & Med. Chem.* **2016**, *24* (6), 1277–1291.

(75) Guo, P.; Paul, A.; Kumar, A.; Farahat, A. A.; Kumar, D.; Wang, S.; Boykin, D.W.; Wilson, W. D. The Thiophene "Sigma-Hole" as a Concept for Preorganized, Specific Recognition of G•C Base Pairs in the DNA Minor Groove. *Chem. Eur. J.* **2016**, *22* (43), 15404–15412.

(76) Racané, L.; Tralić-Kulenović, V.; Pavelić, S. K.; Ratkaj, I.; Peixoto, P.; Nhili, R.; Depauw, S.; Hildebrand, M. P.; David-Cordonnier, M. H.; Pavelić, K.; Karminski-Zamola, G. Novel Diamidino-Substituted Derivatives of Phenyl Benzothiazolyl and Dibenzothiazolyl Furans and Thiophenes: Synthesis, Antiproliferative and DNA Binding Properties. *J. Med. Chem.* **2010**, *53* (6), 2418–2432.

(77) Messaoudi, S.; Anizon, F.; Léonce, S.; Pierré, A.; Pfeiffer, B.; Prudhomme, M. Synthesis

and Cytotoxicities of 7-Aza Rebeccamycin Analogues Bearing Various Substituents on the Sugar Moiety, on the Imide Nitrogen and on the Carbazole Framework. *Eur. J. Med. Chem.* **2005**, *40* (10), 961–971.

(78) Gros, C.; Fleury, L.; Nahoum, V.; Faux, C.; Valente, S.; Labella, D.; Cantagrel, F.; Rilova, E.; Bouhlel, M. A.; David-Cordonnier, M. H.; Dufau, I.; Ausseil, F.; Mai, A.; Mourey, L.; Lacroix, L.; Arimondo, P.B. New Insights on the Mechanism of Quinoline-Based DNA Methyltransferase Inhibitors. *J. Biol. Chem.* **2015**, *290* (10), 6293–6302.

(79) Nguyen, B.; Tanious, F. A.; Wilson, W. D. Biosensor-Surface Plasmon Resonance: Quantitative Analysis of Small Molecule-Nucleic Acid Interactions. *Methods* **2007**, *42* (2), 150–161.

(80) Nanjunda, R., Munde, M., Liu, Y.; Wilson, W. D. Real-Time Monitoring of Nucleid Acid Interactions with Biosensor-Surface Plasmon Resonance. In *Methods for Studying Nucleic Acid/Drug Interactions*; 2011; Edition 1, Chapter 4, Publisher CRC Press, Editors Yitzhak Tor, Meni Wanunu, Boca Raton, Florida, USA, 91–122.

(81) Bayly, C. I.; Cieplak, P.; Cornell, W.; Kollman, P. A. A well-behaved electrostatic potential based method using charge restraints for deriving atomic charges: the RESP model. *J Phys Chem* **1993**, *97* (40), 10269–10280.

(82) Case, D. A.; Babin, V.; Berryman, J.; Betz, R. M.; Cai, Q.; Cerutti, D. S.; Cheatham, T. E., III; Darden, T. A.; Duke, R. E.; Gohlke, H.; Goetz, A. W.; Gusarov, S.; Homeyer, N.; Janowski, P.; Kaus, J.; Kolossváry, I.; Kovalenko, A.; Lee, T. S.; LeGrand, S.; Luchko, T.; Luo, R.; Madej, B.; Merz, K. M.; Paesani, F.; Roe, D. R.; Roitberg, A.; Sagui, C.; Salomon-Ferrer, R.; Seabra, G.; Simmerling, C. L.; Smith, W.; Swails, J.; Walker, R. C.; Wang, J.; Wolf, R. M.; Wu, X.; Kollman, P. A. AMBER 14. University of California, San Francisco, **2014**.

(83) Wang, J.; Wang, W.; Kollman, P. A.; Case, D. A. Automatic atom type and bond type perception in molecular mechanical calculations. *J. Mol. Graph. Model* **2006**, *25* (2), 247–260.

(84) Harika, N. K.; Germann, M. W.; Wilson, W. D. First Structure of a Designed Minor Groove Binding Heterocyclic Cation that Specifically Recognizes Mixed DNA Base Pair Sequences. *Chem. Eur. J.* **2017**, *23* (69), 17612–17620.

(85) Athri, P.; Wilson, W. D. Molecular dynamics of water-mediated interactions of a linear benzimidazole-biphenyl diamidine with the DNA minor groove. *J. Am. Chem. Soc.* **2009**, *131* (22), 7618–7625.

(86) Trott, O.; Olson, A. J. J. AutoDock Vina: improving the speed and accuracy of docking with a new scoring function, efficient optimization and multithreading *Comput. Chem.* **2010**, *31* (2), 455–461.

(87) Ritchie, M. E.; Phipson, B.; Wu, D.; Hu, Y.; Law, C. W.; Shi, W.; Smyth, G. K. Limma Powers Differential Expression Analyses for RNA-Sequencing and Microarray Studies. *Nucleic Acids Res.* **2015**, *43* (7), e47.

Compound Name	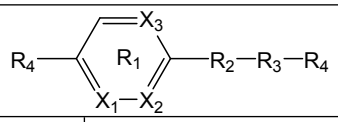								
R_2 as 5-member ring R_3 as 6-member ring	R_1 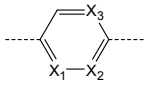			**R_2** 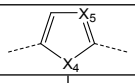 X_4	X_5	R_3 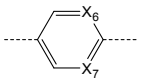			**R_4**
DB421 (**12a**)				O	CH				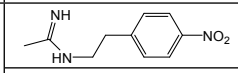
DB75									
DB484					N				
DB351				S	CH				
DB1620					N				
DB1751 (**12b**)				Te					
DB262				NH	CH				
DB883									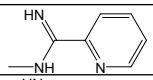
DB884									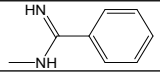
R_2 as 5-member ring R_3 as benzimidazole or derivative	**R_1** 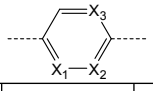			**R_2** 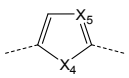		**R_3** 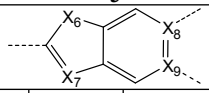			R_4
	X_1	**X_2**	**X_3**	**X_4**	**X_5**	**X_6**	**X_7**	**X_8**	**X_9**	
DB293	CH	CH	CH	O	CH	NH	N	C-R_4	CH	
DB850		C-CH_3								
DB928 (**4a**)		C-OH								
DB915 (**4b**)		N								
DB995 (**4c**)	N	CH								
DB1478 (**11a**)	CH						CH	CH	C-R_4	
DB1481 (**11b**)		N								
DB1878		CH						C-R_4	CH	
DB2430						N-CH_3	N	CH	C-R_4	
DB2005 (**11e**)			CO-CH_3			NH	CH	C-R_4	CH	
DB818			CH	S			N			
DB2651 (**7**)					N					
DB1879 (**11c**)					CH		CH			
DB2529 (**11d**)		N			CH		CH			
DB2429		CH				N-CH_3	N	CH	C-R_4	
DB2223				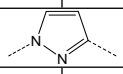		NH		C-R_4	CH	
DB2572 (**19**)	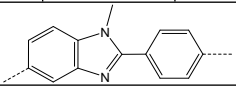			S	CH	N-CH_3		CH	C-R_4	

R2 as 5-members ring R3 as Others	R_1	**R_2**		**R_3**				R_4
	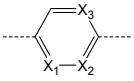	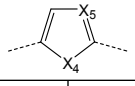		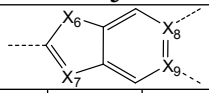				
		X_4	X_5	X_6	X_7	X_8	X_9	
DB828		O	CH	O	N	CH	C-R_4	
DB2708		S		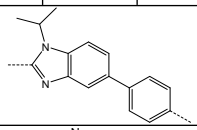				
DB1504 (**18**)				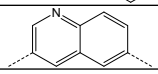				
R_2 as 6-members ring R3 as Others	**R_1**	**R_2**		**R_3**				R_4
	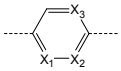	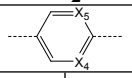						
		X_4	X_5					
DB1055	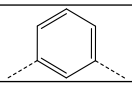	CH	CH	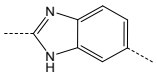				
B911				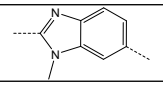				
DB1314 (**14**)								
DB1175				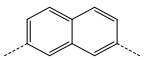				
DB1177		CH	CH					
DB1210		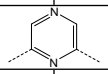		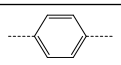				
DB1302				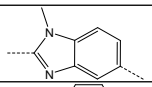				
DB1263		CH	CH	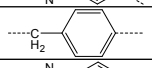				
DB877				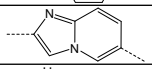				
DB1798				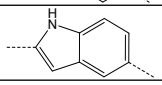				

Table 1. Structures of the 39 evaluated diamidine derivatives.
Numbers in brackets refer to numbering used in the synthesis section and schemes presented in chemistry section

Compound	MTS IC_{50} 72H (µM)	Conc. (µM)	% PI-positive cells 24H	% PI-positive cells 48H	% SubG1 48H
DB818	9.97 +/- 2.40	10	6.95 +/- 0.48	**29.40 +/- 3.29** $	**9.46 +/- 1.91** $
		15	**13.50 +/- 1.37** #	**64.03 +/- 3.25** $	**14.58 +/- 1.30** $
		20	**21.07 +/- 1.25** $	**75.53 +/- 0.60** $	**12.00 +/- 0.90** $
DB1055	14.09 +/- 1.69	15	3.87 +/- 0.03	5.72 +/- 0.06	1.27 +/- 0.20
		20	5.17 +/- 0.35	9.45 +/- 0.52	1.65 +/- 0.37
DB1878	6.34 +/- 1.41	10	8.72 +/- 0.35	**44.93 +/- 1.03** $	**15.94 +/- 1.80** $
		15	11.76 +/- 1.88	**52.73 +/-17.16** #	**27.88 +/- 16.14** *
DB1879	3.58 +/- 0.92	5	7.42 +/- 0.19	**77.87 +/- 0.32** $	**33.64 +/- 15.95** #
		10	**23.83 +/- 0.58** $	**98.17 +/- 0.20** $	na
DB2529	2.24 +/- 0.22	5	6.21 +/- 0.34	**39.40 +/-12.96** #	**4.48 +/- 0.95** †
		10	**13.57 +/- 1.19** #	**96.03 +/- 0.77** $	na
DB883	3.87 +/- 0.17	0.5	5.19 +/- 0.10	8.01 +/- 0.12	1.23 +/- 0.35
		1	**14.43 +/- 0.83** #	**17.60 +/- 1.06** $	1.04 +/- 0.35
DB884	2.14 +/- 0.26	0.5	**12.90 +/- 0.40** #	**18.33 +/- 0.77** $	**2.47 +/- 1.02** *
		1	**68.80 +/- 1.06** $	**99.33 +/- 0.15** $	na
DB1620	23.93 +/- 0.86	15	5.69 +/- 0.21	10.45 +/- 1.50	0.88 +/- 0.10
		20	5.91 +/- 0.15	**22.90 +/- 2.36** $	**1.71 +/- 0.06** †
DB2223	>50	15	8.64 +/- 0.42	6.48 +/- 0.11	0.65 +/- 0.10
		20	10.43 +/- 0.69	6.72 +/- 0.18	0.67 +/- 0.17
DB828	>50	15	8.89 +/- 0.32	7.32 +/- 0.03	0.95 +/- 0.18
		20	8.38 +/- 0.45	7.77 +/- 0.10	0.92 +/- 0.19
None		**Untreated**	9.06 +/- 0.53	8.75 +/- 0.23	0.76 +/- 0.16

Table 2. Cell survival and cell death. Cell survival is determined by using the MTS measurements (n>3) on the HOXA9-expressing murine MigA9 cell line. IC_{50} corresponds to the concentration of compound associated with the presence of 50% cell survival relatively to untreated controls, measured by using MTS reagent. ">50" means that IC_{50} was not reached, even at the maximum amount concentration of 50 µM used in the experiments. Cell death is established from PI-labeling of MigA9 living cells (PI-positive) or as sub-G1 population from PI-labeling of fixed MigA9 cells treated for 24 (PI-positive cells) or 48 hours (PI-positive cells and subG1 quantification) with the indicated concentrations of evaluated compounds. Results are expressed as mean values or mean percentage +/- s.e.m (n=3 to 7). Statistic, student t-test: *,

p<0.05; [#], p<0.01; [†], p<0.001; [$], p<0.0001; na, not applicable due to high proportion of dead cells.

Treatment		Cell Cycle		
Cpd	**Conc. (µM)**	**G0/G1**	**S**	**G2/M**
None	**Untreated**	48.77 +/- 0.19	46.68 +/- 0.21	4.55 +/- 0.16
DB818	10	50.38 +/- 0.77 *	35.42 +/- 1.57 $	**14.19 +/- 1.50 $**
	15	58.30 +/- 3.71 #	**14.80 +/- 3.59 $**	**26.90 +/- 1.96 $**
	20	56.02 +/- 2.41 #	**9.25 +/- 2.09 $**	**34.73 +/- 0.93 $**
DB1055	15	**61.49 +/- 0.19 $**	**34.13 +/- 0.93 $**	4.38 +/- 0.20
	20	**70.98 +/- 0.90 $**	**23.91 +/- 1.29 $**	5.11 +/- 0.38
DB1878	10	**87.28 +/- 0.44 $**	**8.02 +/- 0.24 $**	4.70 +/- 0.58
	15	**85.95 +/- 5.39 $**	**10.06 +/- 5.92 $**	3.99 +/- 1.26
DB1879	5	**77.92 +/- 1.89 $**	**9.15 +/- 2.81 $**	**12.93 +/- 4.68 ***
	10	na	na	na
DB2529	5	**67.95 +/- 1.78 $**	**22.55 +/- 1.80 $**	**9.50 +/- 0.09 $**
	10	na	na	na
DB883	0.5	48.44 +/- 0.35	46.06 +/- 0.58	5.50 +/- 0.27 *
	1	50.15 +/- 0.19 *	43.51 +/- 0.95 #	6.34 +/- 0.23 †
DB884	0.5	53.83 +/- 1.07 $	38.84 +/- 1.18 $	**7.32 +/- 0.30 $**
	1	na	na	na
DB1620	15	54.87 +/- 2.31 #	38.65 +/- 2.94 #	6.47 +/- 0.65 #
	20	**64.53 +/- 1.69 $**	**27.33 +/- 1.99 $**	**8.14 +/- 0.30 $**
DB2223	15	52.29 +/- 0.63 $	43.65 +/- 0.65 †	4.06 +/- 0.33
	20	53.56 +/- 0.53 $	43.02 +/- 0.80 †	3.42 +/- 0.27 #
DB828	15	**58.66 +/- 0.38 $**	37.22 +/- 0.54 $	4.12 +/- 0.22
	20	**62.21 +/- 0.20 $**	33.86 +/- 0.22 $	3.93 +/- 0.11 *

Table 3. Cell cycle. HOXA9-expressing murine MigA9 cells were collected after 48 hours treatment with the indicated concentrations of evaluated compounds or control cells (n=3 to 6) and further analyzed by cytometry for cell cycle using EdU and PI staining on fixed cells. All results are expressed as mean percentage +/- s.e.m. Statistic, student t-test: *, p<0.05; [#], p<0.01; [†], p<0.001; [$], p<0.0001; na, not applicable due to high proportion of dead cells (PI-positive cells, Table 2).

Colony assay	Type of colonies	CTR	DB818	DB1055	DB828
K562 Number	Total	445 +/- 28	448 +/- 17	467 +/- 12	nd
MigA9 Number (%)	Total	148 (100%)	101 (100%)	115 (100%)	170 (100%)
	CFU-GM	64 (43.2%)	**23 (22.8%)**	**0 (0%)**	90 (52.9%)
	CFU-G	49 (33.1%)	**55 (54.5%)**	**58 (50.4%)**	62 (36.5%)
	CFU-M	28 (18.9%)	20 (19.8%)	**55 (47.8%)**	16 (9.4%)
	BFU-E	7 (4.7%)	3 (3%)	2 (1.7%)	2 (1.2%)

Table 4. Anti-clonogenic activities. MigA9 cells (1000 cells/ well) were seeded in duplicates in complete M3434 Mouse Colony-Forming Cell Assays MethoCult® in the presence or absence (CTR) of 2.5µM of the indicated compounds and plated in 6-wells plates for 10 days prior to quantification of clones and further identification of the individual CFU-GM, CFU-M and CFU-G colonies on morphological criteria. na: not applicable; nd: not determined. K562 cells (1000 cells/ well) were treated in the same conditions, plated on H4535 (human) Colony-Forming Cell Assays MethoCult® and counted (Mean +/- s.e.m). Data that are statistically different from the untreated control are presented in bold letters.

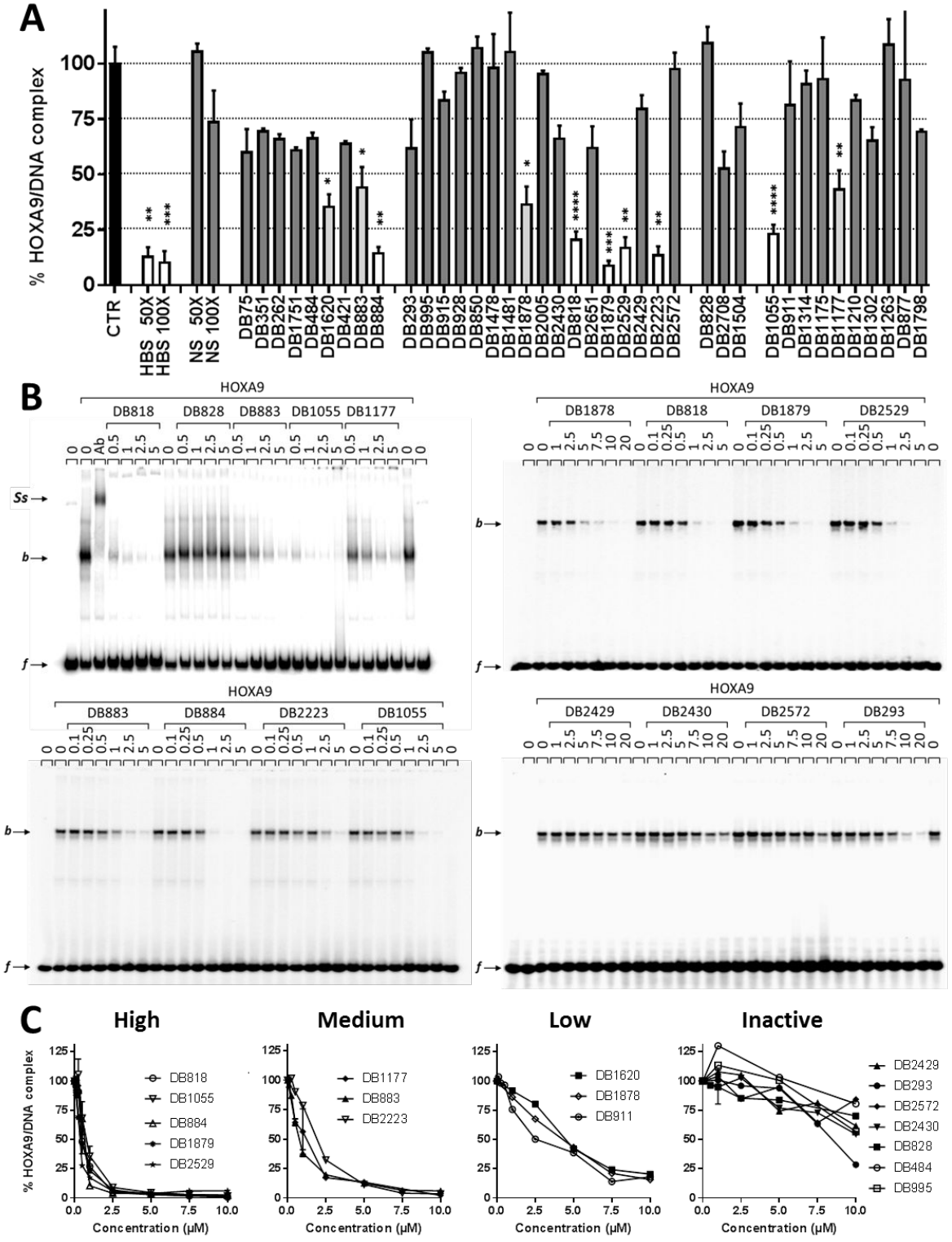

Figure 1. In vitro selection of DB818 and DB1055 as HOXA9/DNA binding inhibitors.

A. ELISA-derived protein/DNA binding inhibition assay for selection of HOXA9/DNA binding inhibitors. HOXA9 protein was expressed from reticulocyte lysate and incubated with immobilized HBS-containing sequence (CTR). Free HBS or non-specific (NS) DNA at 50X or 100X the quantity of immobilized HBS oligonucleotide or the various indicated DB compounds (5 or 10μM) were then added. Black, dark grey, light grey and white bars correspond to control, > 50%, between 25 and 50% or <25% of HOXA9/DNA remaining complexes. Graph represents mean +/- s.e.m. of up to 15 independent measurements.

B. Electrophoretic mobility shift assay (EMSA) gel. 5'-end ^{32}P-radiolabeled HBS DNA sequence ("*f*", free DNA) was incubated with reticulocyte lysate expressing HOXA9 protein ("HOXA9") to form a complex (bound "*b*") and in the presence HOXA9-directed antibody ("*Ab*") to generate a super-shifted ("*Ss*") DNA band, or in the presence of increasing concentrations of the indicated DB compounds (μM).

C. Quantitative analysis of the inhibition of HOXA9/DNA complex formation from EMSA defines sub-groups based on their HOXA9/DNA binding inhibition activity. The percentage of bound HOXA9/DNA complex was quantified from EMSA in panel B, relatively to the mean of the three control samples (100%) and plotted over drug concentration.

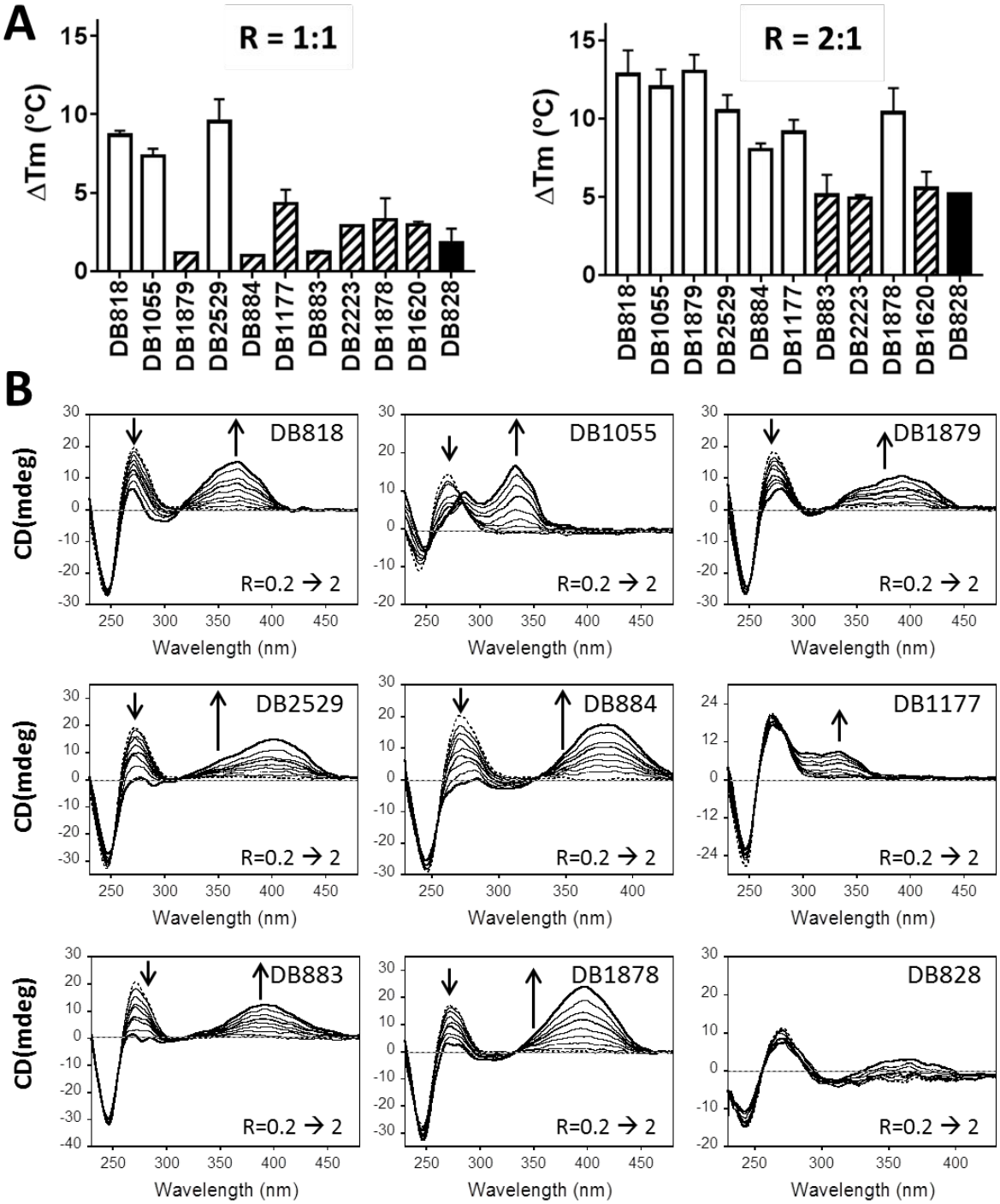

Figure 2. Comparison and mode of binding to an oligonucleotide containing a HOXA9/DNA binding site.

A. Melting temperature studies on the HBS-containing DNA. Double stranded HBS-containing oligonucleotides (0.5μM) were incubated with 0.5μM (R=1:1) or 1μM (R=2:1) of the indicated compounds in TNE buffer prior to be subjected to the measurement of the DNA hyperchromic variation upon step by step heating using absorbance measurement at 260nm. The ΔTm values are calculated from $Tm_{(DNA+DB)}$-$Tm_{(DNA)}$. White and dashed bars highlight an increase of the Tm of more or less than 5°C, respectively, whereas black bars are used for DB828, chosen as a control drug for further cellular analyses.

B. Circular dichroism spectra is showing minor groove binding of duplex DNA. Double stranded HBS-containing oligonucleotides (5μM) were incubated in TNE buffer with increasing concentrations of the indicated compounds at increasing drug/oligonucleotide ratios R, evidencing a strong positive induced CD at the drug wavelength (0, 1, 2, 3, 4, 5, 6, 8, 10 μM of drug, as indicated by arrows from min to max concentrations). Dashed lanes are CD spectra for oligonucleotides in the absence of compounds. Thick lanes highlight CD spectra at R=1:1 and R=2:1.

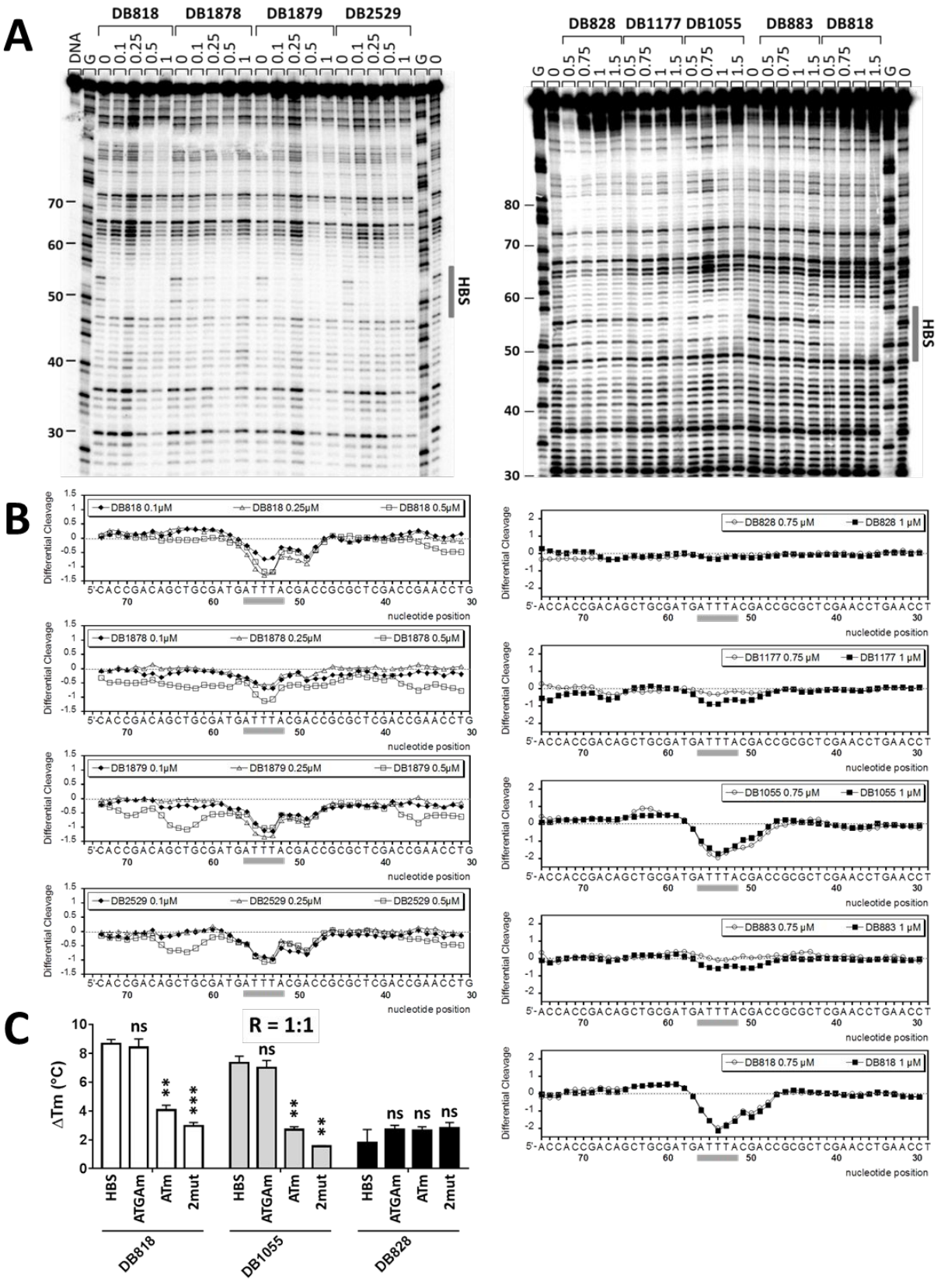
A
DB818
DB1878
DB1879
DB2529
DB828
DB1177
DB1055
DB883
DB818
DNA
HBS
B
Differential Cleavage
nucleotide position
DB818 0.1µM
DB818 0.25µM
DB818 0.5µM
DB1878 0.1µM
DB1878 0.25µM
DB1878 0.5µM
DB1879 0.1µM
DB1879 0.25µM
DB1879 0.5µM
DB2529 0.1µM
DB2529 0.25µM
DB2529 0.5µM
DB828 0.75 µM
DB828 1 µM
DB1177 0.75 µM
DB1177 1 µM
DB1055 0.75 µM
DB1055 1 µM
DB883 0.75 µM
DB883 1 µM
DB818 0.75 µM
DB818 1 µM
C
R = 1:1
ΔTm (°C)
ns
**
***
HBS
ATGAm
ATm
2mut
DB818
DB1055
DB828

Figure 3. Evaluation of the drug interaction to HOXA9 consensus DNA binding site.

A. DNaseI footprinting gels. Increasing concentrations of the indicated compounds (μM) were incubated with a 3'-end ^{32}P-radiolabelled HBS-containing DNA fragment prior to DNaseI mild-digestion prior to be subjected to denaturing gel electrophoresis. "G" lanes, G-track localizes guanines within the radio-labeled DNA sequence. "0" lanes, DNA fragment without drug. Grey line locates the HOXA9-binding site (HBS).

B. Densitometric analyses from DNaseI footprinting gels. Each band from lanes generated in the presence various concentrations of the indicated compounds was quantified regarding each identical base from the untreated lanes ("0") to visualize the differential cleavage at the HBS sequence (grey lines) or not depending on the evaluated compounds from gels in section A.

C. Melting temperature studies on ATGA- and/or AT-mutated sites from the HBS-containing DNA. Experiments were performed at equimolar drug/DNA ratio (R=1:1) in similar conditions as in Figure 2 A but with oligonucleotides mutated on the ATGA sequence (ATGAm), the AT-rich site (ATm) or both (2Mut) (sequences presented in Supplementary Table S1). Statistic, student t-test: ns, $p>0.05$; **, $p<0.01$; ***, $p<0.001$.

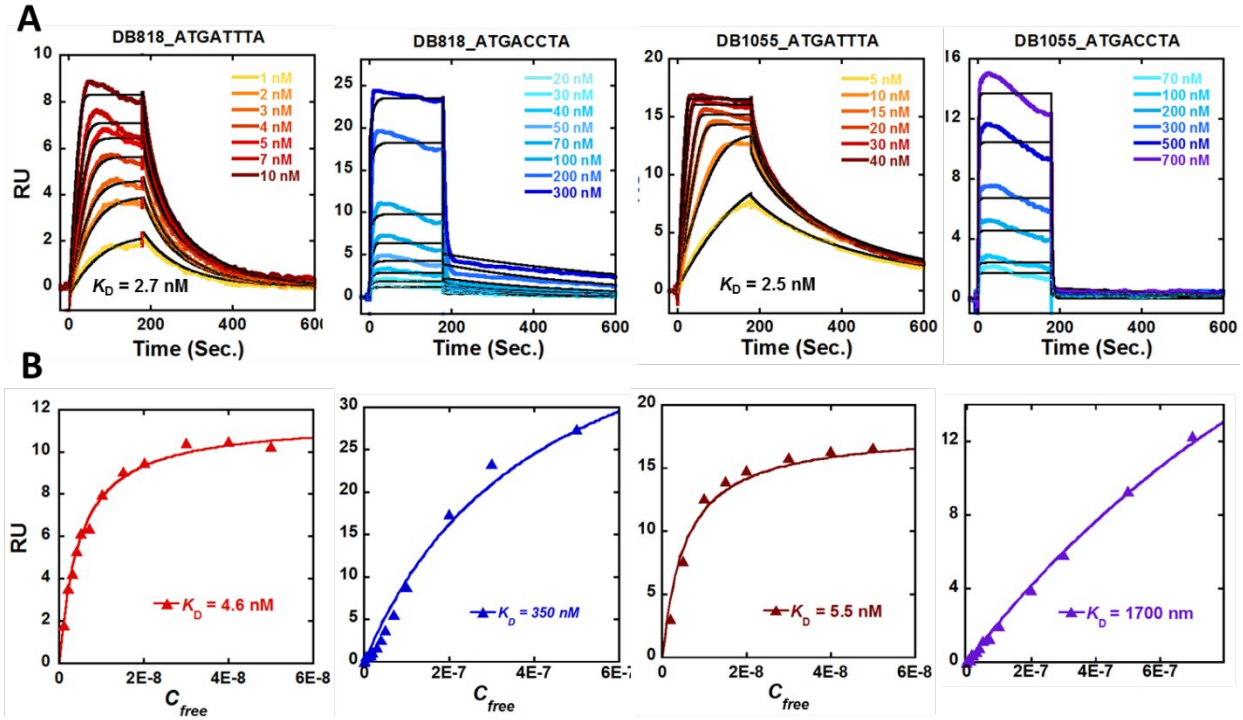

Figure 4. Kinetic and affinity analysis of DB818 and DB1055 binding to HBS and HBS-mut DNA sequences using BIAcore technology.

A. SPR sensorgrams for the evaluation of the interaction kinetics of DB818 and DB1055 with the HBS ("ATGATTTA") or HBS-mut ("ATGACCTA") DNA sequences in P20-TNE binding buffer. The black lines are best fit curves determined by kinetic fitting. The ligand concentrations are indicated in the graphs from bottom to top. The surface interaction of the diamidines at high concentrations causes the drift in the sensorgrams.

B. Steady-state fitting curves for of DB818 and DB1055 on the HBS or HBS-mut DNA hairpin sequences. A stoichiometric value of one was used for data fitting based on the maximum RU values for the different sequences that was similar to that for netropsin binding to AATT sequence used as chip control.

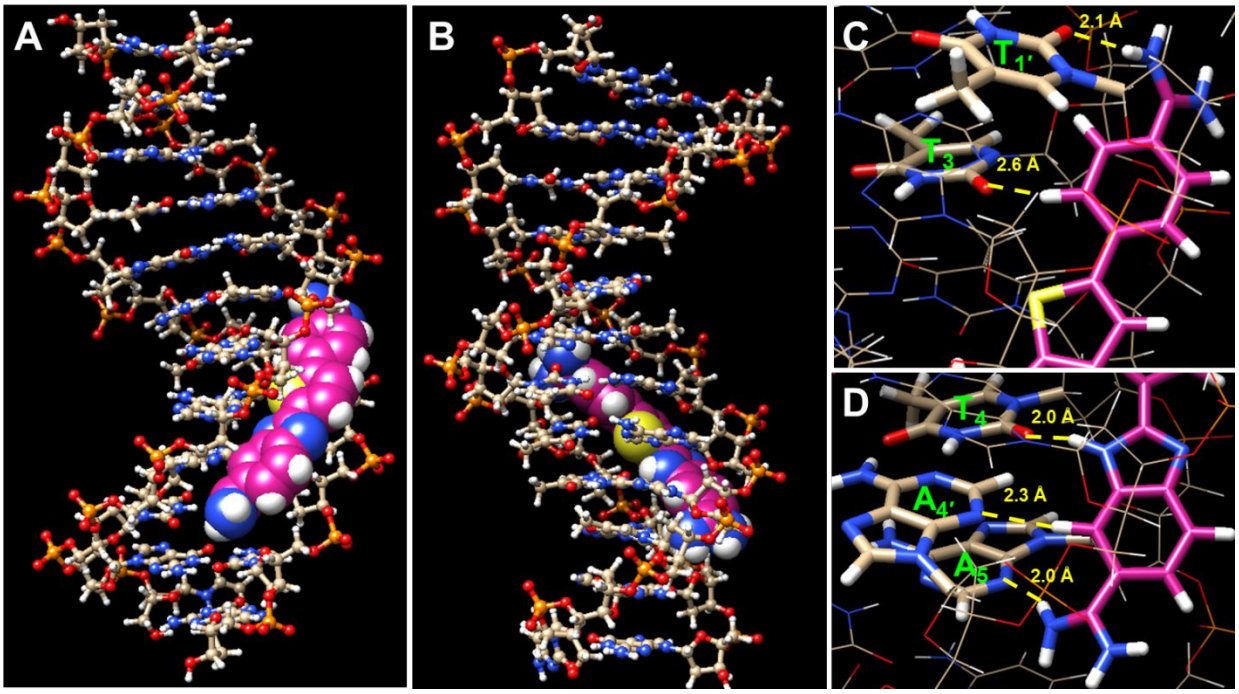

Figure 5. Molecular Dynamics (MD) model of DB818 bound to ds[(5'-CCATGATTTACG-3')(5'-CGTAAATCATGG-3')].

A-B. Ball-stick (DNA) and space-filling (ligand) model viewed into the minor groove (A) and major groove (B) of the ATTTA binding site with bound DB818. The DNA bases are represented in tan-white-red-blue-yellow (C−H−O−N−P) color scheme and DB818 is light purple-white-blue-yellow (C−H−N−S) color scheme.

C-D. The important interactions between different sections of the DB818/DNA complex are presented for the phenyl-amidine (C) and benzimidazole-amidine (D) moieties. Interactions with the indicated bases of HBS sequence are schematized by yellow dashed lanes and the corresponding distances are indicated above (in angstrom).

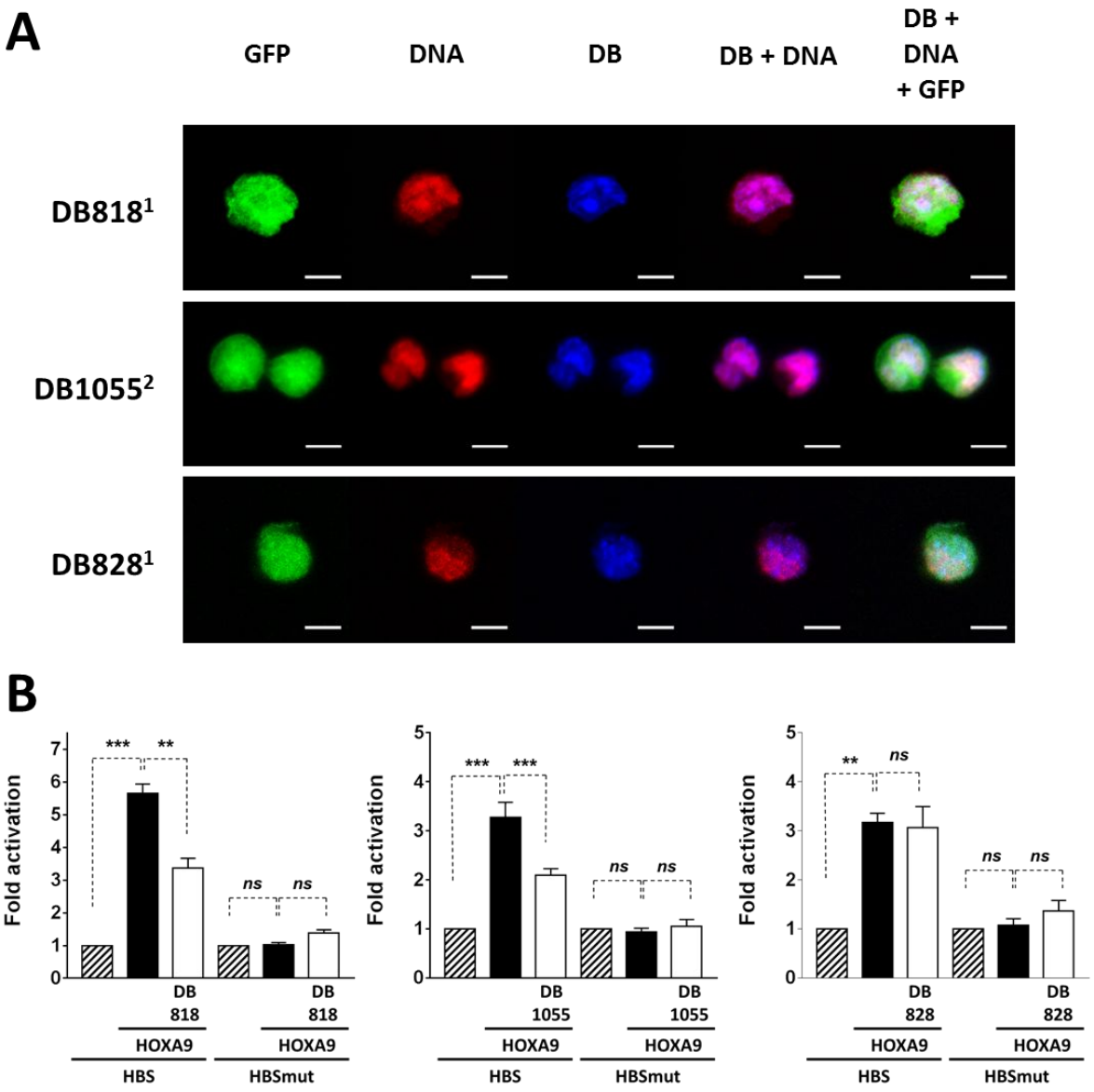

Figure 6. Cellular analysis of HOXA9 transcription factor inhibition by DB818 and DB1055.

A. Subcellular distribution of DB818, DB1055 and DB828 using cell fluorescence microscopy. GFP-positive MigA9 cells (in green) were treated with 20µM of the indicated compounds (in blue) for 2H. Nucleus was counterstained using TO-PRO-3 or propidium iodide (PI) staining of DNA (in red). Merged images are presented on the right. Scale bars correspond to 5µm.

[1]: Images acquired with a confocal Zeiss LSM880 microscope. GFP (Ex488nm, Em495-551nm), TO-PRO-3 (Ex633nm, Em640-735nm), DB818 (Ex405nm, Em445-485nm), DB828 (Ex 405nm, Em425-465nm). [2]: Images acquired with a widefield Leica DMi8 microscope. GFP (ExBP480/40, EmBP527/30), PI (ExBP546/10, EmBP585/40), DB (ExBP350/50, EmBP460/50).

B. Inhibition of HOXA9 transcriptional control by DB818 and DB1055 evidenced by luciferase assays. K562 cells were co-transfected with pGL3-prom reporter vector containing 6-repeated HBS sequences as WT sequence ("HBS") or mutated sequence ("HBSmut") +/- pCMV-AD-HOXA9 ("HOXA9") prior to addition of the indicated DB compounds or vehicle. Graphs represent mean +/- s.e.m. of 3 to 8 independent points. Statistic, student t-test: *, $p<0.05$; **, $p<0.01$; ***, $p<0.001$.

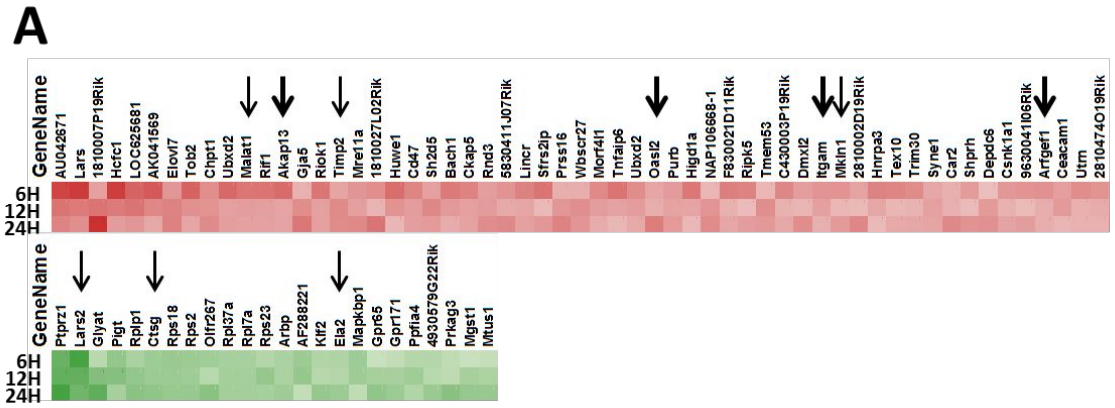

B

DB818 treated MigA9 cells	GSEA analysis C2-CGP	p-value	FDR q-value
Up-regulated genes	NUYTTEN_EZH2_TARGETS_UP	0.0000336	0.00965
	TAKEDA_TARGETS_OF_NUP98_HOXA9_FUSION_8D_DN	0.0000342	0.00965
	GAL_LEUKEMIC_STEM_CELL_DN	0.0000673	0.01140
	GABRIELY_MIR21_TARGETS	0.0001290	0.01890
Down-regulated genes	MARTENS_TRETINOIN_RESPONSE_DN	0.0000324	0.00848
	WANG_IMMORTALIZED_BY_HOXA9_AND_MEIS1_UP	0.0000917	0.01950

C

IPA : Diseases & Functions	p-Value	z-score	# Genes	Gene Names
Differentiation of macrophages	0.0203	1.9800	4	**ITGAM↗**; RGS10↗; TP53↗; CD47↗
Quantity of pro-B lymphocytes	0.0031	-1.7150	4	IGLL1/IGLL5↗; PIM1↗; Tac4↗; TP53↗
Quantity of blood cells	0.0135	-1.5860	20	**AKAP13↗**; ARHGEF1↘; CD47↗; CD74↘; DICER1↗; DNMT3A↗; E2F1↗; FGF7↘; ID1↗; IGLL1/IGLL5↗; **ITGAM↗**; KLF2↘; KLF3↗; Ncoa6↗; ONECUT1↘; PIM1↘; RGS10↗; Tac4↗; TIMP2↗; TP53↗
Quantity of leukocytes	0.0193	-1.5330	18	**AKAP13↗**; ARHGEF1↘; CD47↗; CD74↘; DICER1↗; DNMT3A↗; E2F1↗; FGF7↘; ID1↗; IGLL1/IGLL5↗; **ITGAM↗**; KLF2↘; KLF3↗; PIM1↘; RGS10↗; Tac4↗; TIMP2↗; TP53↗
Quantity of hematopoietic progenitor cells	0.0112	-1.3830	11	**AKAP13↗**; CD47↗; E2F1↗; ID1↗; IGLL1/IGLL5↗; KLF2↘; Ncoa6↗; ONECUT1↘; PIM1↘; Tac4↗; TP53↗
Apoptosis of leukemia cell lines	0.0097	1.2890	8	**ITGAM↗**; PIM1↘; TP53↗; CD47↗; CEACAM1↗; CTSG↘; DICER1↗; E2F1↗

D

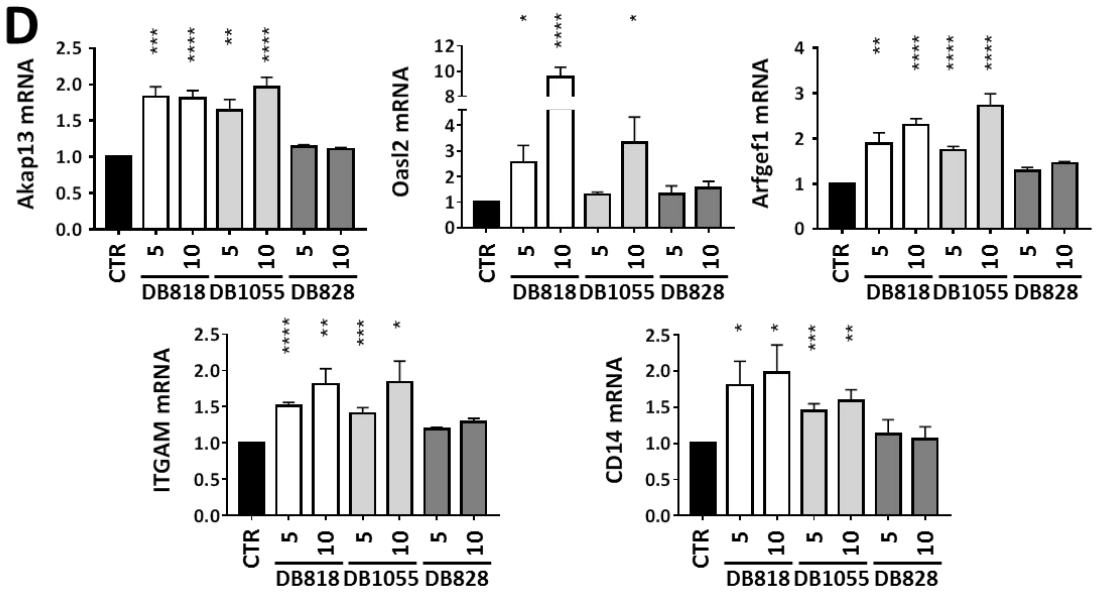

Figure 7. Transcriptomic analysis of MigA9 treated with 2.5µM of DB818 for 6, 12 or 24H.

A. Commonly deregulated genes with |mean fold changes| ≥ 1.5 are presented as heatmap for up-regulated genes (top panel) or down-regulated genes (bottom panel). Arrows identified genes up- or down-regulated during hematopoietic differentiation from progenitors to granulocyte/monocyte differentiated cells as presented in Supplementary Figure S7.

B. GSEA analyses of up-regulated or down-regulated gene expression data on MSigDB C2-Chemical and Genetic Perturbation genesets.

C. Cellular networks ("Diseases and functions" analysis in Hematological systems) deduced from Ingenuity Pathway Analysis of genes that were significantly deregulated (adjusted p-values≤0.05) by DB818 treatment of MigA9 cells with |fold-changes|≥1.5. Z-score, the number of genes ("# Genes"), their names and corresponding up (↗) or down (↘) expression changes are indicated.

D. Quantification of deregulated genes using qRT-PCR on total mRNA from MigA9 cells treated with DB818, DB1055 or DB828 (5 or 10 μM) for 48 hours, as 6 independent replicates. Each gene expression was normalized relatively to that of Gapdh (see primers in supplementary Table S1) and given as mean +/- s.e.m. Statistics (Student t-test): *, $p<0.05$; **, $p<0.01$; ***, $p<0.001$; ****, $p<0.0001$.

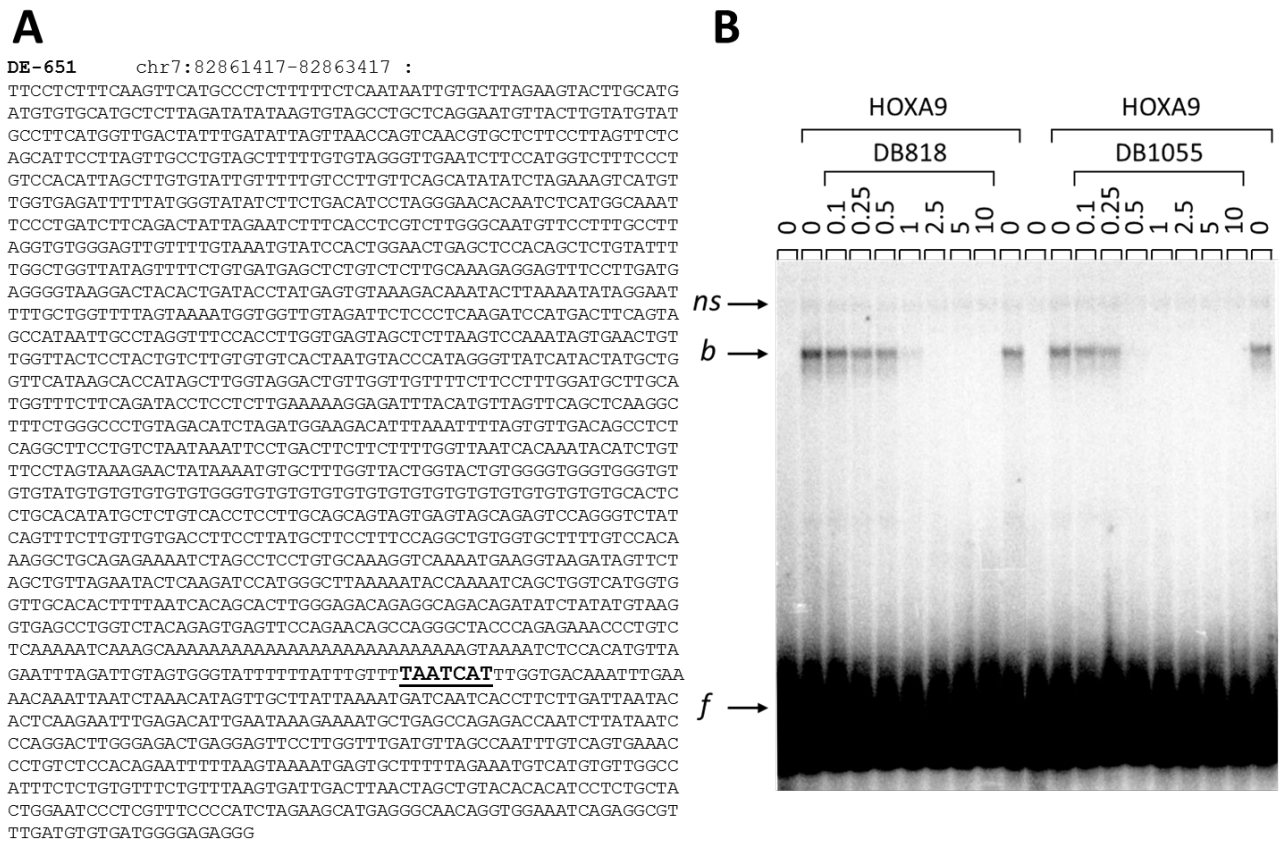

Figure 8. Evaluation of DB818 and DB1055 inhibition of HOXA9 binding to murine Akap13 gene regulatory region.

A. DNA sequence of DE-651 peak, located at position chr7:82861417-82863417 from NCBI37/mm9 mouse reference genome (within Akap13 gene) as identified by Sun et al[57] from ChIP-seq analysis using a hemagglutinin antibody to trap HOXA9 binding site from the murine leukemia model obtained by transformation of murine progenitor cells by co-expression of hemagglutinin (HA)-tagged HOXA9 and MEIS1.

B. Electrophoretic mobility shift assay (EMSA) gel. 5'-end ^{32}P-radiolabeled AKAP13-HBS DNA sequence ("f", free DNA) was incubated with reticulocyte lysate expressing HOXA9

protein ("HOXA9") or not ("0") to form a complex (bound "b") and in the presence of increasing concentrations of DB818 or DB1055 compounds (μM). *ns*, non-specific band.

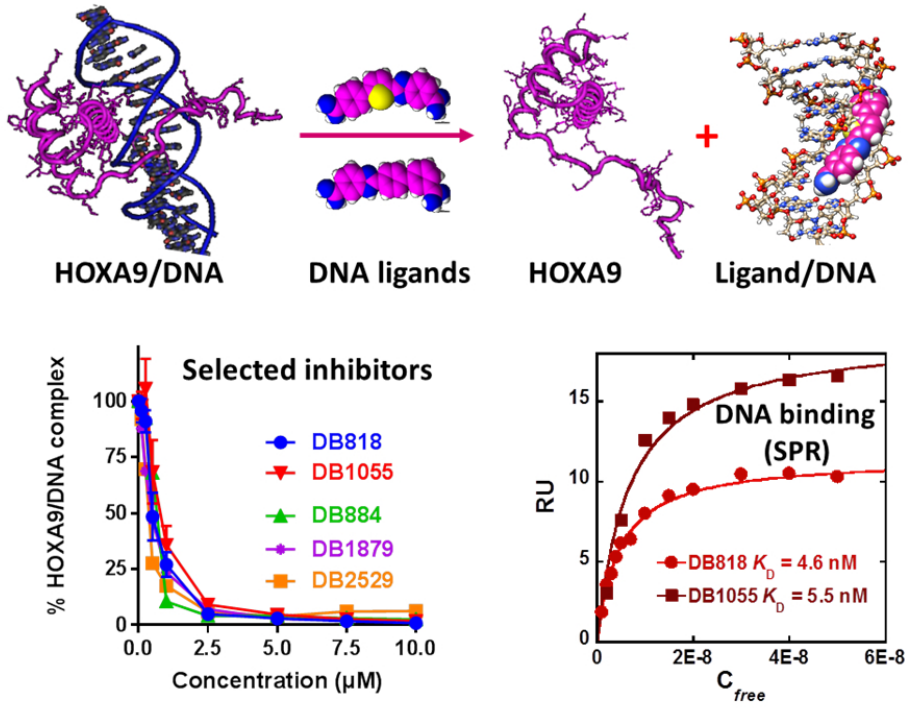

Depauw et al TOC graphic

254x190mm (96 x 96 DPI)